Control and Stability of a Spinning Symmetric Satellite in an Elliptical Orbit

THESIS

James Walter Cole
Captain, USAF

AFIT/GAE/ENY/89D-05

DEPARTMENT OF THE AIR FORCE
AIR UNIVERSITY
AIR FORCE INSTITUTE OF TECHNOLOGY

Wright-Patterson Air Force Base, Ohio

AFIT/GAE/ENY/89D-05

Control and Stability of a Spinning Symmetric Satellite in an Elliptical Orbit

THESIS

Presented to the Faculty of the School of Engineering
of the Air Force Institute of Technology
Air University
In Partial Fulfillment of the
Requirements for the Degree of
Master of Science in Aeronautical Engineering

James Walter Cole, B.S.
Captain, USAF

December, 1989

Preface

This work is a continuation of work done by Shell in the stability evaluation of a scalar control applied to a time periodic system. The scalar controlled satellite is examined in a new controlled modal coordinate system. This coordinate system decouples the four modes of the linearized system with the controller. The stability of each mode can easily be evaluated in the uncoupled form. This technique is demonstrated on a well defined problem and can easily be extended to higher order systems. The comparison of the linear and non-linear equations in the controlled modal coordinates demonstrates some of the limitations of linearized equations in this type of non-linear system.

I must thank Dr. Wiesel for his consultation on the computer programs and help with the Fourier series computations and Major Robinson for his guidance and encouragement through the thesis process. Thanks must also go to Dr. Mark Oxley for his assistance with the mathematics. I am especially grateful to my thesis advisor, Dr. Robert Calico, for the wisdom and insight he has provided me through the past year. Finally, I would like to thank my wife, Barbara for her love and patience during this trying time.

James Walter Cole

Table of Contents

List of Figures

List of Tables

Abstract

The stability of a spinning symmetric satellite in an elliptical orbit is analyzed using phase planes and surface of section techniques. The equations of motion for the satellite attitude are presented in a linearized and a non-linear form. Floquet Theory is applied to the development of a control system for two unstable modes of the satellite. A scalar control is applied using angle rates as feedback. The stability of the new controlled system is examined in controlled modal coordinates. Comparisons of the linear and non-linear system motions are made relative to changes in the control gains. Potential chaotic motion limits the controller gains of the non-linear system.

Control and Stability of a Spinning Symmetric Satellite in an Elliptical Orbit

I. Introduction

We are demanding more accurate control and attitude stability from our satellites while sending them into less stable environments. The control design developed here is relatively easy to implement, yet it compensates for a complex, dynamic environment. This fits well into the control systems for satellites going into elliptical orbits or in other periodic systems that fit the form of the Floquet problem. The non-linear example shows that some caution is warranted as to the limits of control in non-linear systems. In some configurations non-linear behavior can drive the system into instability or chaos.

The stability of a spinning symmetric satellite was examined by Kane and Barba [8:402-405]. The development of the equations of motion from their work is presented in Appendix I. They applied Floquet Theory to determine the stability of the linearized system. Calico and Yeakel developed a control system based on Floquet Theory to control one unstable mode of the same class of problem [3:315-318]. Calico and Wiesel extended this to control two unstable modes [2:671-676]. Myers examined several types of controllers for this kind of system and made some rough evaluation of the performance of each controller type [12:56-59]. Shell examined the scalar controller for a satellite with two unstable modes using phase plane techniques [14:3.24-3.44]. The true performance limits of the controller are still unknown. There are no guidelines for selecting the proper parameter values for this controller design. This thesis addresses these problems.

The theory and concepts developed here can be applied to any system that fits the form of the Floquet problem. The example problem of a spinning symmetric satellite in an elliptic orbit is well defined and exhibits some interesting characteristics. A full description of the coordinates and development of the equations of motion are given in Appendix 1. The equations of motion can be expressed in matrix form as

$$\bar{x}' = A(\tau)\bar{x} \tag{1.1}$$

where $A(\tau)$ is composed of periodic elements that all have the same period. The solution to the this system of equations and the development of the controller involves the application of Floquet Theory.

II. Theory

This chapter examines the equations of motion of a spinning inertially symmetric satellite in an elliptical orbit around a symmetrical attracting body, determines the satellite stability, develops a controller and examines the stability of the controlled system. The satellite spin axis is along the inertial axis of symmetry and perpendicular to the orbit plane, Figure 2.1. The attitude equations of the satellite are developed and linearized about an equilibrium solution in Appendix 1. These linearized attitude equations describe a linear time periodic system. Floquet Theory is applied to determine the stability of this system. A scalar controller is then developed to control two unstable modes of the linearized system. The controller uses two rate variables from the system state vector as feedback inputs. Floquet Theory is then applied to the controlled system to analyze the stability. The system is evaluated in a new controlled modal coordinate system, derived from the Floquet solution. This method decouples the four modes of the system and provides an easy method to determine system stability.

2.1 Floquet Theory

The solution to a system of linear time-periodic equations was developed by Floquet in the late 1800's. Such a system in first order form is given by

$$\bar{x}' = A(\tau)\bar{x} \tag{2.1}$$

where $A(\tau) = A(\tau + T)$. Any set of independent solutions,$\phi(\tau)$ the fundamental matrix, must satisfy the differential equation

$$\phi'(\tau) = A(\tau)\phi(\tau) \tag{2.2}$$

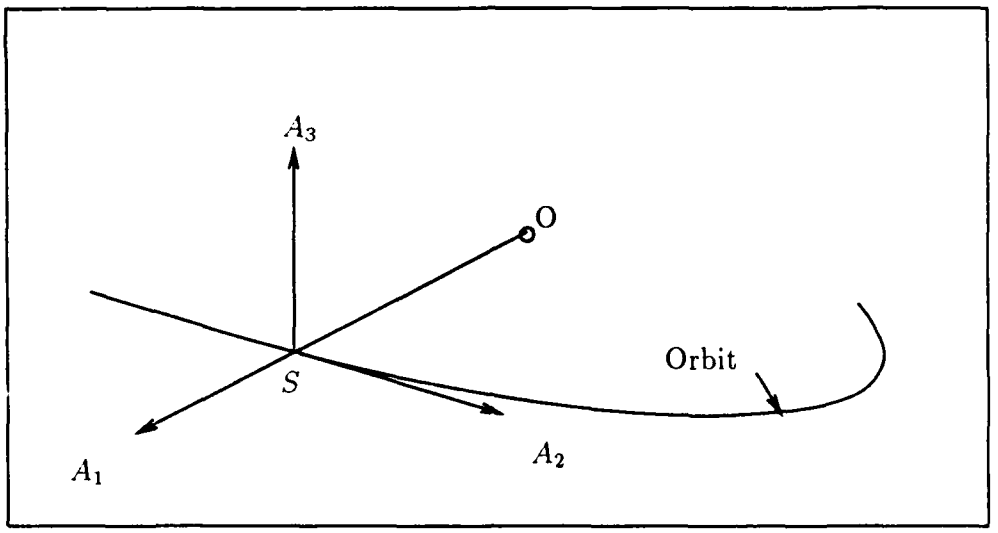

Figure 2.1. Orbit Reference Frame

Floquet found that the fundamental matrix can be expressed as

$$\phi(\tau) = P(\tau)e^{\Gamma\tau} \tag{2.3}$$

where P is a periodic matrix with the period T and Γ is a constant matrix. A more convenient and equivalent form can be developed through a similarity transformation using a constant non-singular matrix B such that Γ is transformed to the Jordan form,

$$\psi(\tau) = B^{-1}\phi(\tau)B = F(\tau)e^{J\tau} \tag{2.4}$$

Then ψ is also a fundamental matrix and $F(\tau)$ is periodic, with a period of T. That is

$$F(\tau) = F(\tau + T) \tag{2.5}$$

and J is the Jordan form of Γ.

Examine equation 2.3 at the end of one period,

$$\phi(\tau + T) = P(\tau + T)e^{\Gamma(\tau+T)} \tag{2.6}$$

since $P(\tau)$ is periodic

$$P(\tau) = P(\tau + T) \tag{2.7}$$

substituting this in to the equation 2.6

$$\phi(\tau + T) = P(\tau)e^{\Gamma\tau}e^{\Gamma T} = \phi(\tau)e^{\Gamma T} \tag{2.8}$$

C, a constant matrix, replaces $e^{\Gamma T}$ and is called the monodromy matrix.

$$\phi(\tau + T) = \phi(\tau)e^{\Gamma T} = \phi(\tau)C \tag{2.9}$$

The monodromy matrix, C, can be found by letting $\tau = 0$

$$\phi(0)^{-1}\phi(T) = C \tag{2.10}$$

If ϕ is the principal fundamental matrix

$$\phi(0) = I \tag{2.11}$$

where I is the identity matrix. C can then be found by numerical integration of equation 2.2 using the initial conditions from equation 2.11. The diagonal elements of J, ρ_i, are the eigenvalues of Γ and are called characteristic exponents. The system stability can be determined from the value of the characteristic exponents. If they have negative real parts, the system is stable. If any have positive real parts, the system is unstable. The J matrix can be determined from the monodromy matrix C. The eigenvalues of C, λ_i (characteristic multipliers), are related to the eigenvalues

of Γ by

$$\rho_i = \frac{1}{T} \ln \lambda_i \tag{2.12}$$

This analysis will allow us to determine the system stability and is a typical application of Floquet Theory. But, to implement a controller based on the solution to the original system [2:671-676] we must solve for the F matrix. To find the differential expression for F, differentiate equation 2.4 with respect to τ.

$$\psi'(\tau) = F'(\tau)e^{J\tau} + F(\tau)Je^{J\tau} \tag{2.13}$$

We note that every fundamental matrix must satisfy the differential equation 2.2.

$$\psi'(\tau) = A(\tau)\psi(\tau) \tag{2.14}$$

Replacing ψ' and ψ in equation 2.14 with the expressions from equations 2.4 and 2.13

$$F'(\tau)e^{J\tau} + F(\tau)Je^{J\tau} = A(\tau)F(\tau)e^{J\tau} \tag{2.15}$$

Dividing both sides by $e^{J\tau}$ and rearranging results in

$$F' = AF - FJ \tag{2.16}$$

To find the initial conditions we write

$$\bar{x}(\tau) = \psi(\tau)\psi(0)^{-1}\bar{x}(0) \tag{2.17}$$

where $\bar{x}(0)$ is the initial state vector and ψ is any fundamental matrix. From Floquet Theory , any fundamental matrix can be expressed in the form of

$$\psi(\tau) = F(\tau)e^{J\tau} \tag{2.18}$$

It has already been shown how to find the J matrix, whose diagonal entries are the eigenvalues of the C matrix. To find an expression for the $F(0)$ matrix, take the inverse of equation 2.18

$$\psi(\tau)^{-1} = e^{-J\tau}F(\tau)^{-1} \tag{2.19}$$

At $\tau = 0$

$$\psi(0)^{-1} = e^{0}F(0)^{-1} = F(0)^{-1} \tag{2.20}$$

Then use this value in equation 2.17

$$\bar{x}(\tau) = F(\tau)e^{J\tau}F(0)^{-1}\bar{x}(0) \tag{2.21}$$

Evaluated at $\tau = T$

$$\bar{x}(T) = F(T)e^{JT}F(0)^{-1}\bar{x}(0) \tag{2.22}$$

Writing equation 2.17 in terms of the principal fundamental matrix

$$\bar{x}(\tau) = \phi(\tau)\phi(0)^{-1}\bar{x}(0) \tag{2.23}$$

Evaluated at $\tau = T$

$$\bar{x}(T) = \phi(T)\phi(0)^{-1}\bar{x}(0) \tag{2.24}$$

From equation 2.10

$$\phi(T)\phi(0)^{-1} = \phi(T)I = \phi(T) = C \tag{2.25}$$

where C is the constant monodromy matrix. Now equate equations 2.22 and 2.24

$$F(T)e^{JT}F(0)^{-1}\bar{x}(0) = C\bar{x}(0) \tag{2.26}$$

performing the necessary linear algebra this becomes

$$F(T)e^{JT} - CF(0) = \bar{0} \tag{2.27}$$

Noting that $F(\tau)$ is periodic, $F(T) = F(0)$, this becomes

$$F(0)e^{JT} - CF(0) = \bar{0} \tag{2.28}$$

Since J is diagonal, this can be written as a set of i equations where i identifies a column in the $F(0)$ matrix.

$$\varrho_i \bar{f}_i(0) - C\bar{f}_i(0) = \bar{0} \tag{2.29}$$

Where ϱ_i is the ith diagonal element of e^{JT} matrix. Or expressed as

$$[\varrho I - C]\,\bar{f}(0) = \bar{0} \tag{2.30}$$

which is an eigenvalue problem. Each column of the $F(0)$ matrix is an eigenvector of the monodromy matrix C. This will provide us with the initial conditions for the F matrix. As previously noted, F is periodic, and if numerically integrated over one period, a set of Fourier series coefficients can be extracted from the data set and used to represent the elements of the F matrix. Each element of F is represented as a Fourier series. Additional information on this technique can be found in reference [6:108-114].

Both F and J matrices may contain complex elements. These can be difficult to work with but equivalent forms can be developed as follows.

- F matrix

  1. If the column vector, $\bar{f}_i$, is real no change is necessary.
  2. If a pair of the column vectors are complex conjugates, separate the real and imaginary components into separate vectors. That is
     $\bar{f}_{real+imag}, \bar{f}_{real-imag} \Rightarrow \bar{f}_{real}, \bar{f}_{imag}$

- J matrix

1. If the eigenvalue, ρ_i, is real no change is necessary.

2. If there are two eigenvalues that form a complex pair, J can be written with the diagonal in the form of blocks

$$\begin{bmatrix} \rho_{real+imag} & 0 \\ 0 & \rho_{real-imag} \end{bmatrix} \Rightarrow \begin{bmatrix} \rho_{real} & \rho_{imag} \\ -\rho_{imag} & \rho_{real} \end{bmatrix}$$

These new equivalent forms of F and J contain only real elements and are much easier to deal with numerically.

2.2 *Control Theory*

This section applies Floquet theory to develop an active control system for a spinning symmetrical satellite in an elliptical orbit. The equations of motion for this system are developed in Appendix 1. Through the use of modal coordinates, a method is demonstrated to stabilize any system that has a two unstable modes. The development of a modal control system for this system differs from a constant coefficient linear system due to the periodic coefficients of the differential equations.

The first step in developing an active control system is to transform the physical coordinates to modal coordinates. The original coordinates, $\bar{x}^T = \left\{\theta_1, \theta_2, \dot{\theta}_1, \dot{\theta}_2\right\}$, are related to the modal coordinates, $\bar{\eta}$, by the F matrix such that

$$\bar{x}(\tau) = F(\tau)\bar{\eta}(\tau) \tag{2.31}$$

Where $F(\tau)$ is the periodic matrix that solves the Floquet problem. Replacing $\bar{x}$ in equation 2.3 yields

$$(F(\tau)\eta(\tau))' = A(\tau)F(\tau)\eta(\tau) \tag{2.32}$$

applying the chain rule to the derivative and reduction yields

$$\eta'(\tau) = F^{-1}(\tau)\left[A(\tau)F(\tau) - F'(\tau)\right]\eta(\tau) \tag{2.33}$$

From equation 2.16, replace F'

$$\eta'(\tau) = F^{-1}(\tau)\left[A(\tau)F(\tau) - A(\tau)F(\tau) + F(\tau)J\right]\eta(\tau) \tag{2.34}$$

This reduces to

$$\eta'(\tau) = J\eta(\tau) \tag{2.35}$$

The eigenvector matrix, $F(\tau)$, transforms the time periodic system to a constant-coefficient system. The new system variables, η, are referred to as modal variables since the transformation in equation 2.31 performs a decoupling similar to a constant-coefficent system.

The controller examined here was developed by Calico and Wiesel [2:673-674]. It is a two mode scalar controller. The system equation with a generalized controller can be written as

$$\bar{x}' = A(\tau)\bar{x} + B\bar{u}(\tau) \tag{2.36}$$

Where the A matrix is from the system description of the uncontrolled system and the B matrix distributes the control in the system. This can also be expressed in the modal variables.

$$\bar{\eta}' = J\bar{\eta} + F^{-1}B\bar{u} \tag{2.37}$$

In general, B has the form

$$B = \begin{bmatrix} 0 & 0 & \cdots & 0 \\ 0 & 0 & \cdots & 0 \\ b_{31} & b_{32} & \cdots & b_{3n} \\ b_{41} & b_{42} & \cdots & b_{4n} \end{bmatrix} \tag{2.38}$$

The number of columns in the B matrix must match the size of the control vector

$\bar{u}$. Each element, b_{ij}, may be time periodic. For the two mode scalar controller

$$B = \begin{bmatrix} 0 \\ 0 \\ 1 \\ 1 \end{bmatrix} \tag{2.39}$$

Which variables are included in the feedback and the gain associated with each variable is determined by the control vector $\bar{u}$. It is defined as

$$\bar{u} = K(\tau)\bar{\eta} \tag{2.40}$$

The general form of the time dependent gain matrix is

$$K(\tau) = \begin{bmatrix} K_{11}(\tau) & K_{12}(\tau) & K_{13}(\tau) & K_{14}(\tau) \\ K_{21}(\tau) & K_{22}(\tau) & K_{23}(\tau) & K_{24}(\tau) \\ \vdots & \vdots & \vdots & \vdots \\ K_{n1}(\tau) & K_{n2}(\tau) & K_{n3}(\tau) & K_{n4}(\tau) \end{bmatrix} \tag{2.41}$$

Again for the two mode scalar controller, a reduced form of the $K(\tau)$ matrix is used

$$K(\tau) = \begin{bmatrix} K_1 & K_2 & 0 & 0 \end{bmatrix} \tag{2.42}$$

where both non-zero elements are periodic functions with a period of T. It is assumed that the first two modes are unstable and need to be controlled. Expanding the control term, $F^{-1}B\bar{u}$, for our two mode scalar controller results in

$$F^{-1}B\bar{u} = \begin{bmatrix} f_{11} & f_{12} & f_{13} & f_{14} \\ f_{21} & f_{22} & f_{23} & f_{24} \\ f_{31} & f_{32} & f_{33} & f_{34} \\ f_{41} & f_{42} & f_{43} & f_{44} \end{bmatrix} \begin{bmatrix} 0 \\ 0 \\ 1 \\ 1 \end{bmatrix} \begin{bmatrix} K_1 & K_2 & 0 & 0 \end{bmatrix} \bar{\eta} \tag{2.43}$$

where f_{ij} is an element of F^{-1}. Applying matrix algebra reduces this equation to

$$F^{-1}B\bar{u} = \begin{bmatrix} f_{13}+f_{14} \\ f_{23}+f_{24} \\ f_{33}+f_{34} \\ f_{43}+f_{44} \end{bmatrix} \begin{bmatrix} K_1 & K_2 & 0 & 0 \end{bmatrix} \bar{\eta} \tag{2.44}$$

and let $R_i = f_{i3} + f_{i4}$ it becomes

$$F^{-1}B\bar{u} = \begin{bmatrix} K_1R_1 & K_2R_1 & 0 & 0 \\ K_1R_2 & K_2R_2 & 0 & 0 \\ K_1R_3 & K_2R_3 & 0 & 0 \\ K_1R_4 & K_2R_4 & 0 & 0 \end{bmatrix} \bar{\eta} \tag{2.45}$$

Substitute this result into equation 2.37 and expand the J matrix

$$\bar{\eta}' = J\bar{\eta} + F^{-1}BK\bar{\eta} = \begin{bmatrix} K_1R_1+\rho_1 & K_2R_1 & 0 & 0 \\ K_1R_2 & K_2R_2+\rho_2 & 0 & 0 \\ K_1R_3 & K_2R_3 & \rho_3 & 0 \\ K_1R_4 & K_2R_4 & 0 & \rho_4 \end{bmatrix} \bar{\eta} \tag{2.46}$$

This is also a Floquet problem and the techniques from Floquet Theory can be applied again to determine the stability of the closed loop system and controller. This Floquet problem can also be expressed in physical coordinates, $\bar{x}$. Substituting into equation 2.36 for $\bar{u}$

$$\bar{x}' = A(\tau)\bar{x} + BK(\tau)\bar{\eta} \tag{2.47}$$

and replacing $\bar{\eta}$

$$\bar{x}' = A(\tau)\bar{x} + BK(\tau)F^{-1}\bar{x} \tag{2.48}$$

This reduces to

$$\bar{x}' = \left[A(\tau) + BK(\tau)F^{-1}\right]\bar{x} \tag{2.49}$$

This is of the same form as equation 2.2. where the new periodic matrix includes the control elements and also has a period of one orbit. The solution set to this Floquet problem will be of the same form and can be expressed as

$$\phi(\tau) = F^*(\tau)e^{J^*\tau} \tag{2.50}$$

where F^* is periodic and bounded, J^* is diagonal and constant. The stability of the controlled linearized system is determined by the diagonal elements of the J^* matrix. If the real part is negative then the system is stable, if positive then the system is unstable. A new set of modal variables for the controlled system can be defined by the transformation

$$\bar{x} = F^*\bar{\eta}^* \tag{2.51}$$

The controller design problem is to find the proper $K(\tau)$ matrix so the Poincar/'e exponents are all negative [2:674] [12:27]. Working with modal variables this problem reduces to two coupled differential equations.

$$\eta_1^{*\prime} = (K_1R_1 + \sigma)\eta_1^* + (K_2R_1 + \omega)\eta_2^* \tag{2.52}$$

$$\eta_2^{*\prime} = (K_1R_2 - \omega)\eta_1^* + (K_2R_2 + \sigma)\eta_2^* \tag{2.53}$$

where ρ_1 and ρ_2 are a complex pair that have been transformed into two real parts σ and ω. There is no known conventional solution method for these two equations. Since the system is periodic, it can be written in the form of a Floquet problem.

$$\bar{\eta}' = X(\tau)\bar{\eta} \tag{2.54}$$

And applying another theorem

$$\lambda_1\lambda_2 = \exp\left\{\int_0^T tr\,[X(s)]\,ds\right\} \tag{2.55}$$

shows a relationship that provides some insight into the correct values for the K matrix. Here λ_i are the characteristic multipliers and $tr[X(s)]$ is the trace of the X matrix. If the constant terms in the Fourier series form of the F matrix are large enough to be of practical use in the feedback, then K_1 and K_2 can be constants. and the trace becomes

$$tr\,[X(s)] = (K_1\alpha_1 + K_2\alpha_2 + 2\sigma) + P(\tau) \tag{2.56}$$

where the α_i are the sum of the respective constant Fourier terms and $P(\tau)$ is the remaining periodic terms. Now

$$\ln(\lambda_1\lambda_2) = \int_0^T [K_1\alpha_1 + K_2\alpha_2 + 2\sigma + P(\tau)]\,d\tau \tag{2.57}$$

Completing the integration over one period yields

$$\ln(\lambda_1\lambda_2) = (K_1\alpha_1 + K_2\alpha_2 + 2\sigma)T \tag{2.58}$$

or

$$\frac{1}{T}\ln(\lambda_1) + \frac{1}{T}\ln(\lambda_2) = K_1\alpha_1 + K_2\alpha_2 + 2\sigma \tag{2.59}$$

Note that $(1/T)\ln\lambda_i = \rho_i$, the characteristic exponent. This results in

$$\rho_1 + \rho_2 = K_1\alpha_1 + K_2\alpha_2 + 2\sigma \tag{2.60}$$

For the characteristic exponents to be negative, the sum must also be negative. Unfortunately the converse is not true. We cannot guarantee both exponents will be negative if the sum is negative, except in the case of a complex pair. This relationship will define a starting region for values of K but cannot always give stable solutions.

In summary, we have examined the stability of the uncontrolled system using Floquet Theory, developed a controller that can control two unstable modes with

the proper selection of the feedback gains, and also looked at the controlled system stability again with Floquet Theory. This stability determination applies only to the linearized system and the controller can only be shown mathematically to be effective controlling the linearized system. What happens when it is applied to the non-linear system? This will require some special analysis techniques.

III. Stability Analysis

This chapter describes the analysis techniques used to examine the linearized and the non-linear system. Some of the tools have been known since the late 1800's but one of the most powerful tools is a recent development, the digital computer. For without digital computer and graphical output devices the other tools are almost unusable. Even in relatively simple problems, like our example with four differential equations, computers and graphical output is essential to compute, manipulate and display the data.

3.1 Classical Methods

In any undergraduate text on control methods for linear systems a few basic methods of determining the stability of a system will be presented. These are quite effective for linear system design and performance evaluation. Two principal methods that apply graphic output are the root locus and Bode plots.

3.1.1 Root Locus The root locus plot describes the path of the roots in the complex plane as some parameter, usually the feedback gain, is varied. This is an effective design tool for linear systems. Identifying the source of instability and the selection of a gain that will stabilize the system is fairly easy for linear systems. With the use of Floquet theory and modal coordinates, this technique can be applied to the example problem by plotting the characteristic exponents on the complex plane as the gain of the feedback circuit is changed.

3.1.2 Bode Plots Bode plots provide a display of the frequency response of a linear system. The gain and phase of the system are plotted versus the input frequency. Complete design and stability can be determined from the two plots. But as with the root locus, it too is limited to linear constant coefficient systems.

Modal coordinates can be applied to linear time periodic systems. Through a modal coordinate transformation the periodic system can be represented as a linear constant coefficient system. This allows all of the linear methods to be applied to a linear time periodic system. Floquet theory provides that type of transformation.

3.2 Non-linear Methods

Several methods have been developed that can be applied to non-linear systems. Often they do not provide detailed design information but they show trends in the behavior and define the regions of stability. These techniques can be applied to linear systems but the specialized linear methods give precise design information.

3.2.1 Phase Space The use of phase space to examine non-linear systems provides a geometric representation of the system motion. Each point of the phase space represents a system state. A time trace in the phase space shows the transformation of the system from one state to another. A typical example of a two dimensional phase space is a pendulum, where the position (θ), and velocity ($\dot{\theta}$), are used as a Cartesian coordinate system, Figure 3.1. This provides a two dimensional space or phase plane to examine the motion. The origin of the axis represents the equilibrium position, the pendulum is stationary. It is surrounded with a series of concentric rings, each representing a stable periodic motion. As one examines the phase plane further from the equilibrium point, the non-linearity of the system becomes apparent. Other equilibrium points are located at values of θ that correspond to a vertical position of the pendulum, these are all unstable. If the pendulum is given enough energy it will swing completely around the pivot point. This motion is represented by the wavy lines outside of the closed orbits.

This is a simple non-linear system with no damping or forcing input. It can easily be shown in only two dimensions, and yet the phase plane shows complex motion. Higher dimensional systems with damping and forcing functions can exhibit

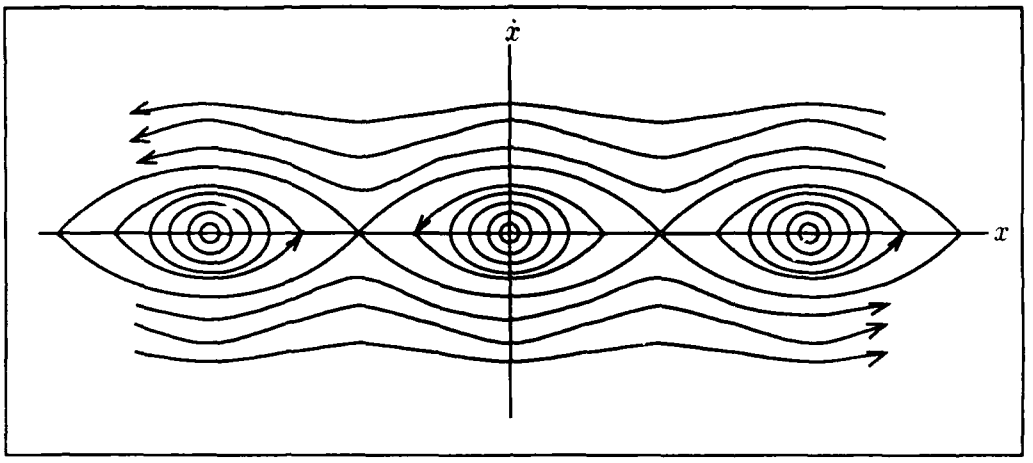

Figure 3.1. Pendulum Phase Space

highly complex motion in their respective phase space.

On the phase plane there several geometric patterns that can be classified according to the behavior of the trajectories in the vicinity, Figure 3.2. These structures represent solutions to a two dimensional system.

- A node is characterized on the phase plane by the intersection of trajectories from the surrounding space. They may be either stable or unstable. If the trajectories move toward the node as time progresses then it is a stable node. If the trajectories move away from the node as time moves forward, the node is considered unstable.
- A center is an equilibrium point surrounded by closed path trajectories.
- An orbit surrounds a center and represents a periodic solution.
- A saddlepoint is an unstable solution that is identified by the intersection of two or more trajectories. The distinguishing characteristic is half of the trajectories approach the solution and the other half of the trajectories move away from the point.

- A spiral is a special type on node. The trajectories do not actually intersect but spiral around the node. Spirals can be stable or unstable.
- A limit cycle is a closed trajectory and represents a periodic solution. It differs from an orbit in that the surrounding trajectories will converge or diverge to the limit cycle orbit. If they converge to the limit cycle it is considered a stable limit cycle. If the trajectories diverge from the orbit, it is unstable.

Stable structures are also known as attractors and the unstable structures are repellers because of the way the phase paths are attracted or repelled from the regions of the structure. All of these structures can appear on the phase plane in various combinations. For a full discussion of these structures see references [10:170-206] and [7:1-54].

A domain of attraction can be defined for each stable structure [15:49]. This is the region of the phase space that trajectories lead to that stable solution. If all trajectories in the phase space lead to a solution then the domain of attraction is the entire phase space and it is considered globally stable.

Stable structures are easily identified by the converging flow of the trajectories in the surrounding phase space. Unstable structures can be identified by examining the flow of trajectories in a negative time period. This is usually accomplished by running the numerical integrator with a negative time step. The unstable nodes, spirals and limit cycles can be easily identified and appear as stable structures in reverse time. The behavior of an orbit or a center will be unchanged and a saddle point will still be unstable and exhibit a complementary structure.

Phase space is a useful tool, especially when the system can be represented with only two variables. Higher dimensional phase space is difficult to model and visualize, however there are other methods that will provide insight into higher dimensional phase space.

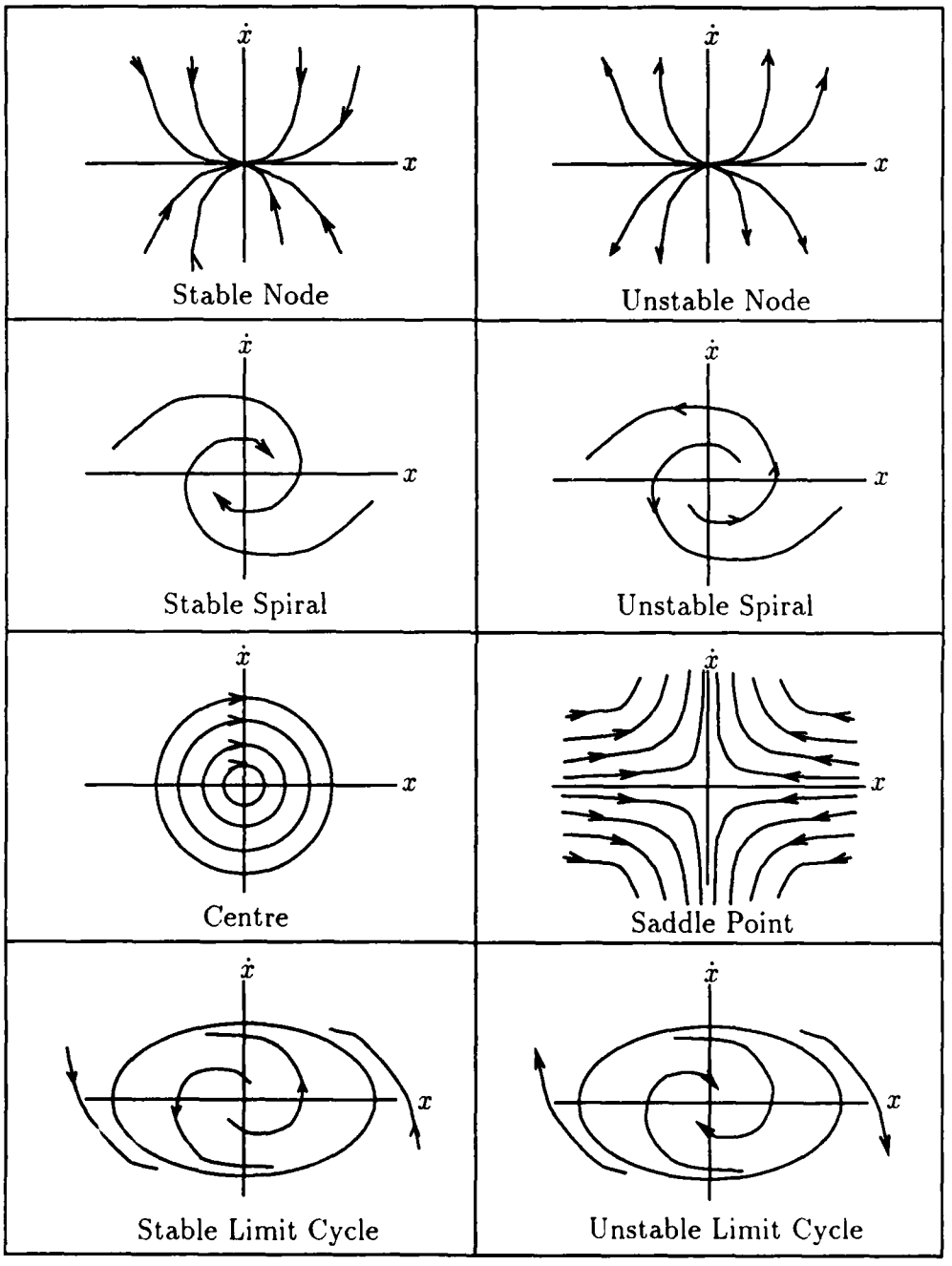

Figure 3.2. Example Phase Plane Structures

3.2.2 Poincaré Maps A Poincaré map, also referred to as a Poincaré section, is constructed by defining a plane in three or higher dimensional phase space. Every time the trajectory passes through the plane, it is mapped as a point on the plane. If many trajectories are mapped in this way, the underlying behavior of the system can be determined. According to Dr. Francis C. Moon, the Poincaré maps can be categorized by the patterns that are generated [11:53]. These structures are observed on a two dimensional plane in the phase space that the trajectories are allowed to puncture as they travel in a three or higher dimensional space.

- A finite number of points indicates a periodic motion or harmonic oscillation.
- Closed curves indicate a quasiperiodic motion or a combination of two periodic motions that are not harmonic.
- A fractal shaped curve is a strange attractor in a higher dimension phase space.
- A fuzzy or dispersed collection of points has several possible causes due to the lack of definition. It could be a system with three or more non-harmonic frequencies, a lightly damped strange attractor or a strange attractor in more that three dimensions. Other tests will have to be used to determine the true nature of the system.

3.2.2.1 Damping Effects A Hamiltonian system is conservative and has no damping. The Poincaré maps for Hamiltonian systems will tend to fill a region on the phase plane. The structure of the attractor will be so disperse that no pattern will be evident. The trend is for damping to reduce the dispersion of the map and if increased sufficiently it will cause a fractal shape to reduce to a single curve [11:63].

3.2.2.2 Torus Mapping A system that has a dominant frequency can be mapped on the surface of a torus. One cycle of the forcing function is mapped as a polar coordinate from the center of the torus. The phase plane of the Poincaré map is perpendicular to the torus and cuts a cross-section, Figure 3.3. The motion

of a periodic system will make lines around the torus, similar to a barber pole. A quasiperiodic system will completely cover the surface of the torus with paths. A chaotic system will have a highly deformed torus with a fractal cross-section on the Poincaré section. This type of map can be used to examine strange attractors and quasiperiodic attractors as they change in relation to the phase of the dominant period. By taking Poincaré maps at several phases in the cycle of the dominant frequency a time picture of the strange attractor can be examined. Just move the cross-section of the Poincaré map around the torus to create new maps.

All of the previous techniques apply to third order systems. For example, the phase space coordinates would be x, $\dot{x}$, and $mod(\omega t, 2\pi)$. Dr. Moon has demonstrated a method referred to as a 'Double Poincaré Map' [11:142]. This method will find strange attractors in higher dimension phase space by taking multiple cuts in to higher dimension torus. He demonstrates the method on a fourth order system and states it can be generalized to higher order systems.

3.2.3 Power Spectrum The power spectrum or Fourier spectrum can be applied to differentiate between a periodic system and a chaotic one. The power spectrum will identify any periodic component of the system as a spike. A quasiperiodic system will have multiple spikes at the basic frequencies involved and mixed harmonics of the basic frequencies. Chaotic systems will have a broad spectrum, the regions between spikes, if any, will be filled [1:314-337].

3.3 Chaos

To quote James Gleick, 'Where Chaos begins, classical science stops.' [5:3]. Until recently, random motion was an area that had to be dealt with stochastically. A continuum of complexity is presented by Heinz Pagels, leading from highly ordered to seemingly random systems. The crystal lattice of a diamond is highly structured and predictable, a rose presents a complex structure with order but not as predictable,

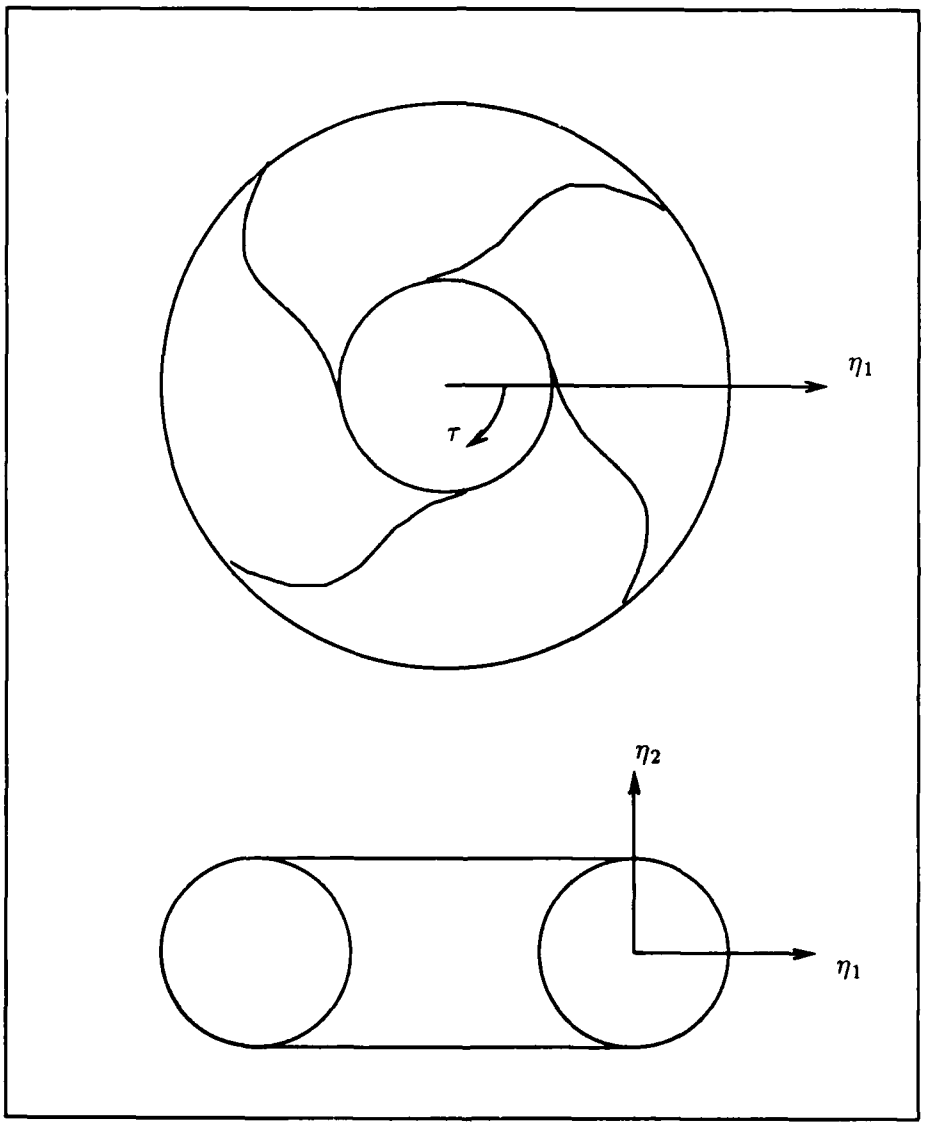

Figure 3.3. Torus for Poincaré Map

the motion of gas molecules in a volume presents a highly complex system will very little order and difficult to predict the future motion.

In these highly random systems one can speak of the average behavior by the use of statistics [13:69-70]. Why should one have to resort to statistics in a deterministic problem? For a dynamic system whose motion is described by a system of ordinary differential equations, given a set of initial conditions, the future motion of the system is prescribed. There is nothing left of chance.

For example, one of the simplest of dynamic systems that is considered a "random event" is the result of a coin toss. The result of the coin toss is determined by it's initial velocity and spin rate. The apparent randomness comes from 'sensitive dependence on initial conditions'. From various readings this is the basic requirement for a chaotic system. Any slight variation in either velocity or spin rate can cause a change in the result of the coin toss.

To create a plot of phase space for the coin, one axis is the velocity and the other the spin rate. Color the regions that result in heads black and in tails white. There will be areas of white and areas of black, but the majority of the phase space will consist of finely intermixed regions. It is this mixed region that causes us to think of the deterministic system as being random. The initial conditions cannot be set precisely enough to be able to predict the result. The small changes in the initial conditions end at a different solutions [13:64-68]. A extreme example of this is found in trying to predict the weather. Referred to as 'The Butterfly Effect', the system is so sensitive to disturbance a butterfly perturbing the air in Peking today causes storms in New York next month [5:20-23].

3.3.1 Strange Attractors Apparently random motion from a deterministic system was studied by Lorenz from a set of three differential equations he was using as a weather model. His discovery of the strange attractor in phase space lead to new understanding of deterministic chaotic systems. This started a revolution in the

analysis of non-linear systems.

An attractor is a region in phase space that is occupied by a steady state trajectory. The simplest attractor is a node, with dimension of 0. The limit cycle is an attractor with a dimension of 1. A quasiperiodic torus is also an attractor and has a dimension of 2. A strange attractor is a region or surface in the phase space into which the steady state solution resides and has a non-integer dimension. The basin of attraction fills the region around an attractor. Any starting point in the basin of attraction will result in a steady state solution to that attractor.

A strange attractor will confine the solution to a bounded region of the phase space. The trajectory will move through this region on a continuous path that never intersects. Any two trajectories, arbitrarily close, in this region will diverge rapidly over time. The other attractors do not exhibit this property, in their basins of attraction two trajectories, arbitrarily close, will remain close. When viewed on a Poincaré section a strange attractor will have a fractal shape [4:200].

3.3.2 Transitions to Chaos As mentioned earlier, there is a continuum that exits from the simple to the complex. In this realm of non-linear dynamics, there are paths that a system can take in transitioning from a simple stable system into a chaotic one. Many dynamic systems exhibit period doubling or bifurcations as the control parameter is varied. This is required in one-dimensional systems but cannot be generalized as a requirement for higher order systems but is sometimes observed [15:126-128]. Higher order systems have been observed to have homoclinic orbits. Homoclinic orbits have the property that from an initial circular starting region, as the system moves in time the initial region is mapped into a horseshoe shape. As time continues the mapping will be repeated. This results in a finely dispersed map with a fractal pattern [11:161].

IV. Results

In this chapter, some of the previous work on the example problem is examined and several of the techniques discussed in chapter 3 are applied to reveal new stability information. The software used to run the simulations was written in Fortran77 and Microsoft Fortran 4.1 used the IMSL math libraries. All calculations were performed using double precision routines. Some of the code was developed by Captain Gregory Myers and then expanded by Captain Dale Shell to include the non-linear equations of motion. I have added the code to handle real as well as complex roots, deal with the period doubling of the system and perform the controlled modal coordinate transformation. The simulations of the linearized system were run on an Zenith 248 microcomputer under MSDOS operating system. The non-linear runs were executed on an Elxsi 6400 superminicomputer under the EMBOS operating system.

4.1 Uncontrolled System

The uncontrolled system is classified as a Hamiltonian system. There is a conservation of energy in the system. It's behavior was examined by both Myers and Shell in both physical and modal coordinates.

4.1.1 Physical Coordinates Myers found that the linearized equations of motion when examined in physical coordinates exhibited some instability. This was determined by examining the parameter ϕ, the angle between the satellite spin axis and the A_3 coordinate axis. Over a period of six orbits the size of ϕ grew from the perturbed value to a larger average value as shown on figure 4.1.

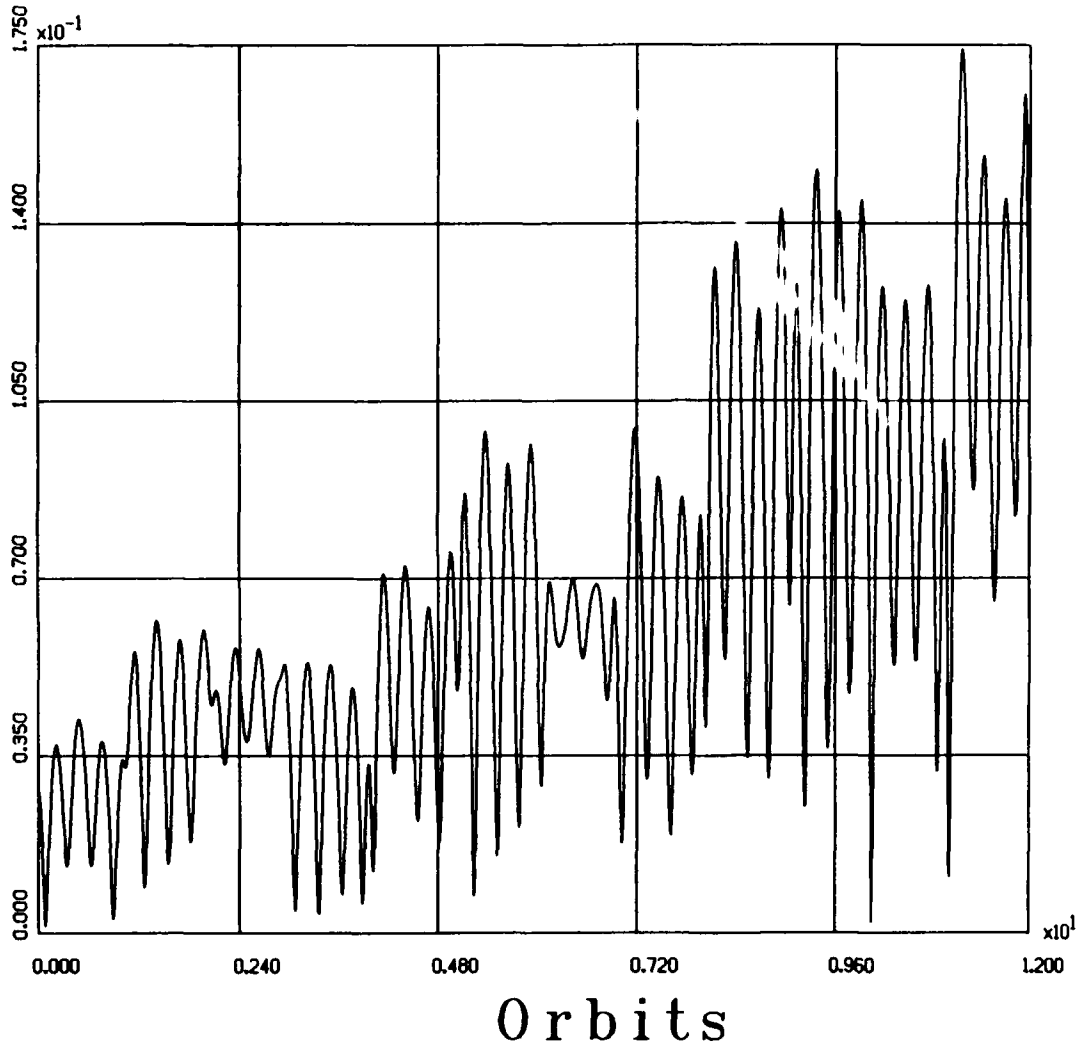

Figure 4.1 Uncontrolled Linearized ϕ Response for 12 orbits

4.1.2 Modal Coordinates When Myers plotted this data in the modal coordinates defined by the Floquet solution as

$$\bar{\eta} = F^{-1}(\tau)\bar{x} \tag{4.1}$$

Over the first six periods, modes one and two appear to be unstable and modes three and four are stable. See figures 4.2, 4.3, 4.4 and 4.5. Shell extended this work by examining the non-linear equations of motion in the same coordinate system and extending the integration of the equations to twelve orbits. Still it appears that the uncontrolled system has two unstable modes and two stable. He did note the irregular motion of the stable modes as they approached the center and did correctly identify it as coupling of the non-linear terms with the other two modes. See figures 4.6 and 4.7.

If he had continued the integration a little further in time, a undiscovered feature of the system would have presented itself. Figures 4.8 and 4.9 show the uncontrolled system for 40 orbits. This is more than sufficient time to observe full motion of the system. With the modes lightly coupled there is an energy exchange that occurs between the modes. Remember this is a conservative system. If one set of modes is declared stable and the other two unstable, the energy from the stable set is being transferred to the unstable set. As the η_1 and η_2 modes spiral out, the η_3 and η_4 modes spiral inward to the center. The non-linear terms are apparent in the η_3 and η_4 modes first. When the non-linear terms become dominant, it causes a reversal in the energy exchange. η_1 and η_2 make a very irregular path back to a low energy state while η_3 and η_4 move along an irregular path to a high energy state. This energy exchange continues through all time and never runs down or becomes more unstable as long as there are no other external influences.

4.1.3 Poincaré Map As stated in Chapter 3, a Poincaré map of a conservative system will cover a region of phase space with a disperse scatter of points. See

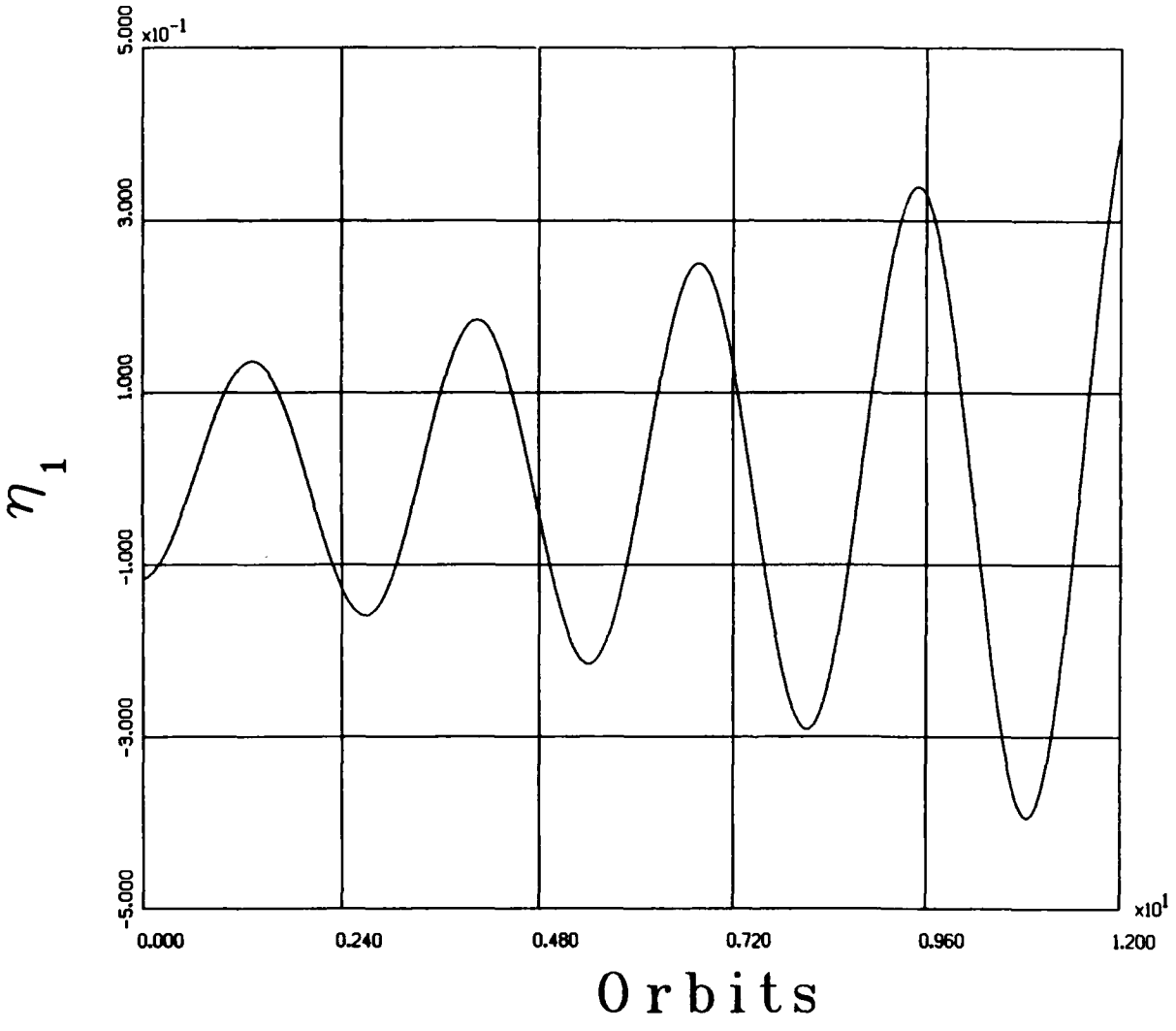

Figure 4.2 Uncontrolled Linearized η_1 Response for 12 orbits

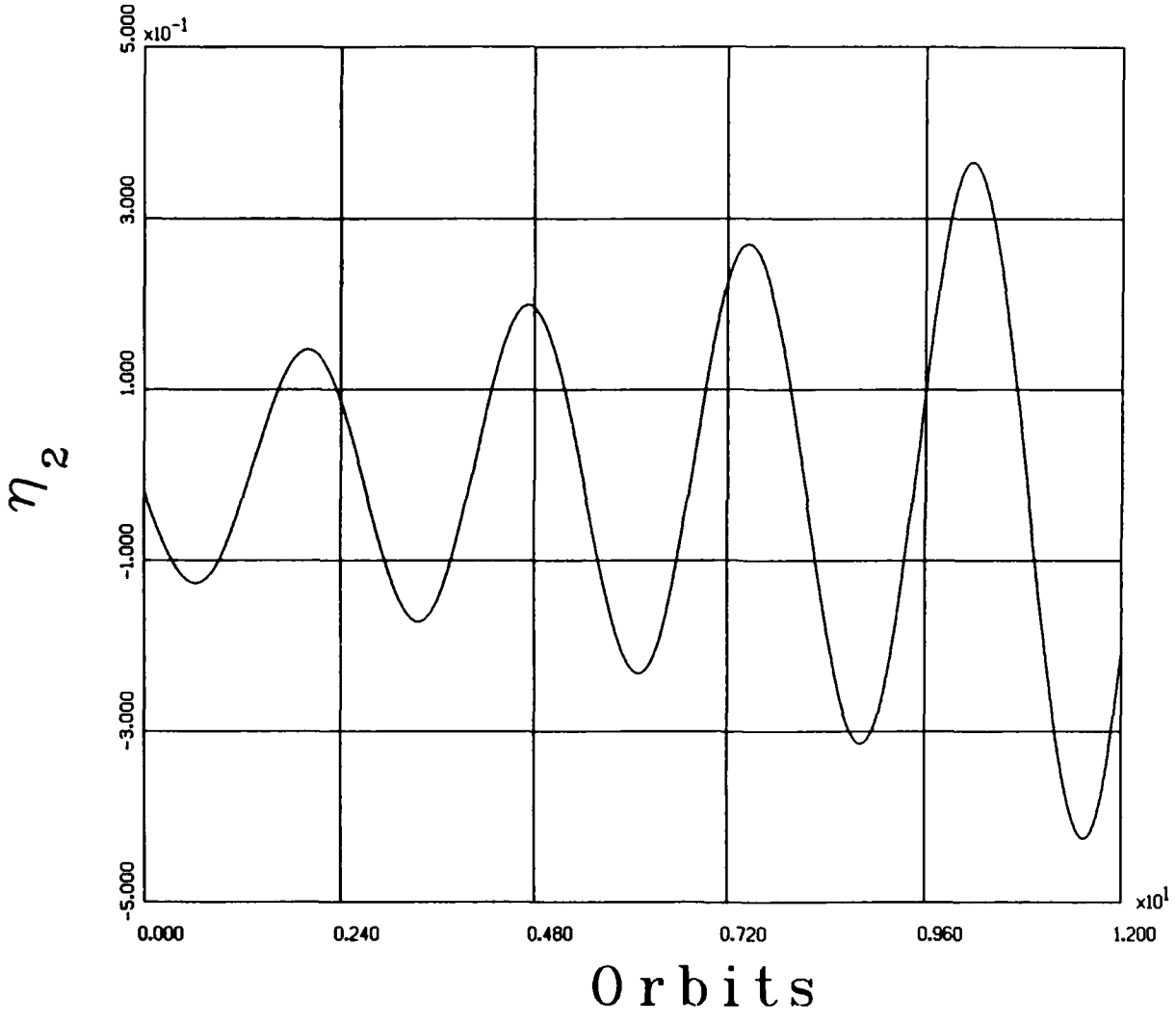

Figure 4.3 Uncontrolled Linearized η_2 Response for 12 orbits

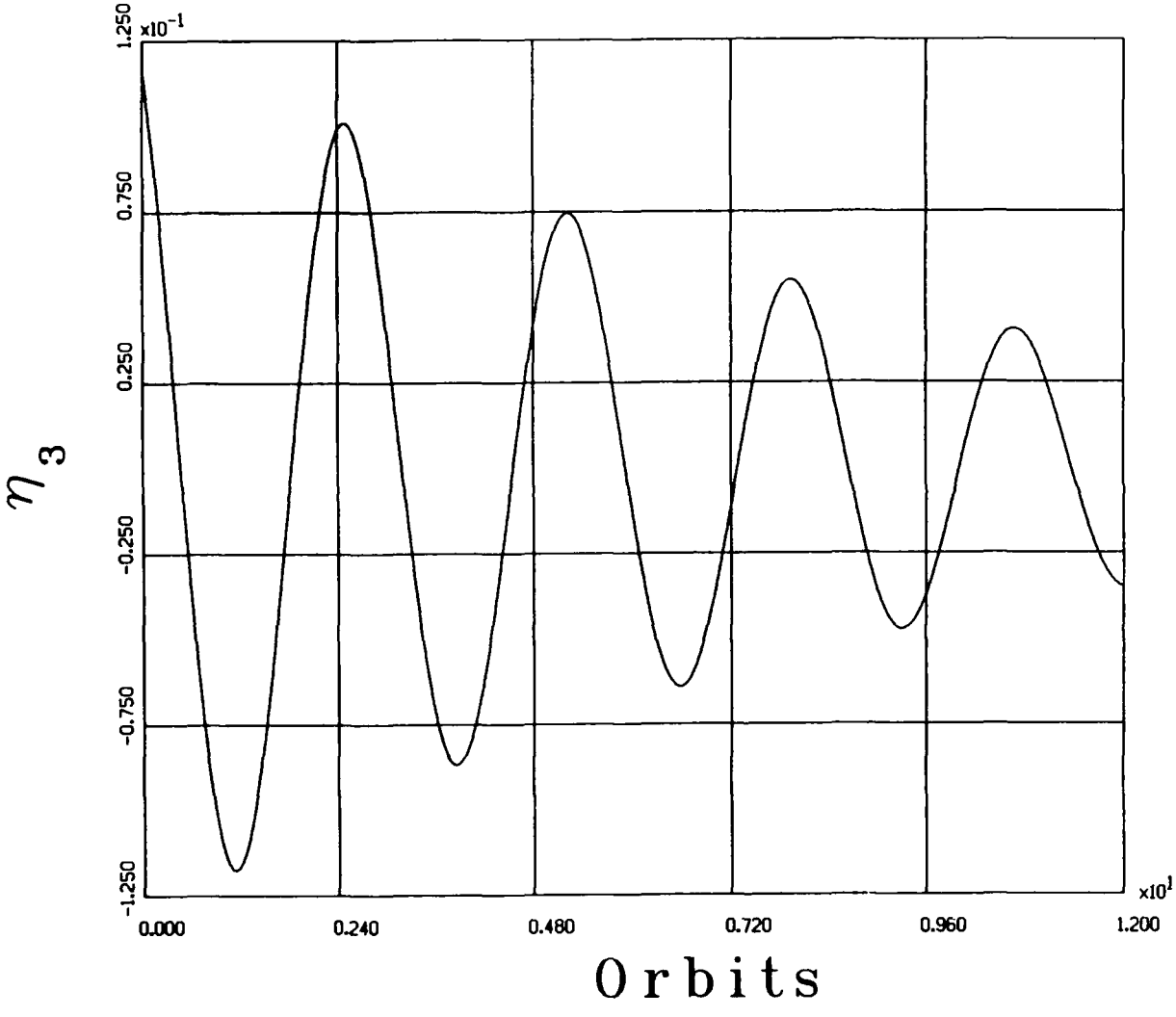

Figure 4.4 Uncontrolled Linearized η_3 Response for 12 orbits

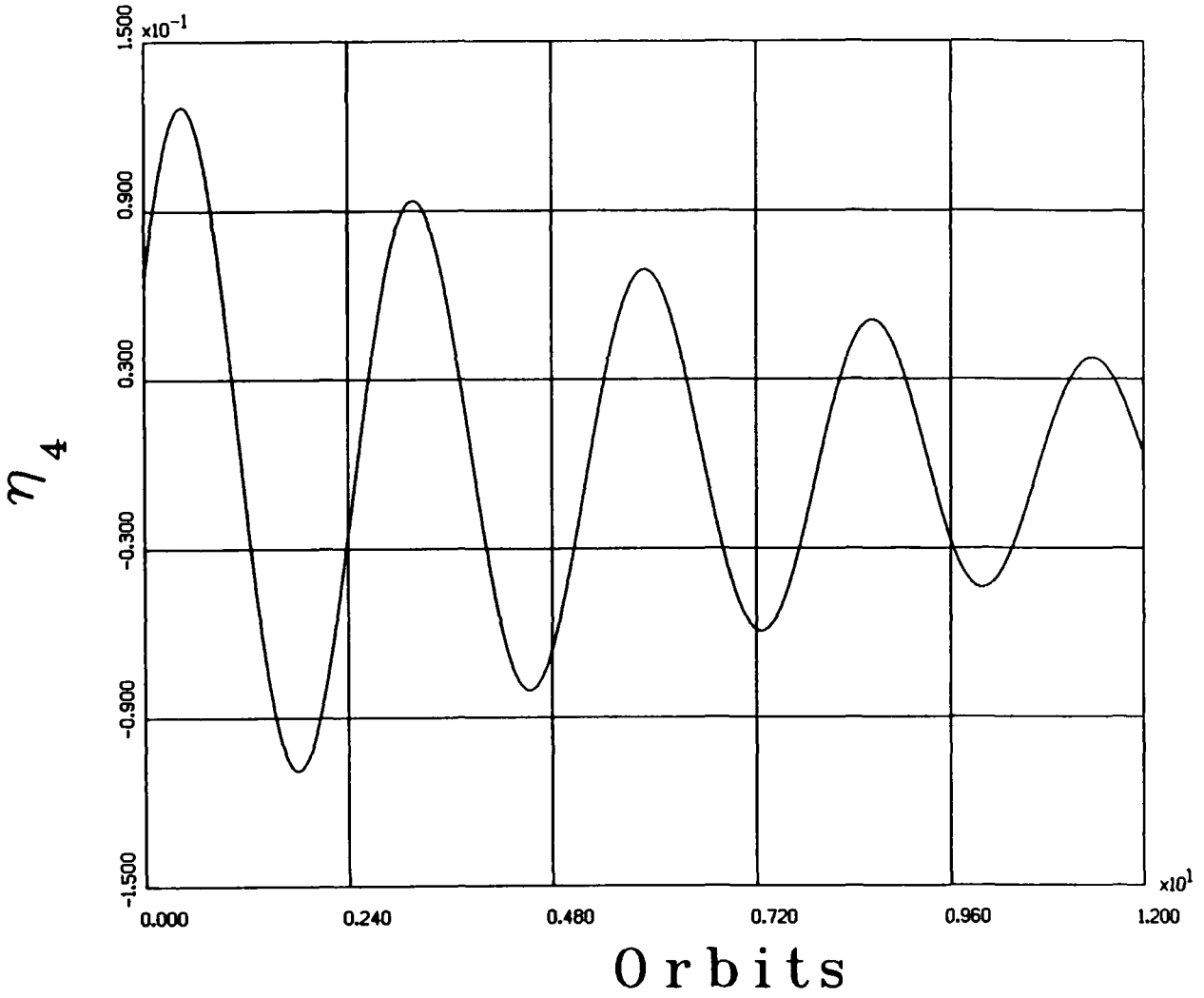

Figure 4.5 Uncontrolled Linearized η_1 Response for 12 orbits

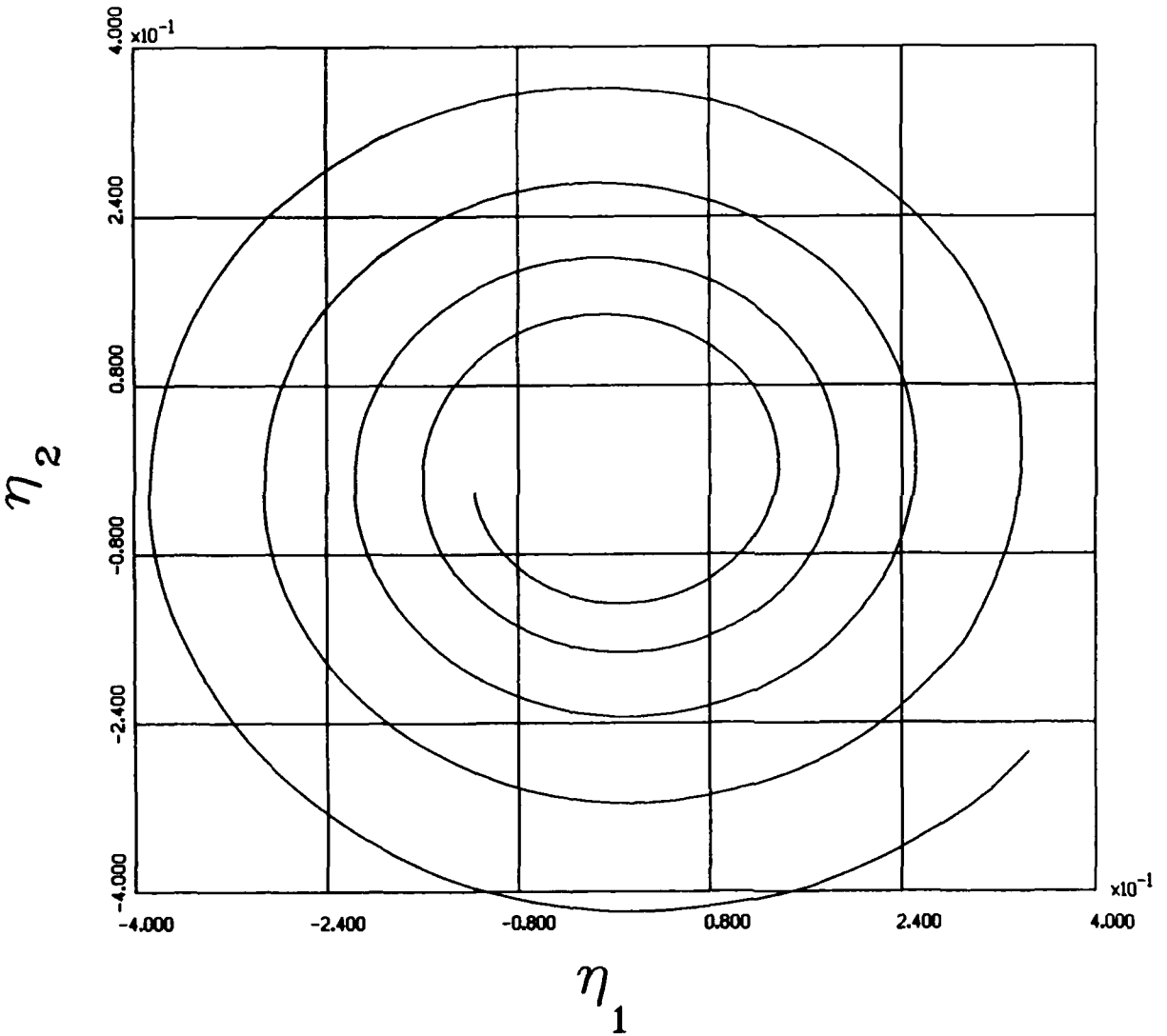

Figure 4.6 Uncontrolled Non-linear η_1 vs η_2 Phase Space for 12 orbits

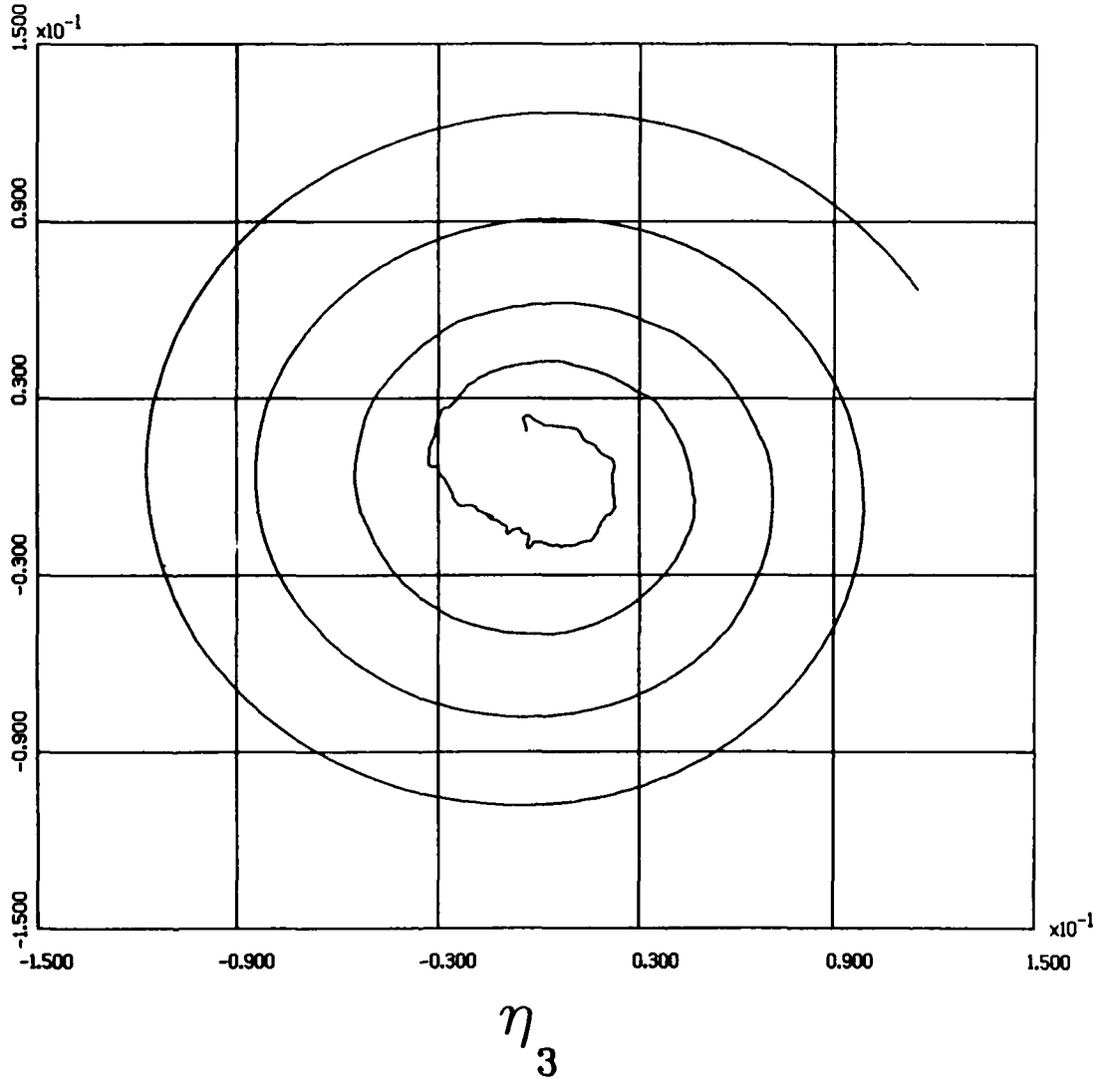

Figure 4.7 Uncontrolled Non-linear η_3 vs η_4 Phase Space for 12 Orbits

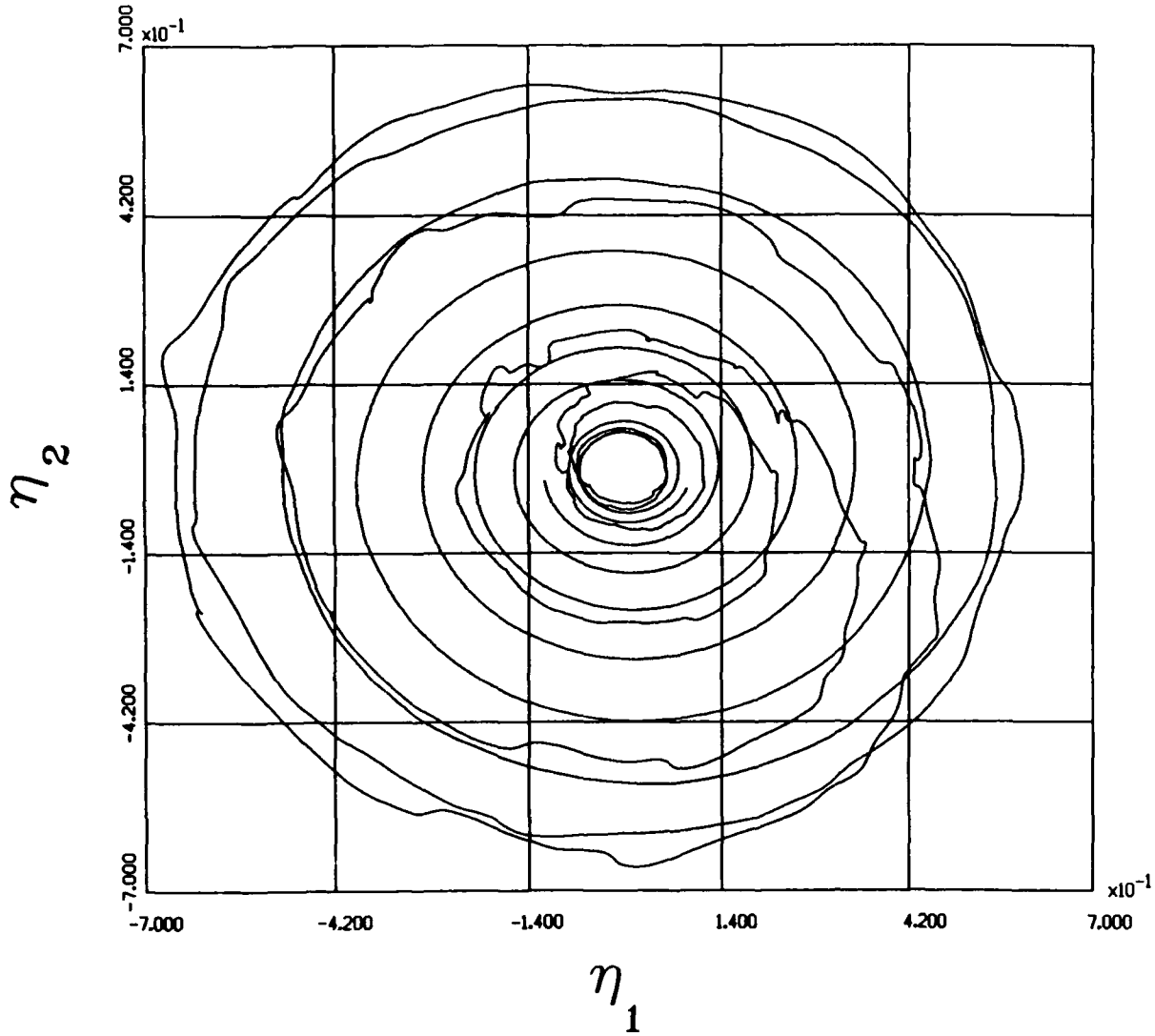

Figure 4.8 Uncontrolled Non-linear η_1 vs η_2 for 40 orbits

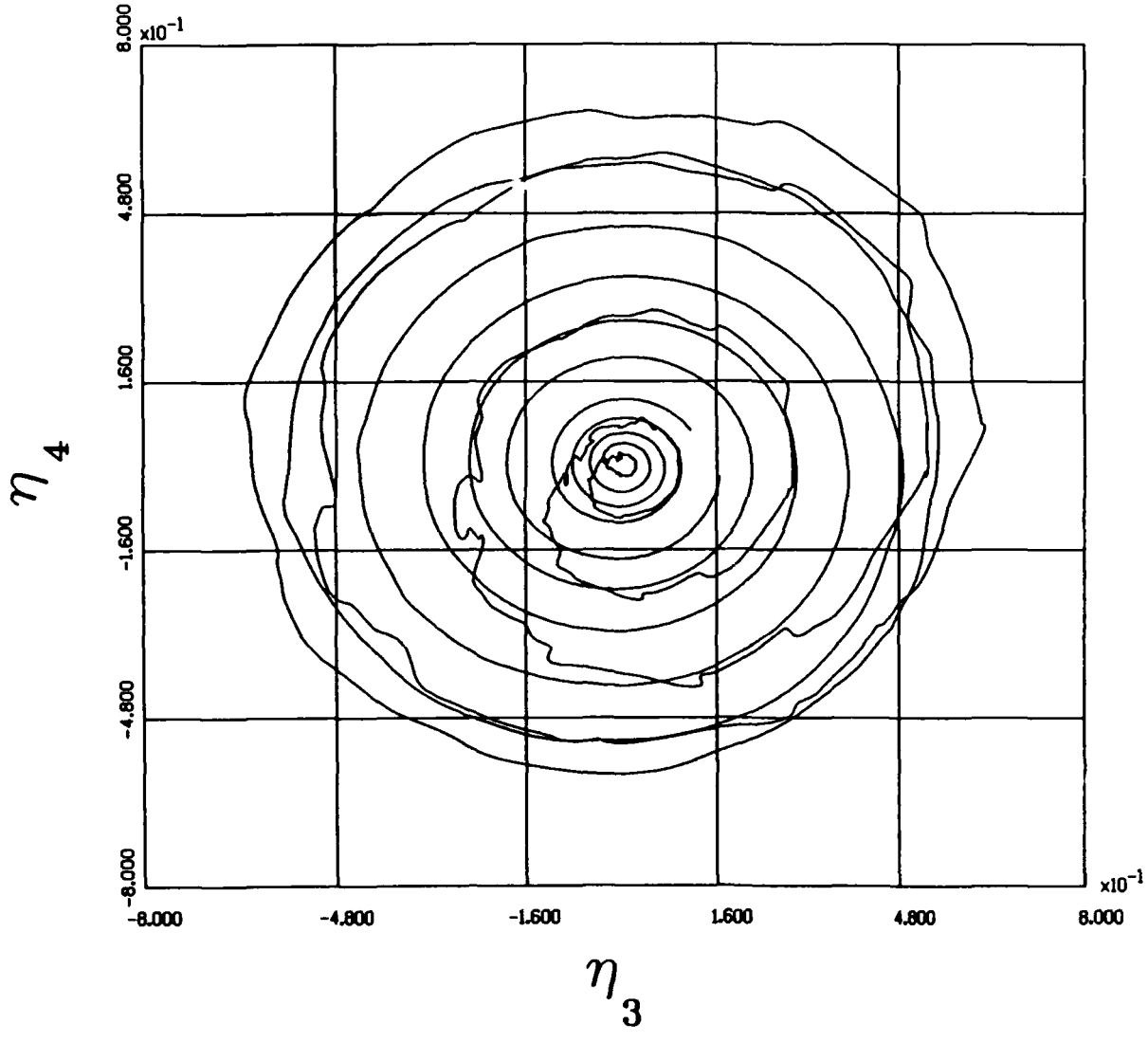

Figure 4.9 Uncontrolled Non-linear η_3 vs η_4 for 40 orbits

figures 4.10 and 4.11. This a new technique in the use of Poincaré maps, the four dimensional system is broken into two, two dimensional maps. This is possible due to the modes being independent and spanning the space completely. These two maps give little further information than confirming what was already know of the non-linear system.

4.2 Controlled System

A control system added to the satellite is supposed to damp out the perturbations and return the system to the preferred equilibrium position. Examining the controlled system, we have two goals

- determine how effective the control system is or how large of a perturbation will it correct
- determine the proper setting of the controller gain and examine how it influences the performance of the controller

4.2.1 Physical Coordinates Myers examined the linearized system in his thesis and was able to determine a method for selecting a gain level for a stable system and projected that a "most stable" solution would be found at the point where the complex roots intersect with the real axis. He also successfully selected gain levels that stabilized the linearized system and plotted the system response in physical coordinates [12:56]. The use of physical coordinates shows little detail of the system behavior other that an general trend of the decrease in magnitude of the perturbed motion.

4.2.2 Root Locus Myers also sketched a root locus plot of the control systems he examined but he never actually computed the necessary data to make an exact plot. There is a hidden difficulty in this system, the phenomena know as period doubling occurs in this periodic system. This can be resolved without too much

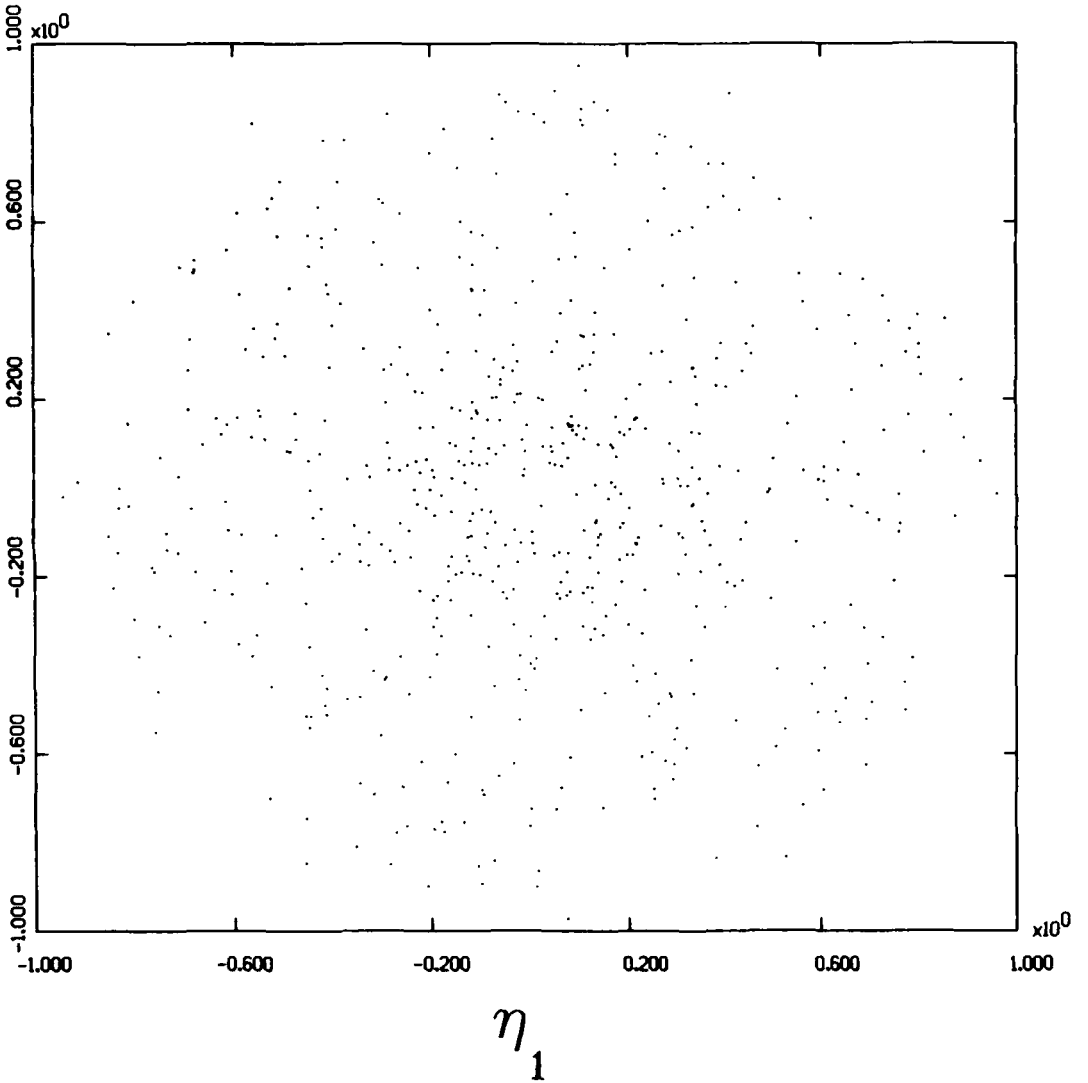

Figure 4.10 Uncontrolled Non-linear η_1 vs η_2 2 Pi Poincare Map for 600 orbits

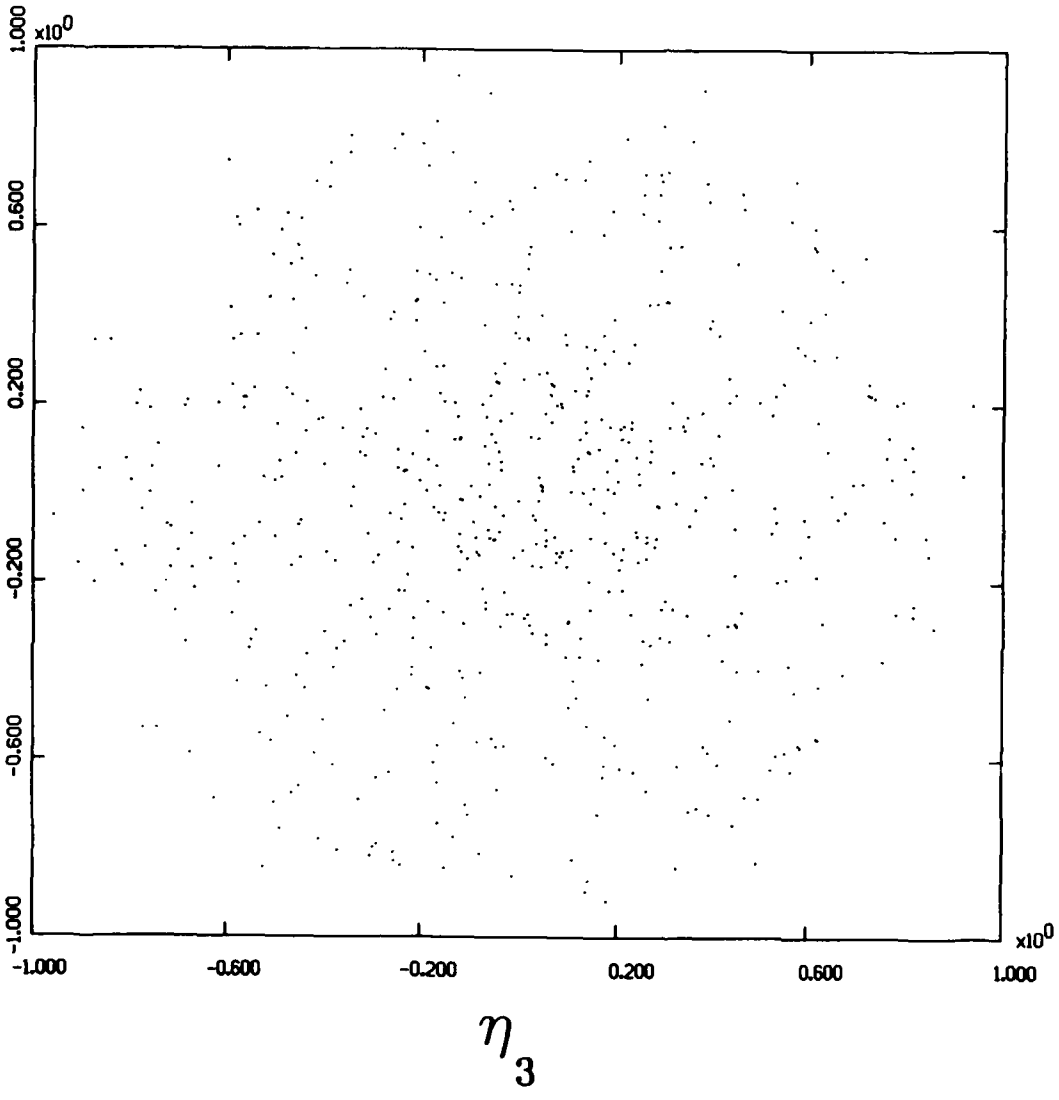

Figure 4.11 Uncontrolled Non-linear η_3 vs η_4 2 Pi Poincare Map for 600 orbits

difficulty if it is noted that any system that has a period of 2π can be treated as if it had a period of 4π. Figure 4.12 is a plot of the Poincaré exponents as a function of gain for the linearized system. The transition from a 2π period to 4π occurs at the intersection of the real axis. I should point out that there is one false point on the plot at the intersection of the real axis. I had to 'create' this one to make the plotting package cause an intersection of the two complex roots with the axis.

A close examination shows that with a gain setting of zero, there are two stable roots and two unstable roots, as the gain is increased on the controller the two unstable roots cross the imaginary axis. When the gain is about 0.2 the roots intersect at the real axis, at 0.4 there are two distinct real roots.

This does provide some detailed information about the linearized system. Classical control techniques can be used to optimize the system for the desired performance based on this kind of plot. This will help us select the gain required for our controller but it falls short in predicting controller performance in the non-linear system. As long as the system is restricted to the region around the equilibrium point, it can be expected to perform in a near linear manner.

4.2.3 Modal Coordinates Shell, in his examination, used the modal coordinates and phase planes to examine the system response. He examined the linearized and the non-linear equations of motion in the modal phase plane. He limited his examination to a fixed gain level and just varied the perturbation to the system to determine its response. His use of the modal coordinates for the uncontrolled system, defined by

$$\bar{\eta} = F^{-1}(\tau)\bar{x} \tag{4.2}$$

was not effective in decoupling the modes of the controlled system. This requires the use of a controlled modal coordinate system defined as

$$\bar{\eta}^* = F^{*-1}(\tau)\bar{x} \tag{4.3}$$

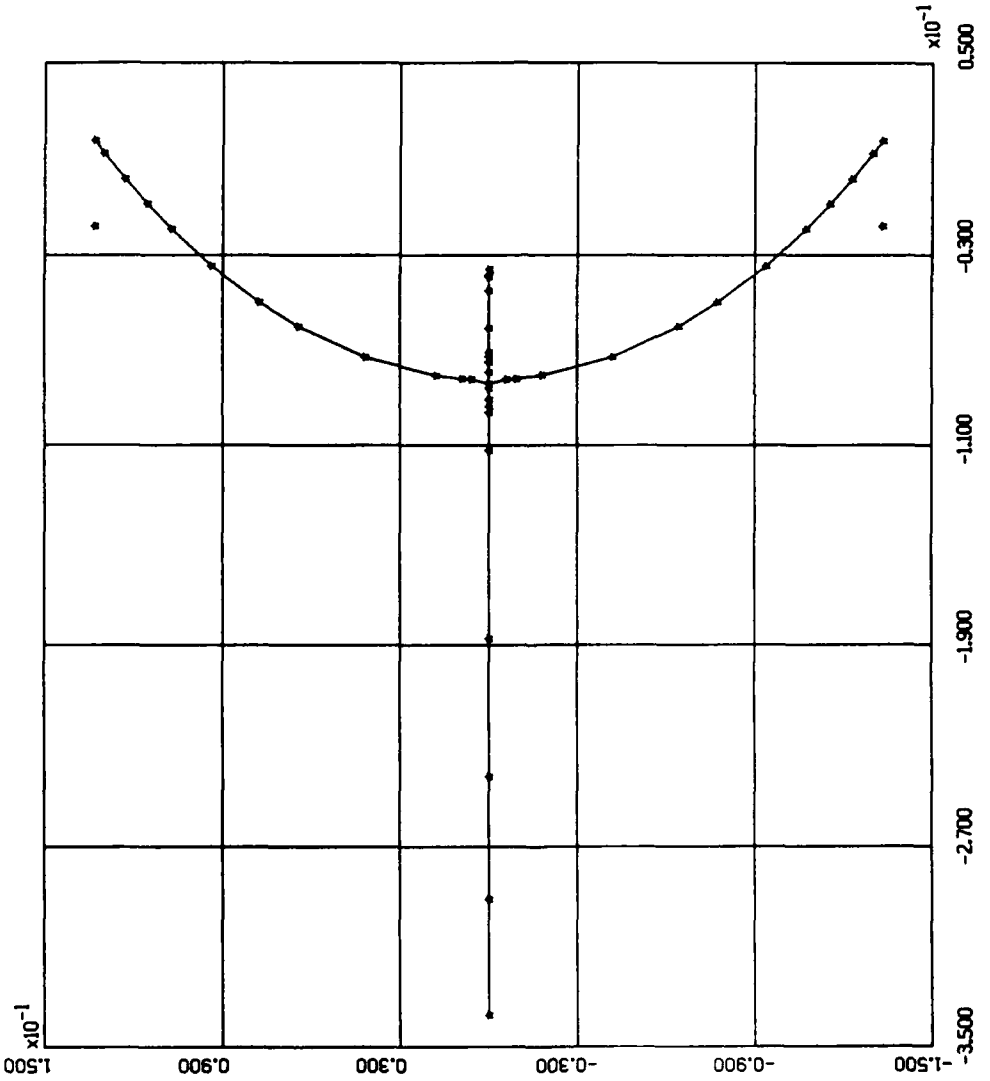

Figure 4.12 Root Locus of Linearized System

Table 4.1. Starting values for linearized system

	η_1	η_2	η_3	η_4
A	0.5	0.0	0.0	0.0
B	1.0	0.0	0.0	0.0
C	1.5	0.0	0.0	0.0
D	2.0	0.0	0.0	0.0
E	3.0	0.0	0.0	0.0
F	4.0	0.0	0.0	0.0
G	5.0	0.0	0.0	0.0
H	6.0	0.0	0.0	0.0
I	7.0	0.0	0.0	0.0

that can be derived from the solution to the Floquet problem presented by the controlled system, equation 2.49. This will define a system of independent coordinates that span the phase space and decouple the modes of the linearized controlled system. It should also be noted that it is invertible and there is a one to one correspondence between the physical coordinates, $\bar{x}$, and the modal coordinates, $\bar{\eta}^*$.

If the gain is set at 0.4, as Shell did in his analysis, the system performance can be examined in the phase space of the controlled modal coordinates. First the linearized system is examined using the starting values in Table 4.1. The phase plane traces are shown in Figures 4.13 and 4.14. These figures present several interesting features of the linearized system. The controller works over the entire phase space in a predictable manner. All four modes are stable and in a linear system the designer could proceed to optimize the gain for the desired performance features. Also note that the equilibrium point is transformed from $\bar{x} = [0,0,0,0]^T$ to $\bar{\eta} = [0,0,0,0]^T$. This is not true for other points in the two spaces.

This gives very little additional information than the root locus. It was already known the linearized system would be stable for this value of the gain and the phase portraits of the system support that fact. Let us now turn to the non-linear equations of motion and examine them in the phase space. To start, select a perturbation point

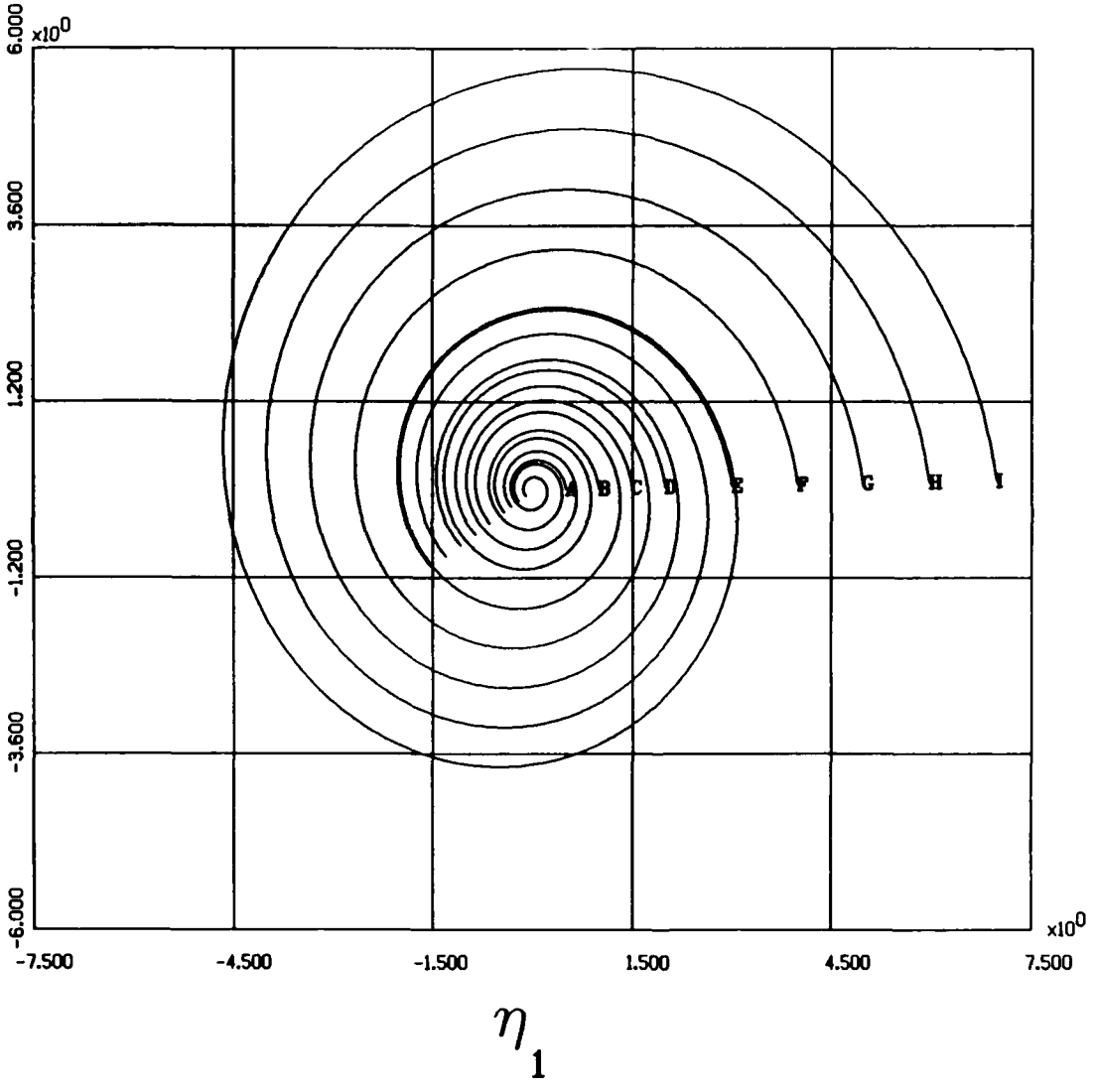

Figure 4.13 Linearized η_1 vs η_2 for 12 orbits

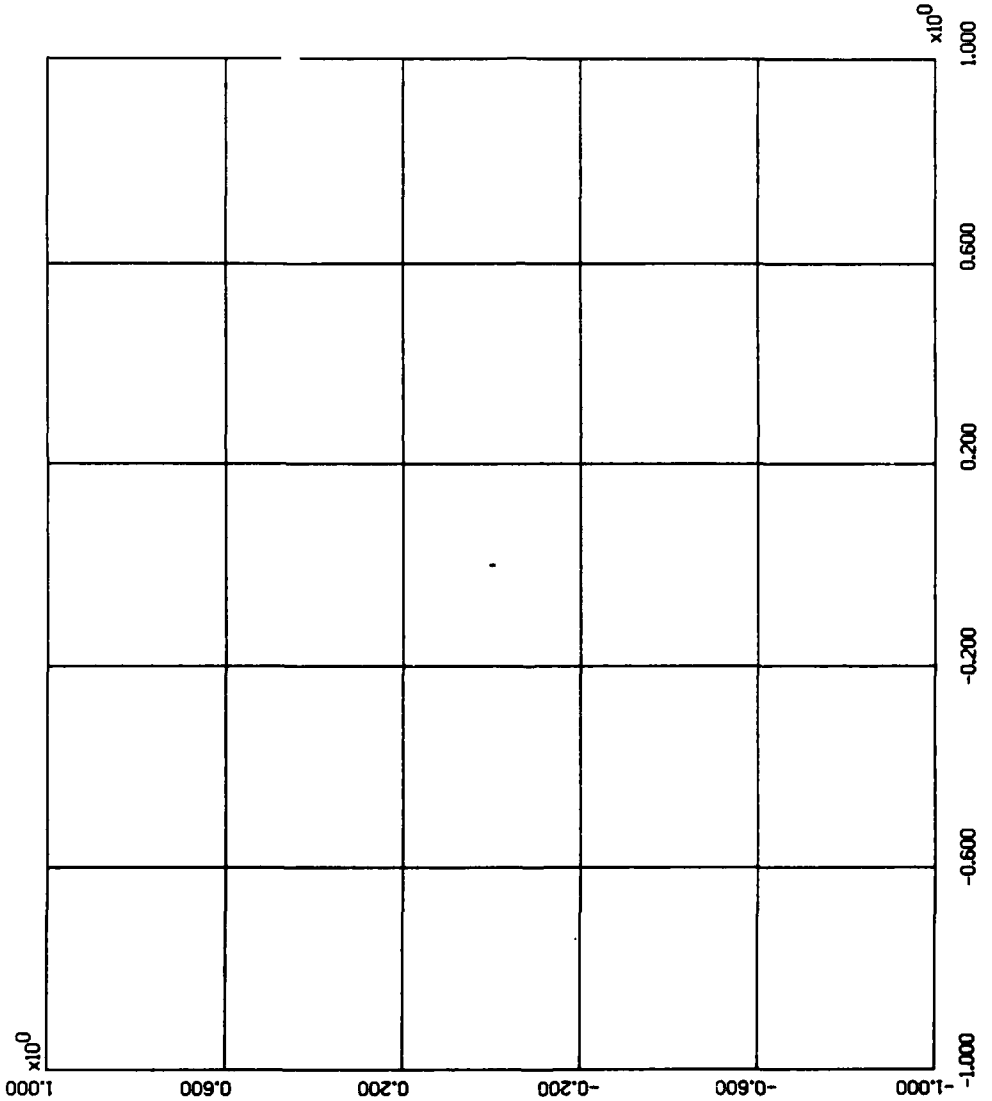

Figure 4.14 Linearized η_3 vs η_4 for 12 orbits

Table 4.2. Starting values for θ quadrants

	θ_1	θ_2	$\dot{\theta}_1$	$\dot{\theta}_2$
A	0.15	0.15	0.0	0.0
B	−0.15	0.15	0.0	0.0
C	0.15	−0.15	0.0	0.0
D	−0.15	−0.15	0.0	0.0

Table 4.3. Starting values for η_1 axis

	η_1	η_2	η_3	η_4
A	0.5	0.0	0.0	0.0
B	0.6	0.0	0.0	0.0
C	0.7	0.0	0.0	0.0
D	0.8	0.0	0.0	0.0
E	0.9	0.0	0.0	0.0
F	1.0	0.0	0.0	0.0
G	1.1	0.0	0.0	0.0
H	1.2	0.0	0.0	0.0

in each quadrant of θ_1 and θ_2 in the physical phase space. The starting values are presented in Table 4.2 and the phase portraits are on Figures 4.15 and 4.16. These paint a different picture from the linearized system. As expected, in the region of the equilibrium point the system shows behavior almost identical to the linearized system, but in the regions further out it is clearly non-linear and does not immediately show any signs of being stable and may even be chaotic.

Exploring the phase space at several points along the η_1 axis, at about $\bar{\eta} = [1, 0, 0, 0]^T$ the traces no longer appear to converge to the equilibrium point, Table 4.3 and Figures 4.17 and 4.18. A similar adventure along the η_2 axis shows a similar state is reached at about $\bar{\eta} = [0, 1, 0, 0]^T$, Table 4.4 and Figures 4.19 and 4.20.

The operational limits of the controller are slowly being outlined but this is not the final answer, a period of 12 orbits is not sufficient to determine the final trajectory

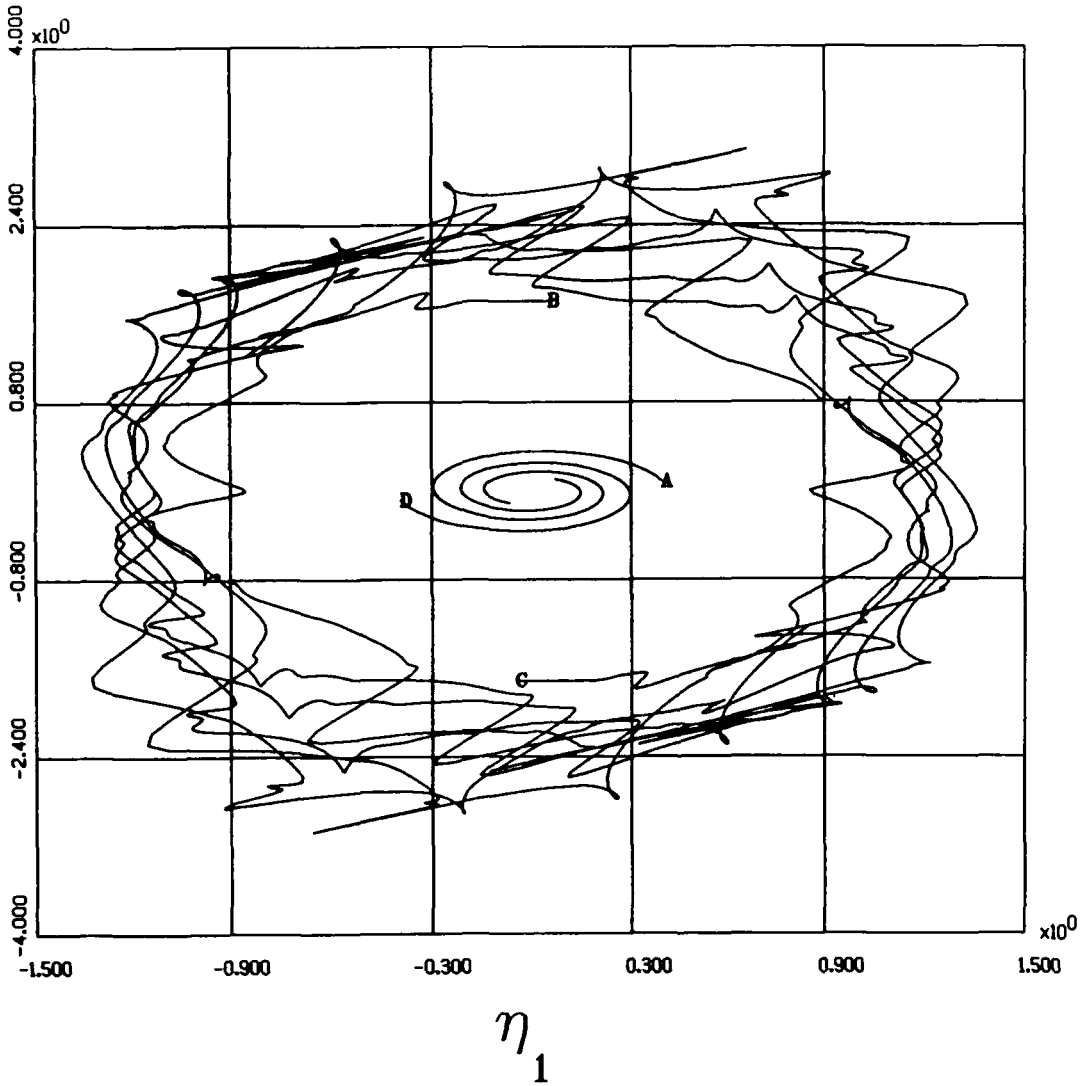

Figure 4.15 Non-linear η_1 vs η_2 for 12 orbits

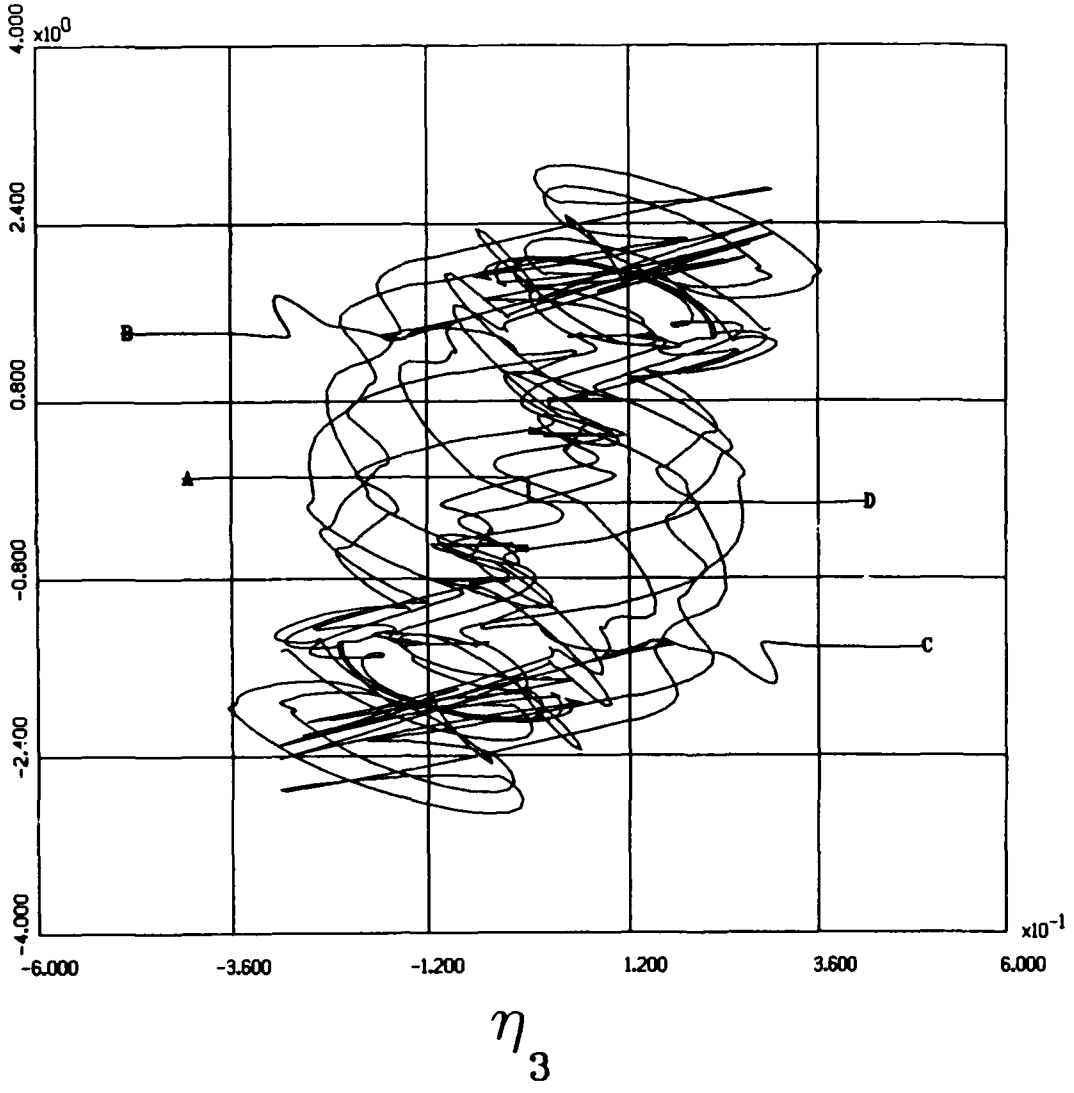

Figure 4.16 Non-linear η_3 vs η_4 12 orbits

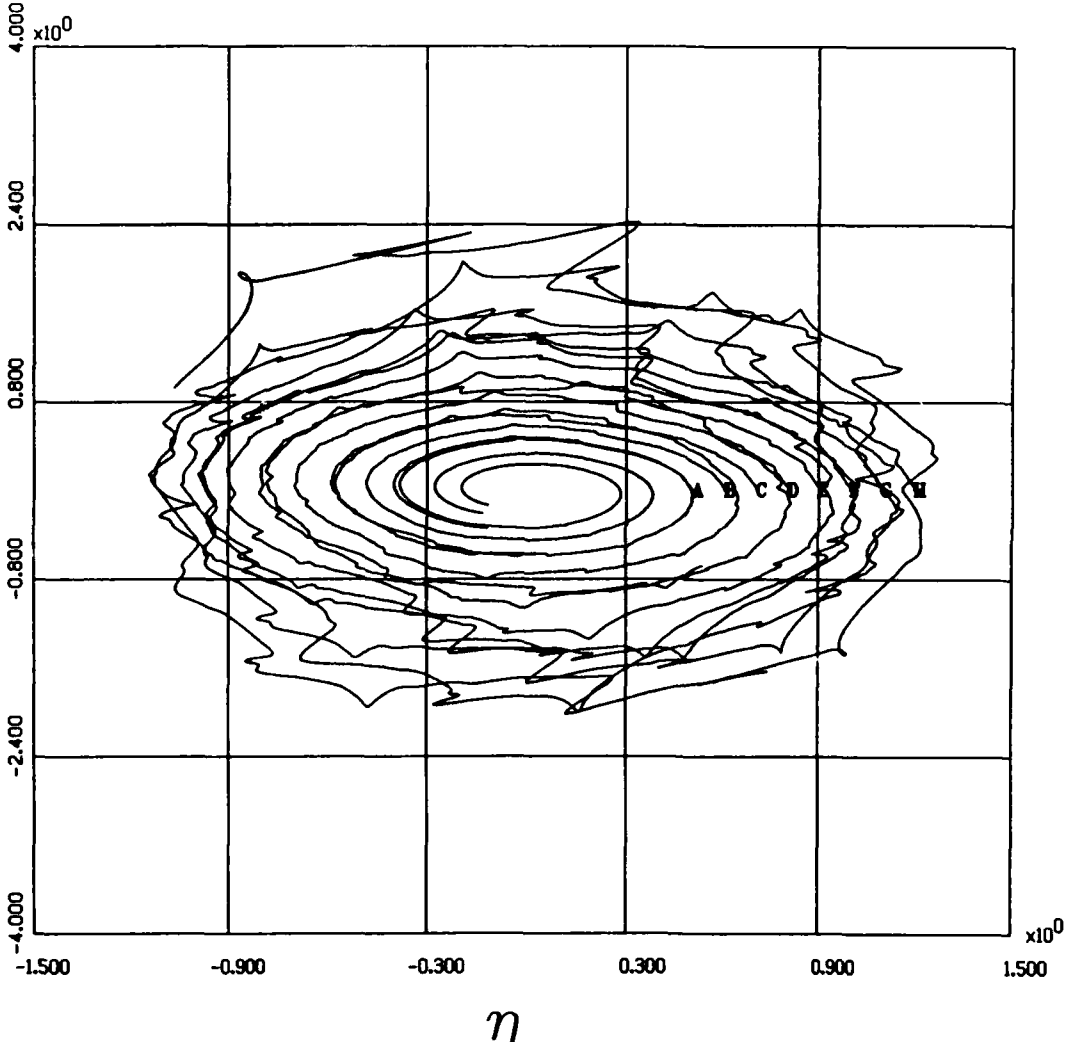

Figure 4.17 Non-linear η_1 vs η_2 for 12 orbits

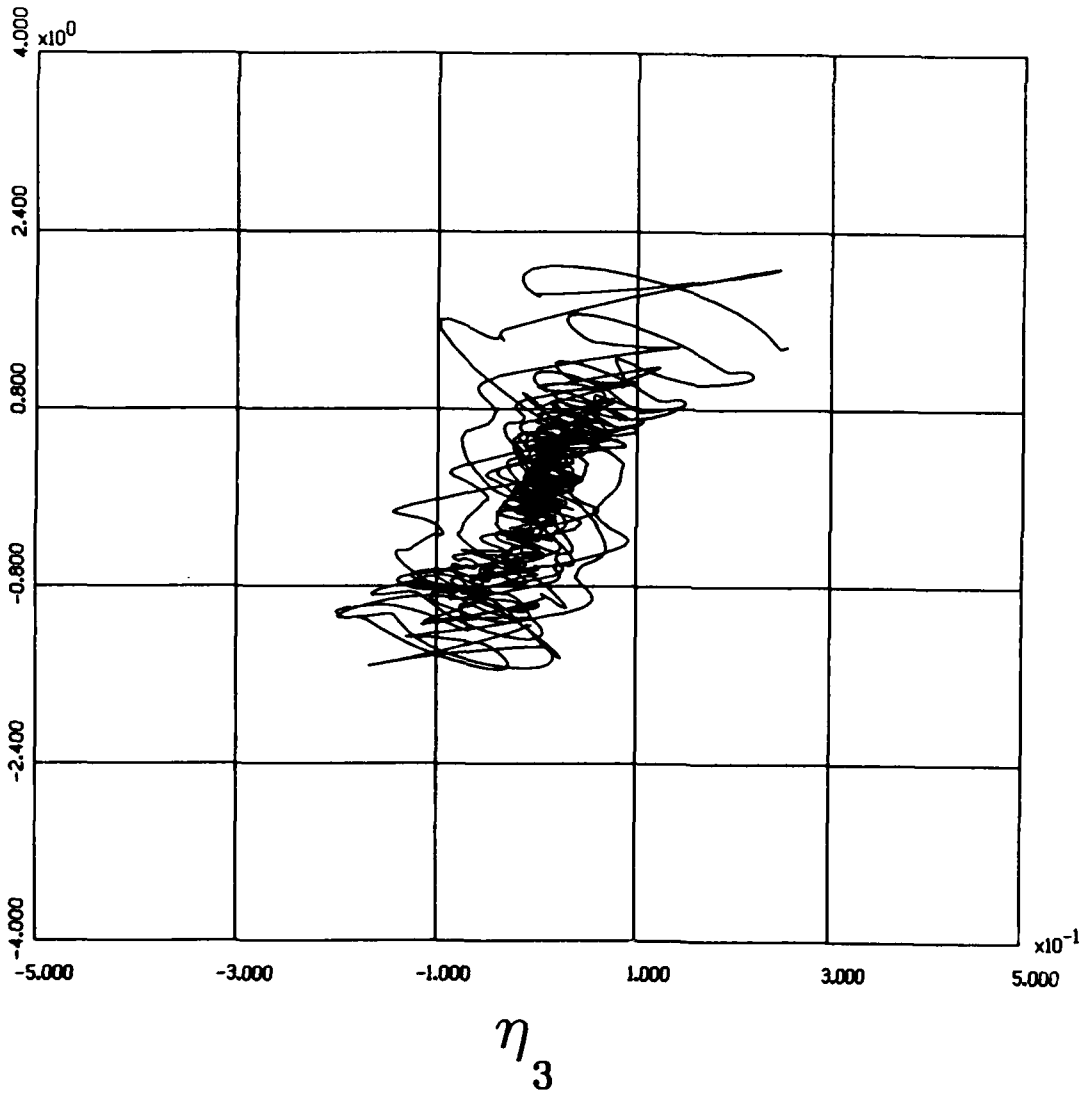

Figure 4.18 Non-linear η_3 vs η_4 for 12 orbits

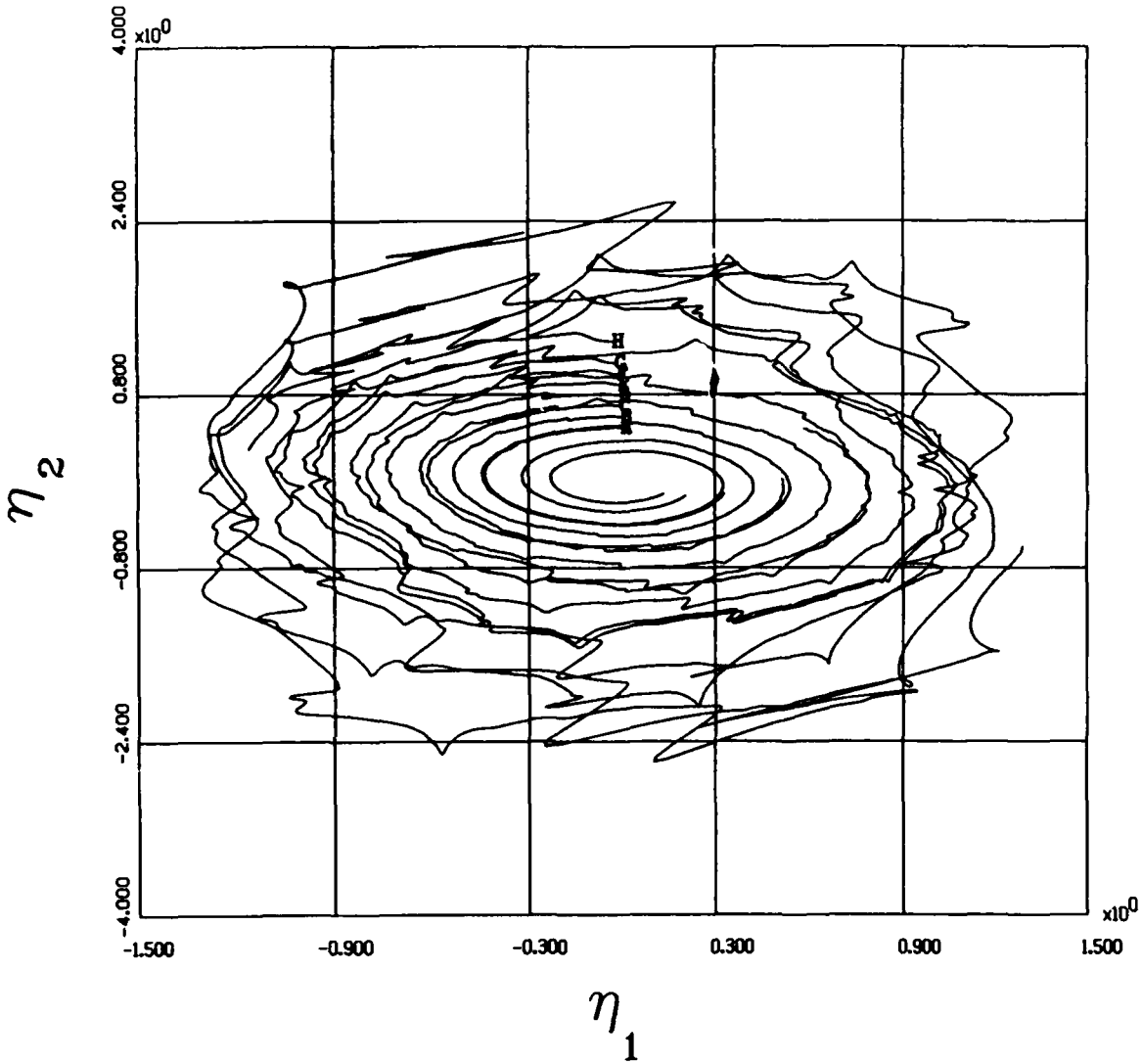

Figure 4.19 Non-linear η_1 vs η_2 for 12 orbits

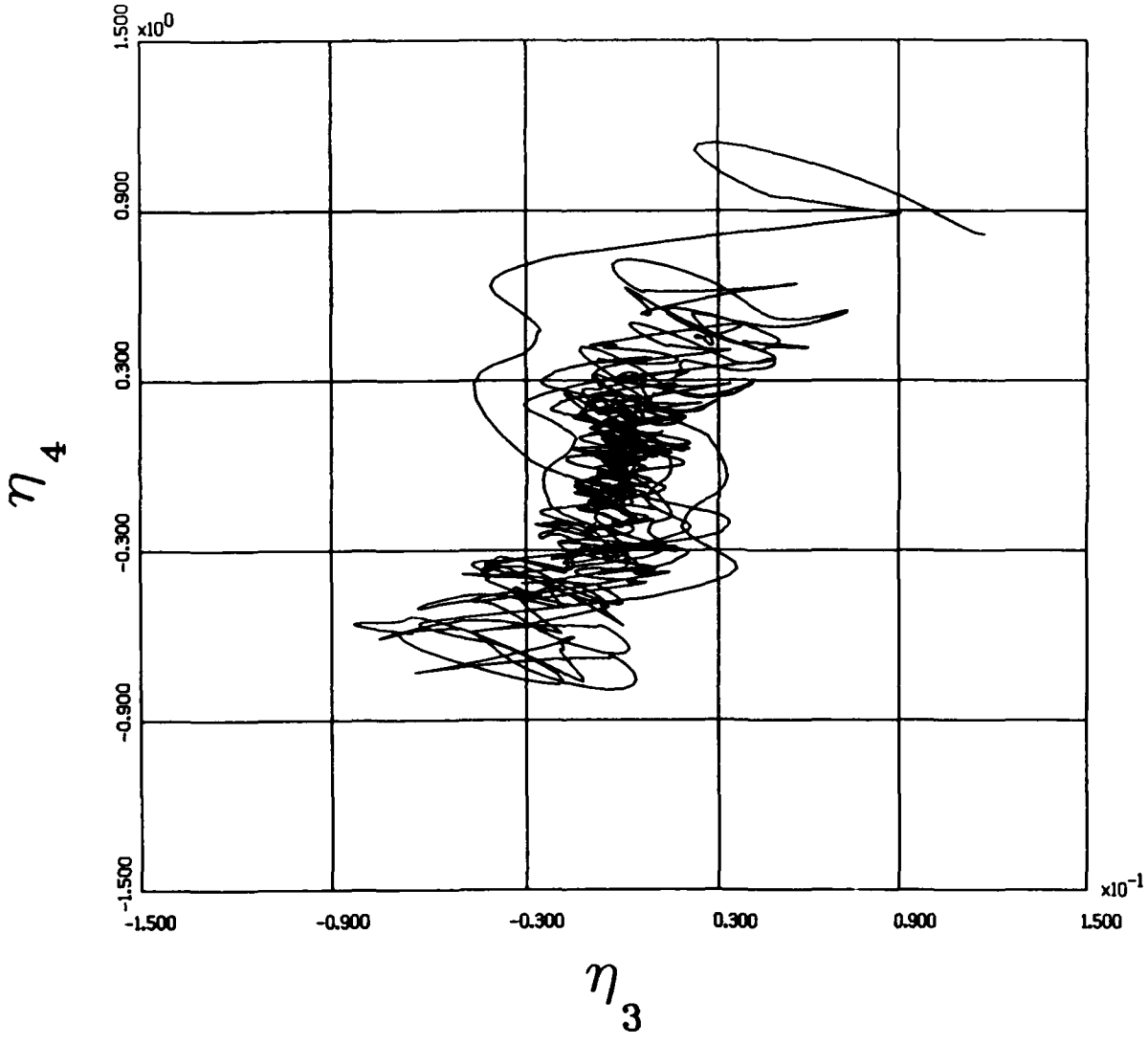

Figure 4.20 Non-linear η_3 vs η_4 for 12 orbits

Table 4.4. Starting values for η_2 axis

	η_1	η_2	η_3	η_4
A	0.0	0.5	0.0	0.0
B	0.0	0.6	0.0	0.0
C	0.0	0.7	0.0	0.0
D	0.0	0.8	0.0	0.0
E	0.0	0.9	0.0	0.0
F	0.0	1.0	0.0	0.0
G	0.0	1.1	0.0	0.0
H	0.0	1.3	0.0	0.0

of the points started in the non-linear region. Start a trajectory at $\bar{\eta} = [0.9, 0, 0, 0]^T$ and integrate it for 200 orbits, the results are shown in Figures 4.21 and 4.22. These figures indicate the controller is effective at this condition.

At a starting point of $\bar{\eta} = [0.95, 0, 0, 0]^T$ the results are completely different as shown in Figures 4.23 and 4.24. The first few orbits are found on the interior of this structure and then the system appears to settle into an orbital type structure. This would not be desirable for a satellite control system, it would quickly exhaust its fuel supply.

There is a region around the equilibrium point that exhibits a stable behavior and if it can be assured of not exceeding those bounds, the controller will perform its intended function. Examining points outside of this orbital structure, for example $\bar{\eta} = [3, 0, 0, 0]^T$, the trajectories all appear to converge in to the orbital structure. The controller is still working at damping large perturbations but another attractor has appeared in the phase space. Any point in its basin of attraction will result in a steady state at that non-linear attractor. To gain more information about this attractor will require some other non-linear analysis tools, especially the Poincaré map.

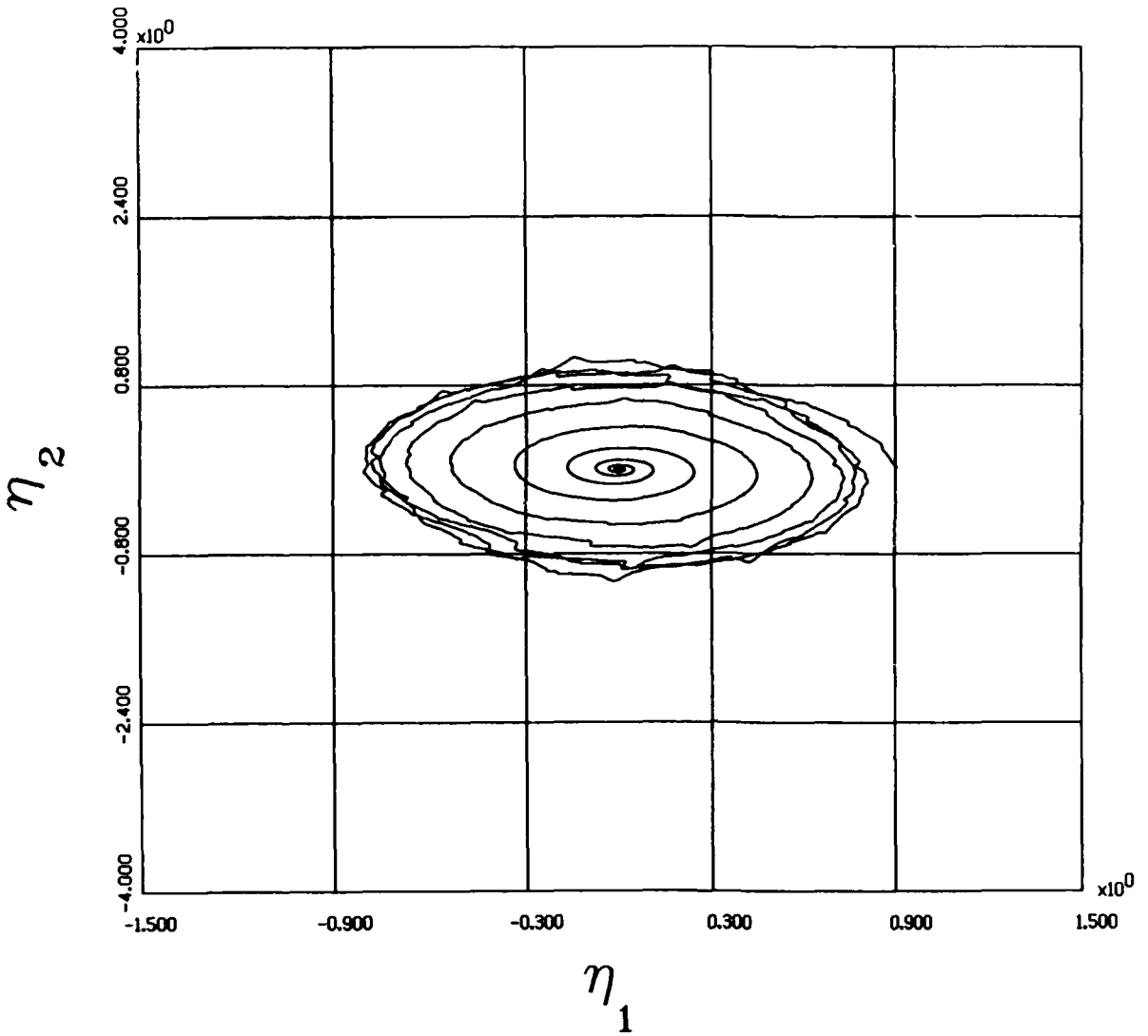

Figure 4.21 Non-linear η_1 vs η_2 for 200 orbits

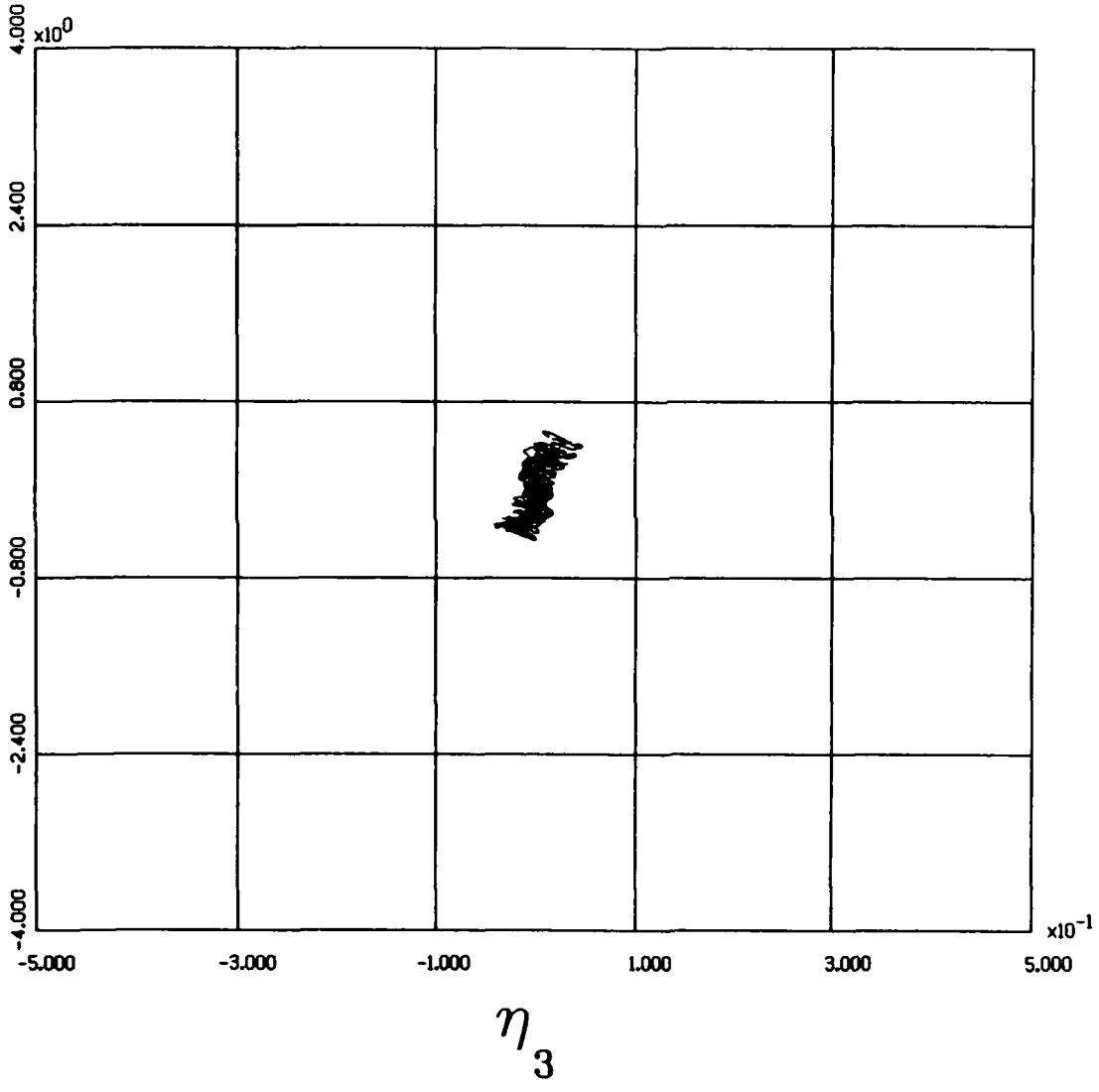

Figure 4.22 Non-linear η_3 vs η_4 for 200 orbits

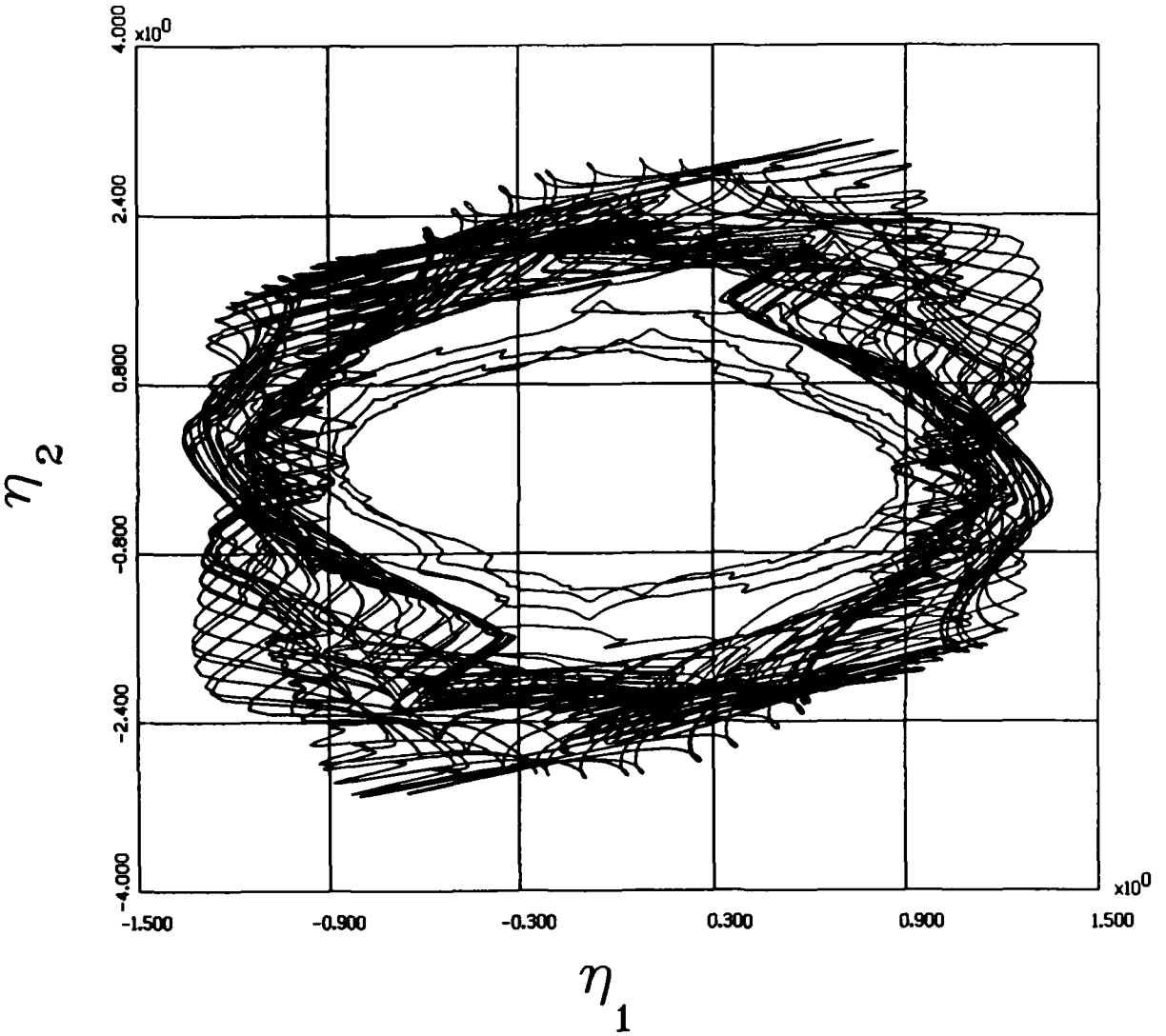

Figure 4.23 Non-linear η_1 vs η_2 for 200 orbits

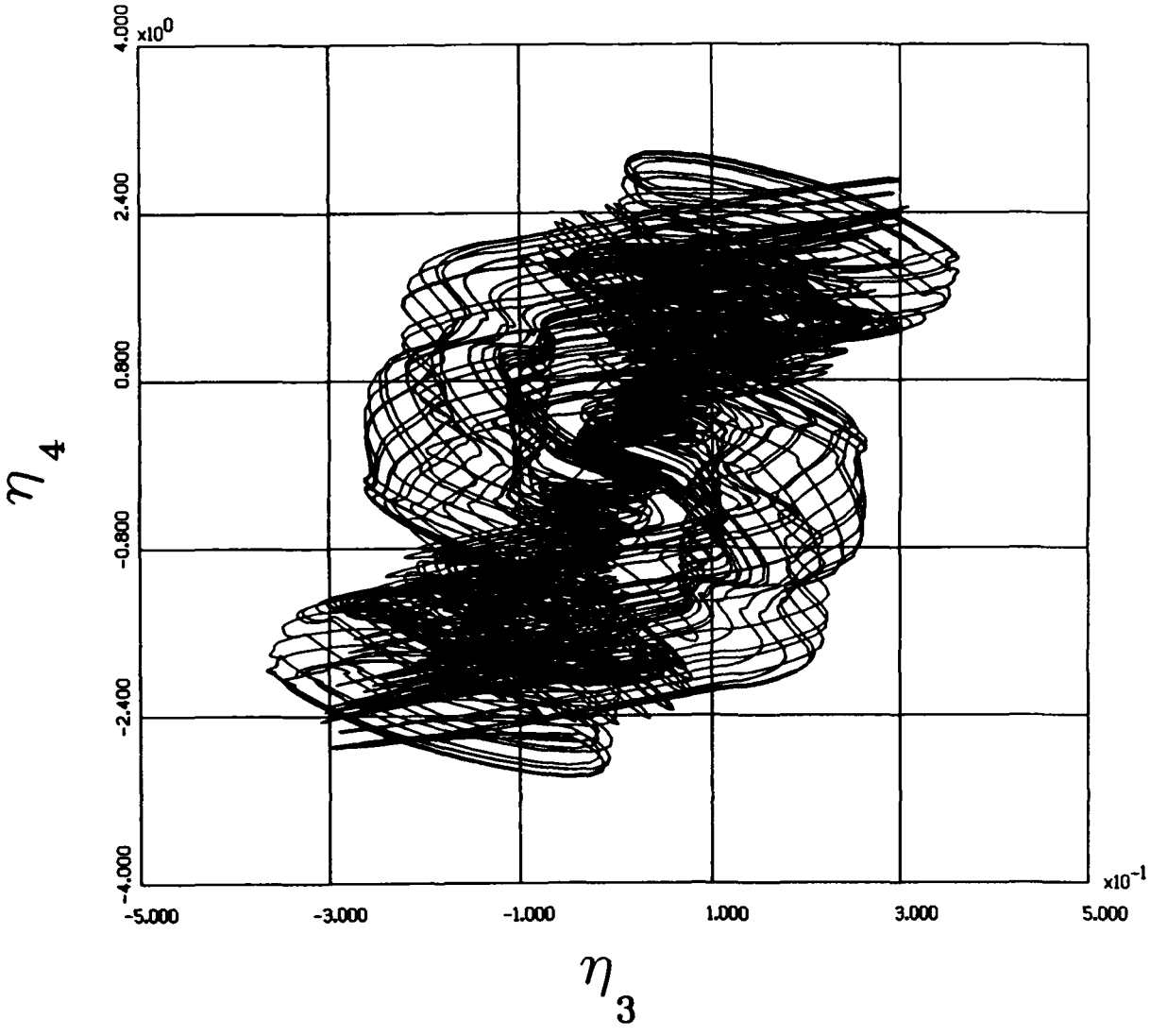

Figure 4.24 Non-linear η_3 vs η_4 for 200 orbits

4.2.4 Poincaré Map To observe a strange attractor with a Poincaré map in a space higher that two dimensions requires a little ingenuity. Dr. Moon presented ideas on how to slice up a three dimensional attractor and view portions of it at a time and then piece together the whole attractor. The real difficulty in viewing this attractor is the fact it resides in a four dimensional space. This can be achieved in our modal coordinates by using what I call a dual torus, Figure 4.25. This is done by stacking two doughnuts on top of one another and running the time coordinate as the angle in the center of the tori. They are synchronized to the same time axis. Then η_1 vs η_2 axis is at the center of the first torus ring and η_3 vs η_4 axis is at the center of the second torus ring. This will allow us to display all four dimensions and take a time slice over n periods. Each system state is represented by a pair of points. Since the system has doubled the original period, start the map with a 4π period.

The system of equations are integrated for many orbits, one point is plotted in each coordinate system as the trajectories pass through the zero angle point on the tori. Figures 4.26 and 4.27 show the results of 2500 orbits. There are four well defined regions mapped in the phase space. At first glance they do not appear to be fractal nor do they fit any of the other cataloged forms. The few scattered points off of the shapes are the initial startup disturbance, before it settles into the attractor. Let us take a series of slices around the torus and examine the shape over one 4π period. Ten maps are shown evenly spaced around the tori. Figures 4.28, 4.29, 4.30, 4.31, 4.32, 4.33, 4.34, 4.35, 4.36 and 4.37 show the attractor in the η_1 vs η_2 space. Figures 4.38, 4.39, 4.40, 4.41, 4.42, 4.43, 4.44, 4.45, 4.46 to 4.47 show the η_3 vs η_4 phase space. The shape of the attractor seems to remain in a ring type shape with no apparent fractal geometry. One thing to note, examine the shape on the left of Figure 4.28 and trace it through the 4π cycle, it does not return back to the same region, but to the region that is the bottom shape in Figure 4.28. Continuing this process for a total of four times will map back to the original region on the left. This indicates period for the attractor is not 4π. The attractor actually

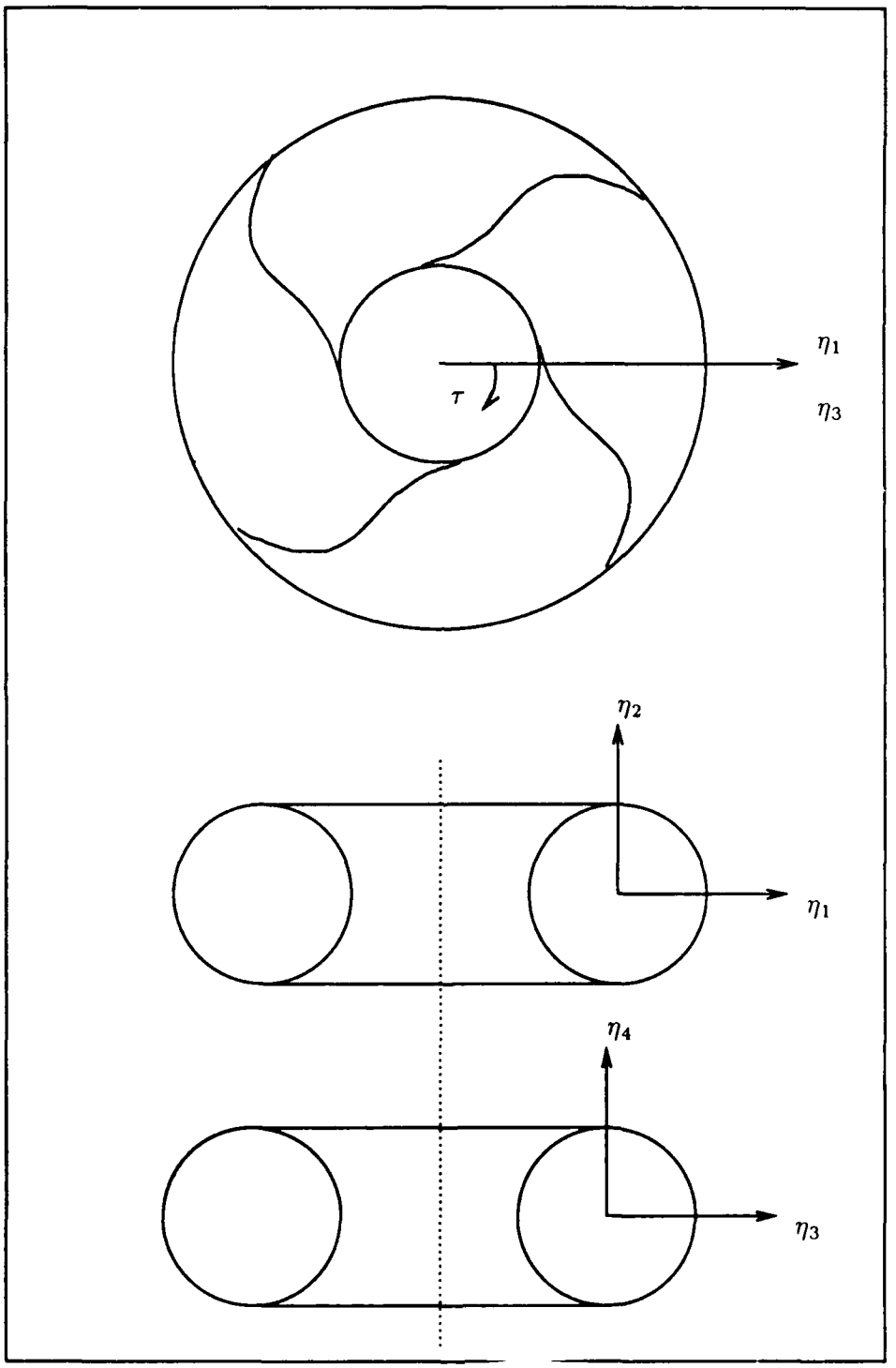

Figure 4.25. Dual Torus Map

has a period of 16π. Increasing the time distance around the tori to 16π and making a Poincaré map of the data can be seen in Figures 4.48 and 4.49. Time slices could be taken to examine the attractor as it changes in time.

4.3 Bifurcations of Cycles

Where did this attractor come from? How can it be removed or compensation added? These questions are important to the designer and operator of the satellite. The hint lies back in the linearized system. The period of the system has doubled, this is usually an indicator of a process called bifurcation. A process called a Hopf bifurcation has been examined in lower order systems that transitions a stable node in to a limit cycle. An extension of this idea is the secondary Hopf bifurcation, where a limit cycle transitions to a torus [15:126-128]. In our case, setting the gain level beyond the bifurcation point has caused the appearance of a 4-dimensional torus around the equilibrium point. By lowering the gain below the bifurcation point, the torus attractor should disappear.

Using the starting points from Table 4.5, Figures 4.50 and 4.51 present typical results from several searches. It appears that the equilibrium point is now globally stable and very non-linear. The controller is effective over the entire phase space. However this increased stability region has not come without a price. The controller now takes a longer time to dissipate a given perturbation.

By slowly increasing the gain and examining the phase space, the appearance of the new attractor can be observed. Figures 4.52, 4.53, 4.54, 4.55, 4.56, 4.57, 4.58 and 4.59 show the formation of the arractor. This provides the designer with enough information to specify upper gain limits for the controller. With the gain set at 0.36 and starting at $\bar{\eta} = \{2, 0.0, 0\}^T$ and examing the system behavior after 75 orbits we find the limit cycle structure, Figures 4.60 and 4.61.

Also a two dimensional analogy can be developed that provides some insight into this system, figure 4.62. This system behaves similar to a marble in a bowl.

As we adjust the gain, the contour of the bottom of the bowl changes. With a gain setting of 0.0, the system exhibits bounded behavior over a region of the phase space or the bottom of the bowl is flat and has no preferred equilibrium. If the gain is raised to 0.2, the system is stable over the entire phase space and is attracted to only the equilibrium point or this bowl has a conventional shape with the center being the lowest point. At a gain of 0.35, the system is developing a limit cycle type attractor or the bowl now has a near flat region surrounding the center. With the gain at 0.4, the phase space is clearly divided into two regions and large perturbations will not return to the equilibrium point or the bowl is now a bowl surrounded by a ringshape.

One could proceed on to determine exactly what type of attractor, strange or quasiperiodic, is appearing with the bifurcation. For controller design, and evaluation this information is not necessary but could be obtained from a power spectrum.

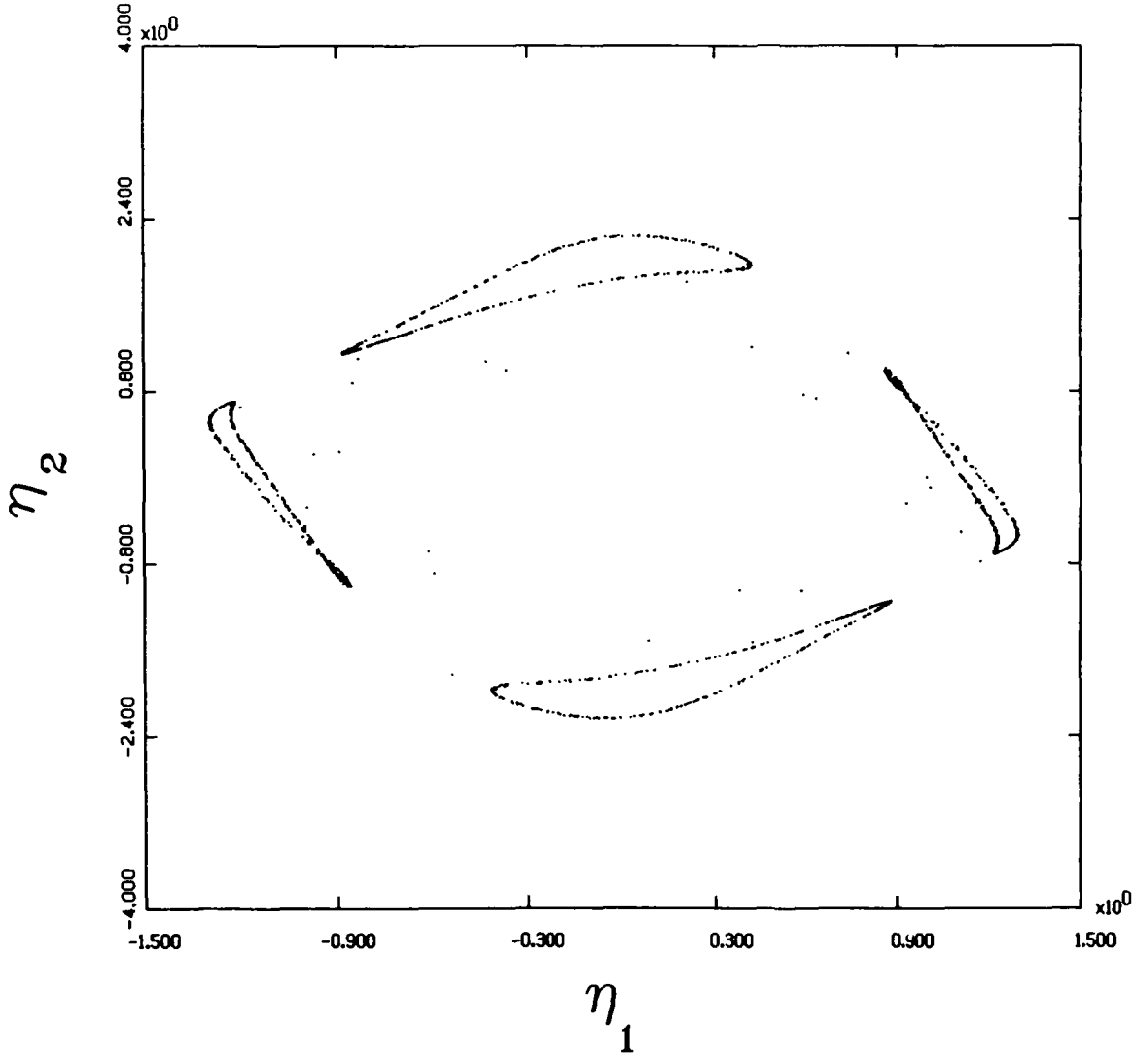

Figure 4.26 Non-linear η_1 vs η_2 Poincare Map for 2500 orbits

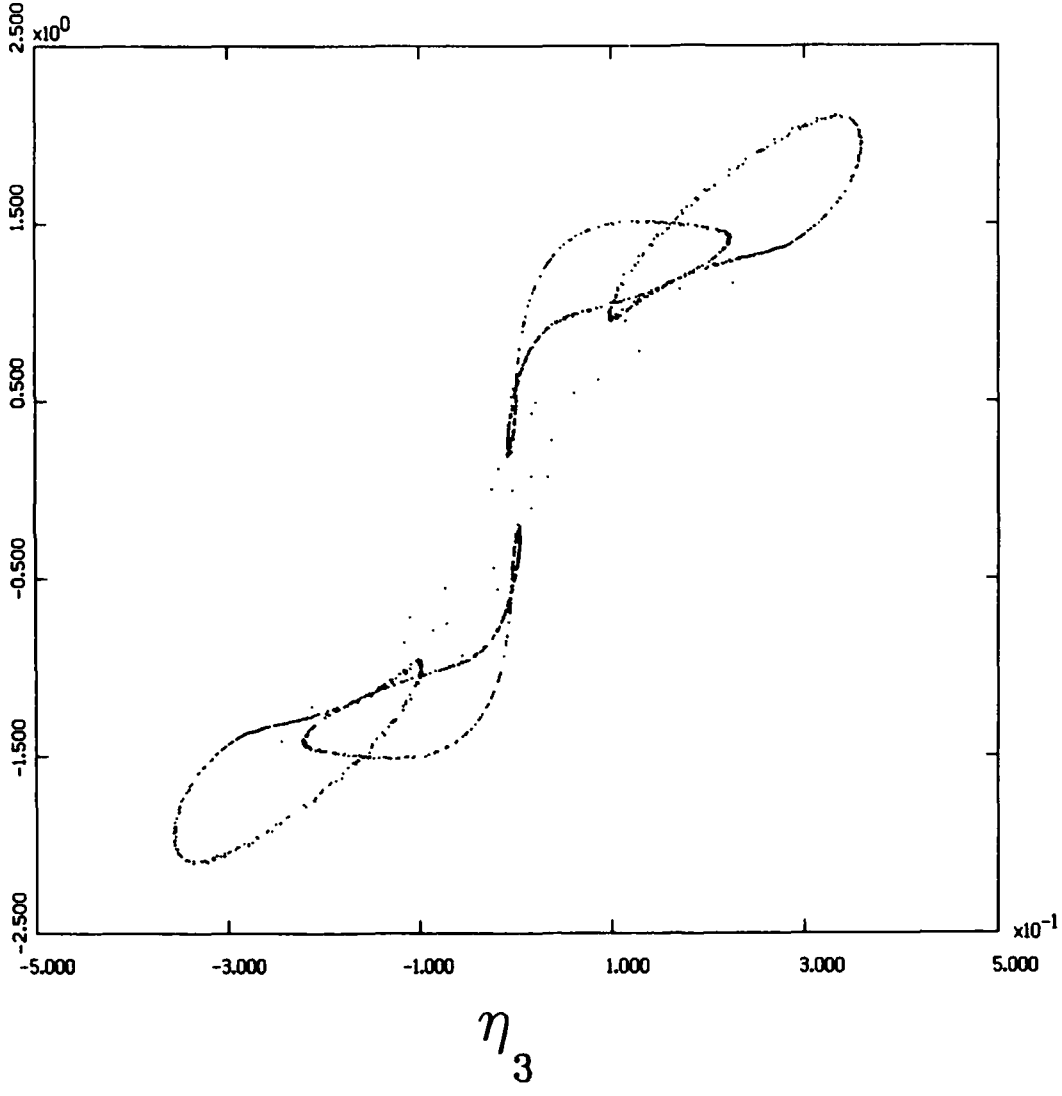

Figure 4.27 Non-linear η_3 vs η_4 Poincare Map for 2500 orbits

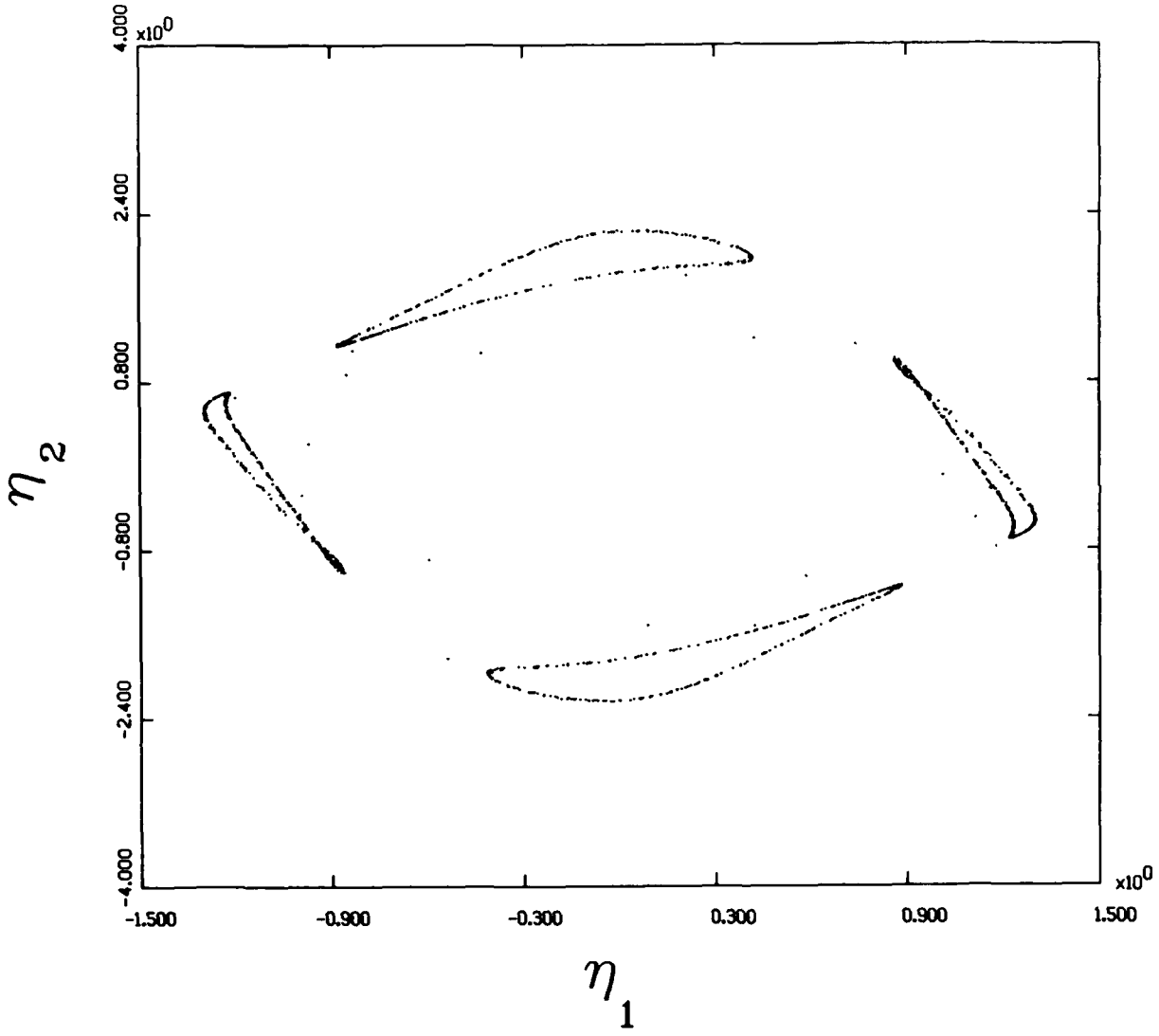

Figure 4.28 Four Pi Poincare Map of η_1 vs η_2, phase 0

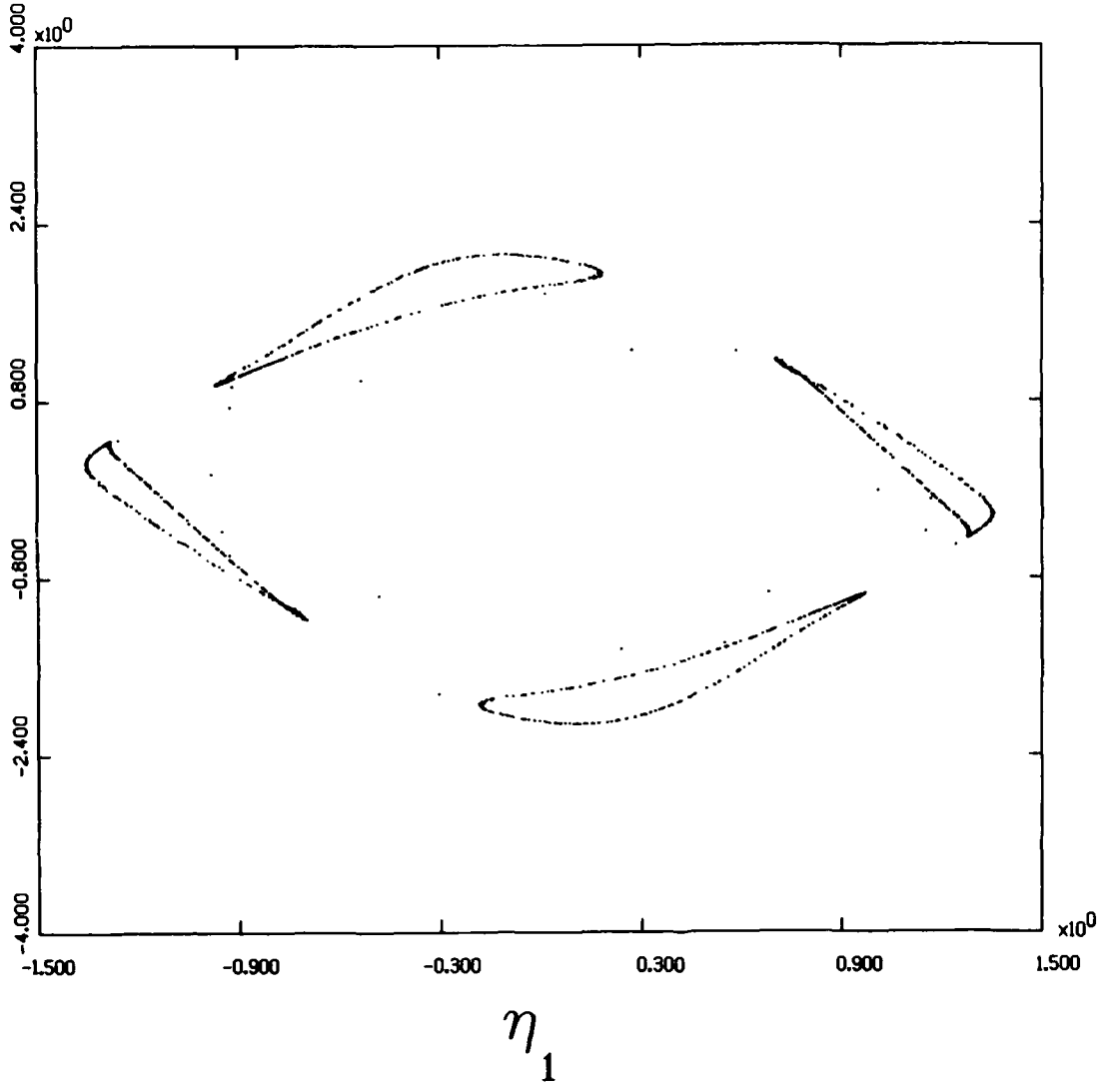

Figure 4.29 Four Pi Poincare Map of η_1 vs η_2, phase 0.4 Pi

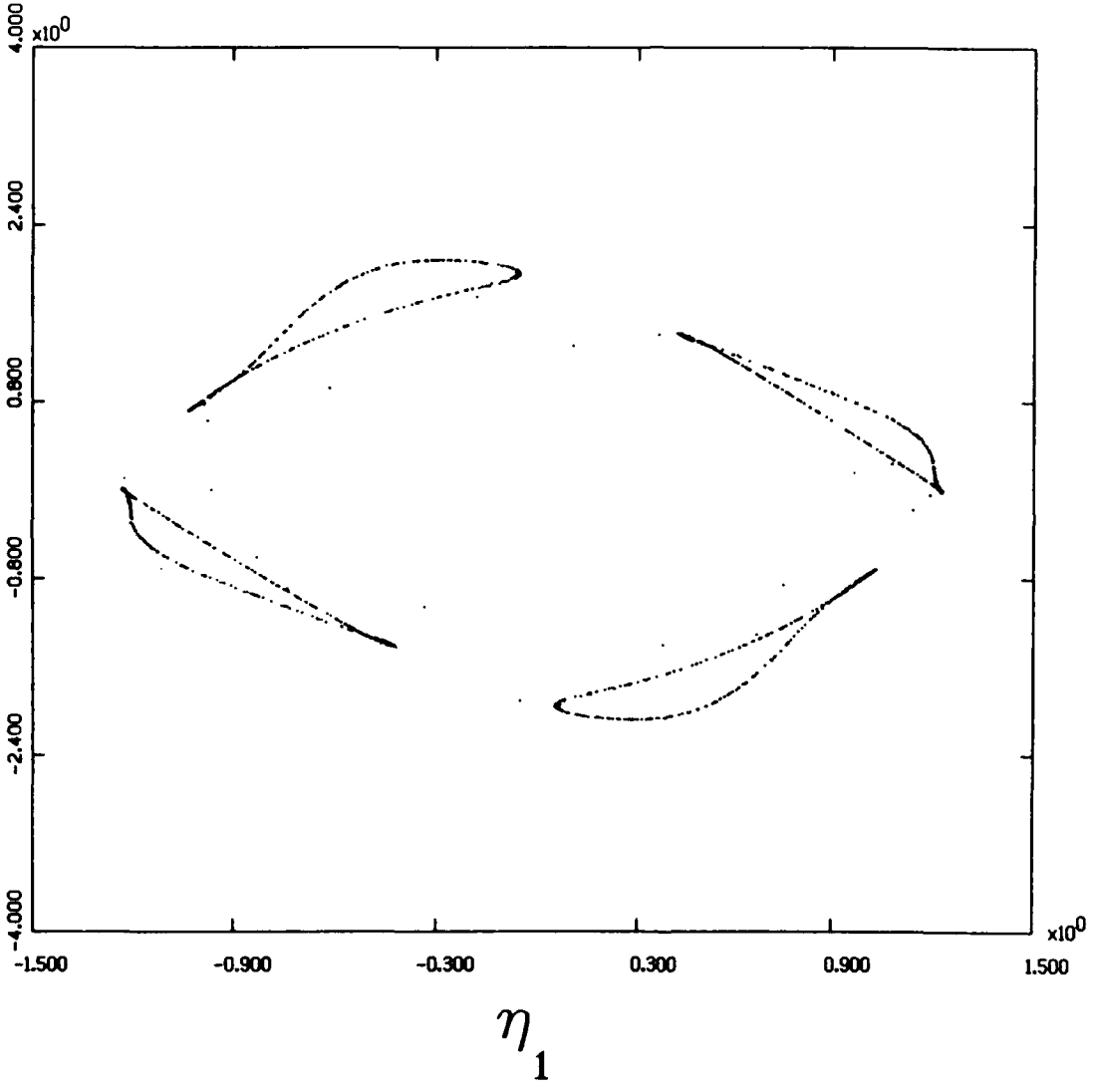

Figure 4.30 Four Pi Poincare Map of η_1 vs η_2, phase 0.8 Pi

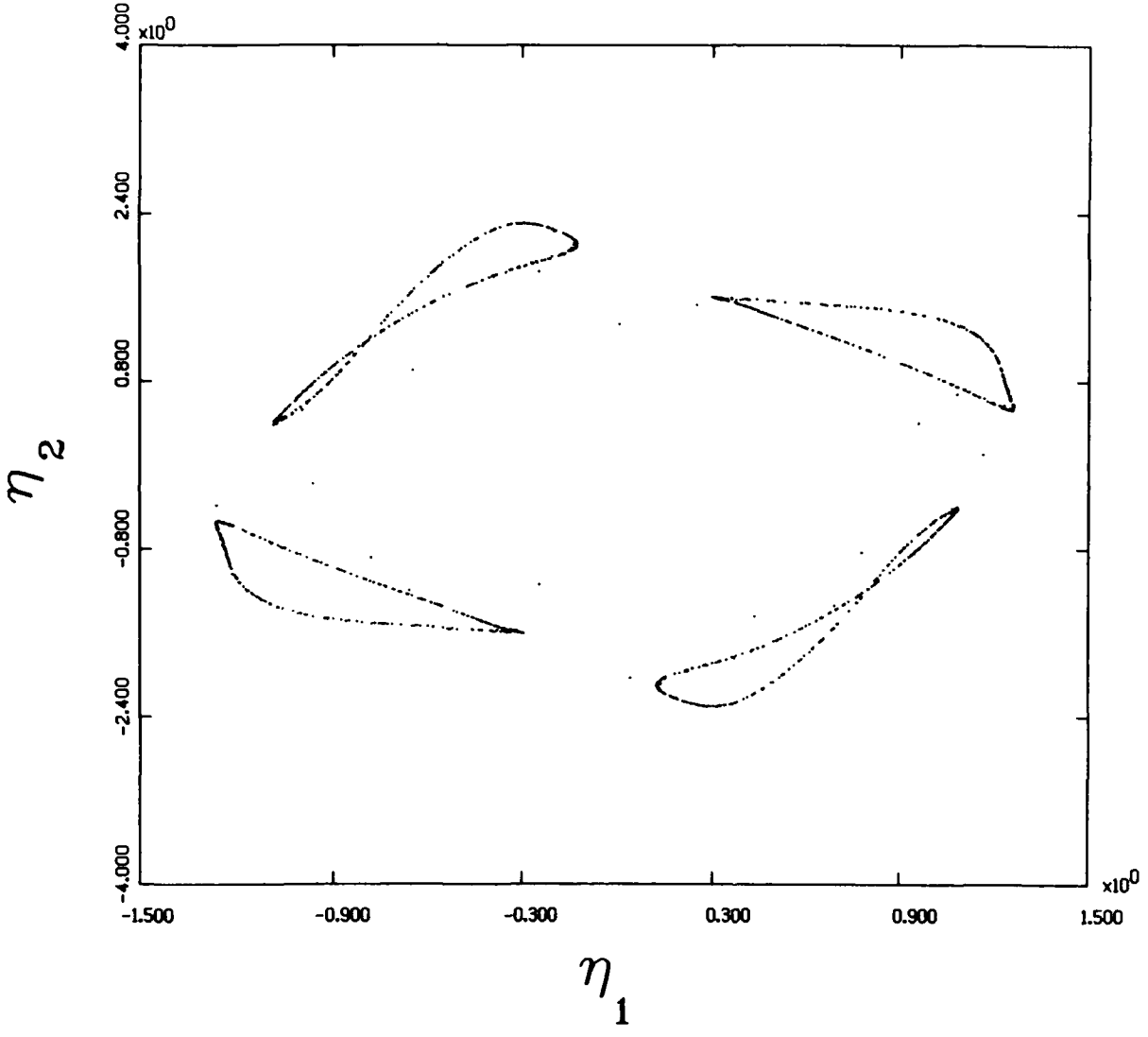

Figure 4.31 Four Pi Poincare Map of η_1 vs η_2, phase 1.2 Pi

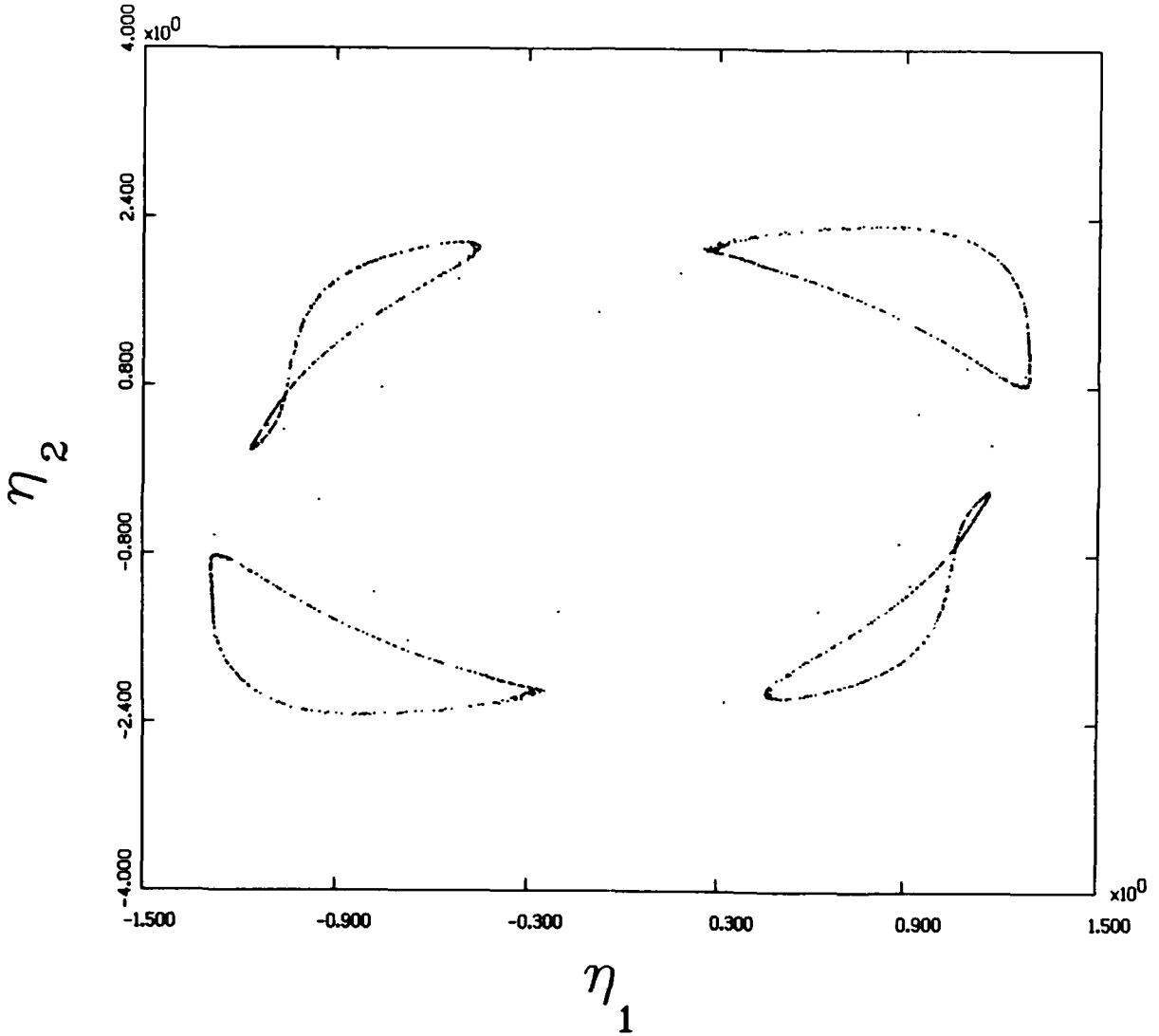

Figure 4.32 Four Pi Poincare Map of η_1 vs η_2, phase 1.6 Pi

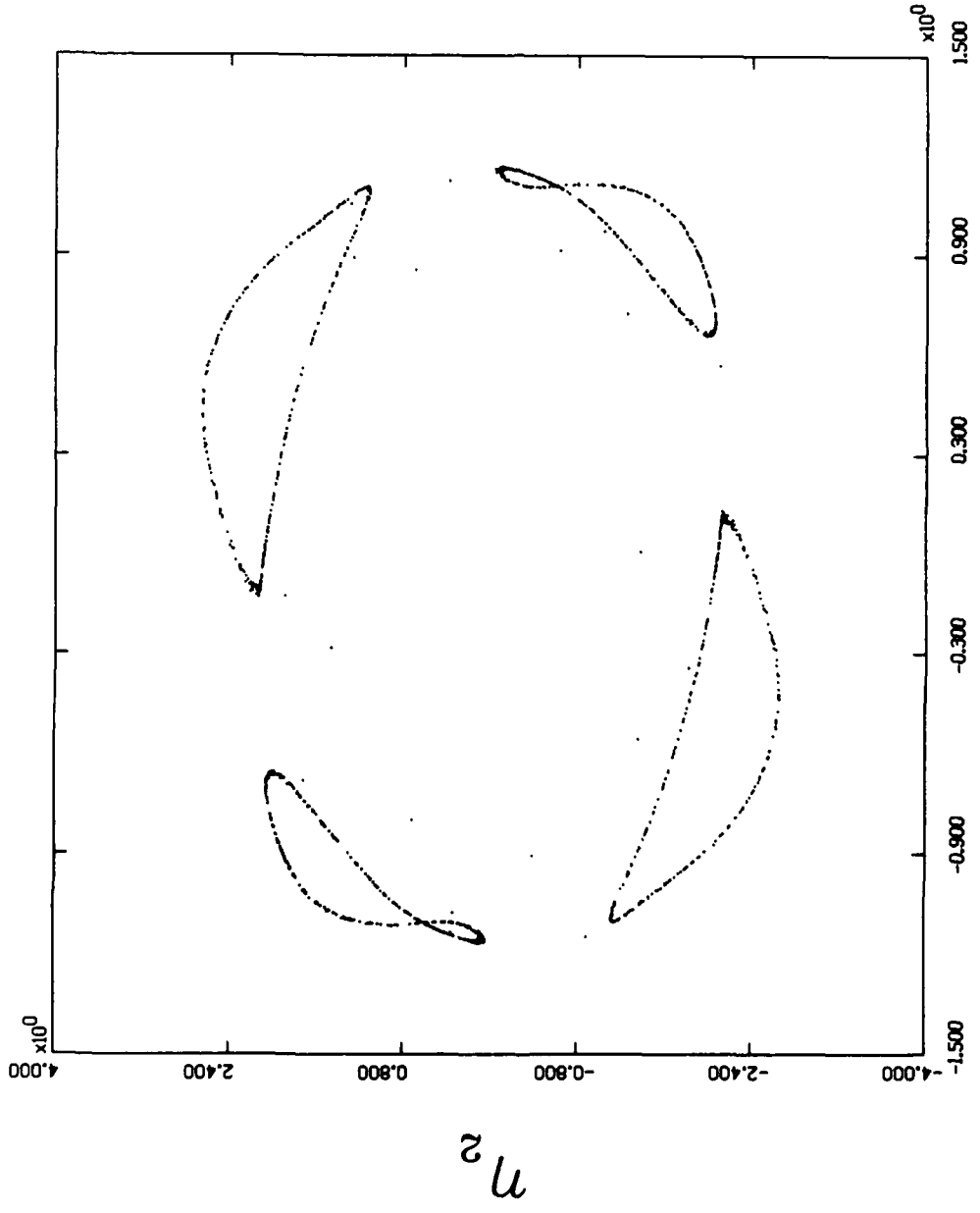

Figure 4.33 Four Pi Poincare Map of η_1 vs η_2, phase 2.0 Pi

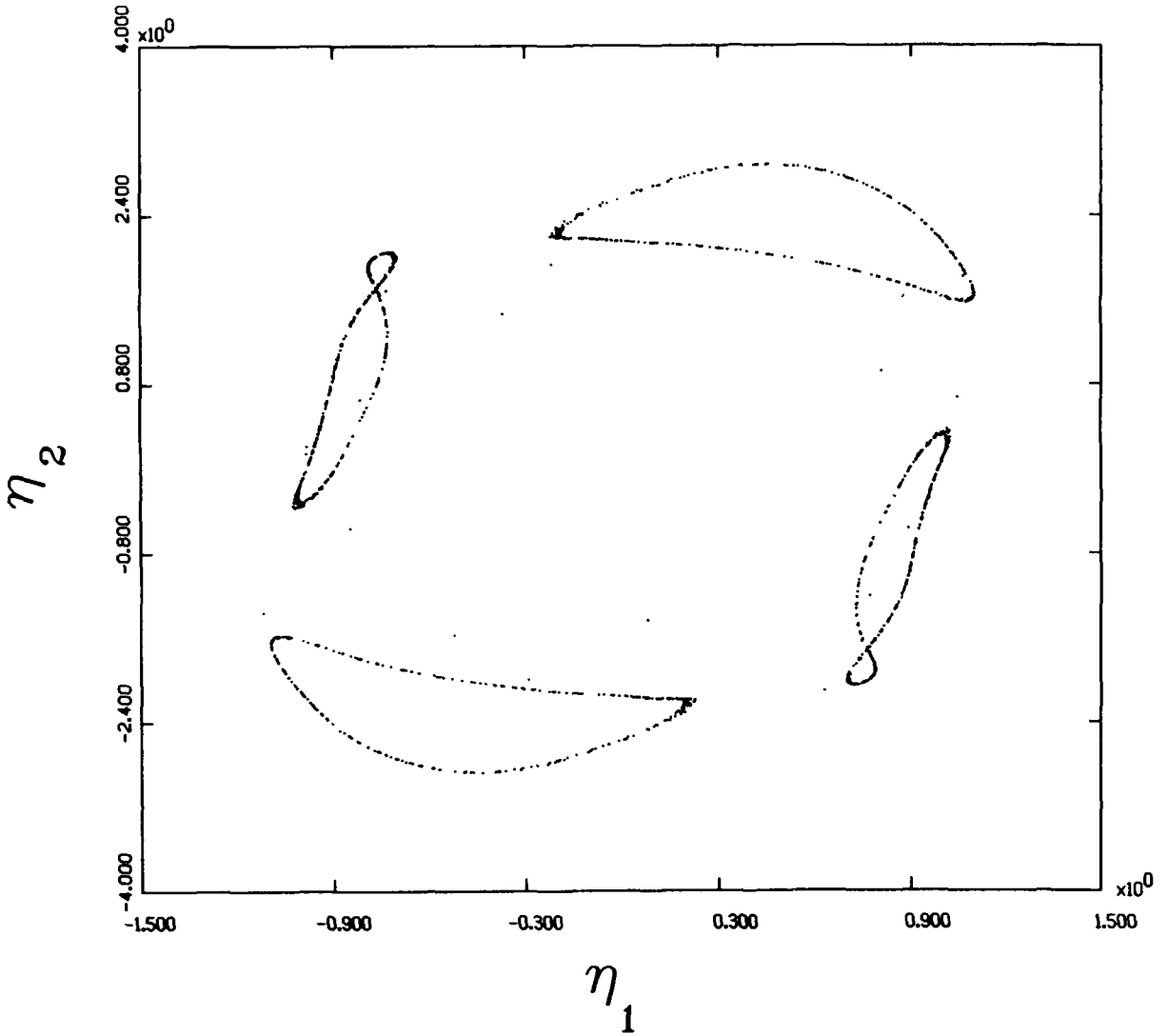

Figure 4.34 Four Pi Poincare Map of η_1 vs η_2, phase 2.4 Pi

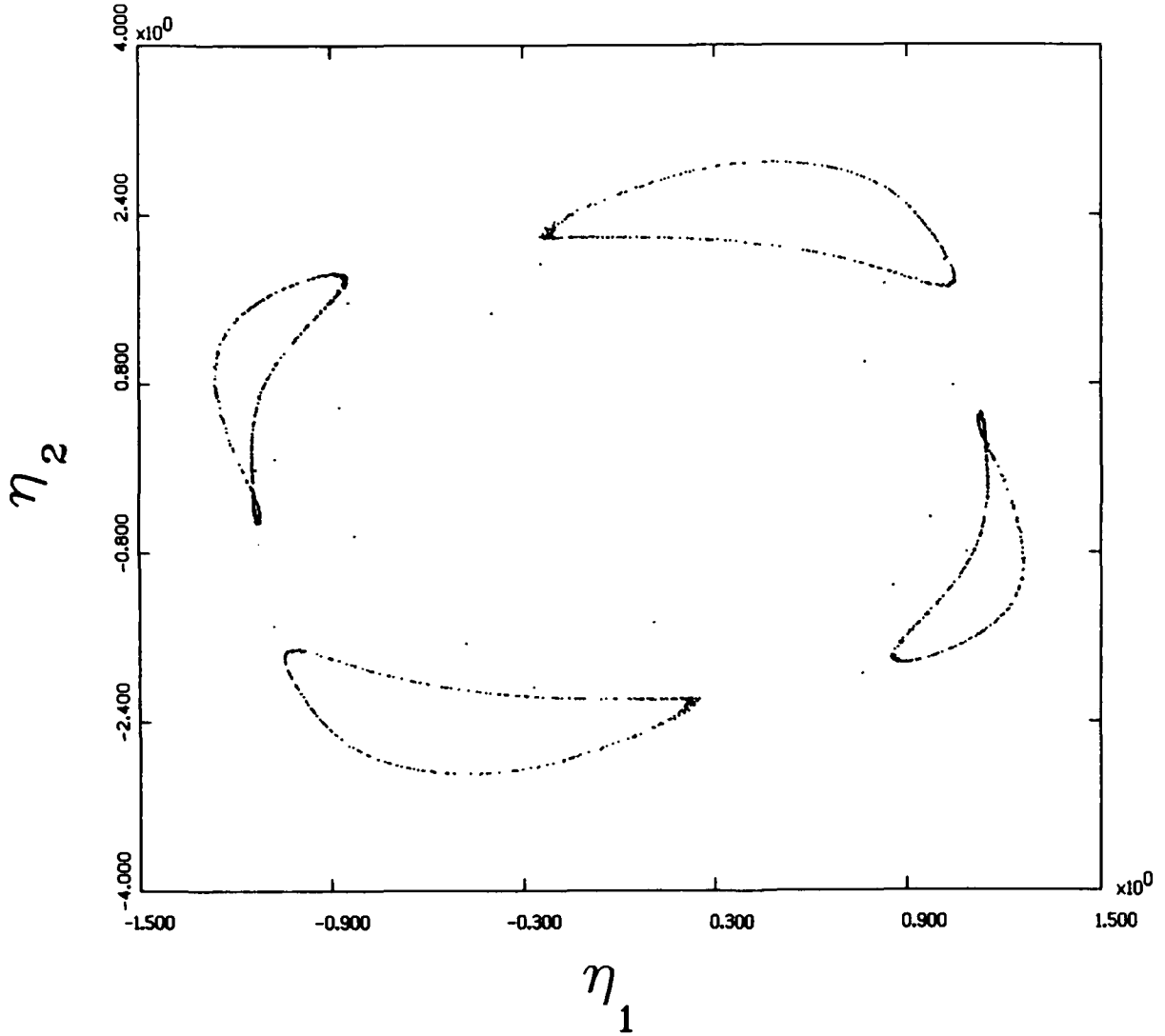

Figure 4.35 Four Pi Poincare Map of η_1 vs η_2, phase 2.8 Pi

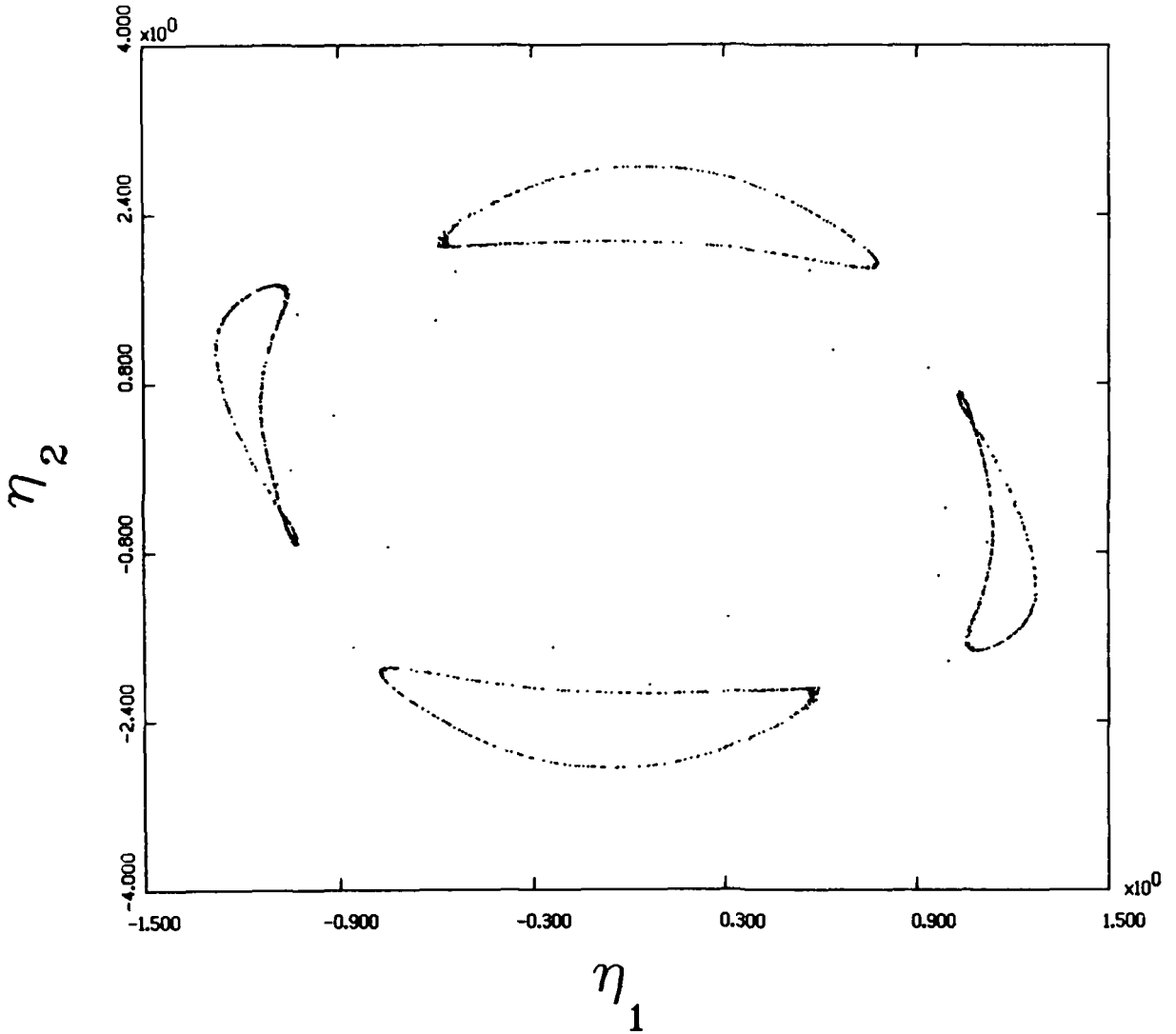

Figure 4.36 Four Pi Poincare Map of η_1 vs η_2, phase 3.2 Pi

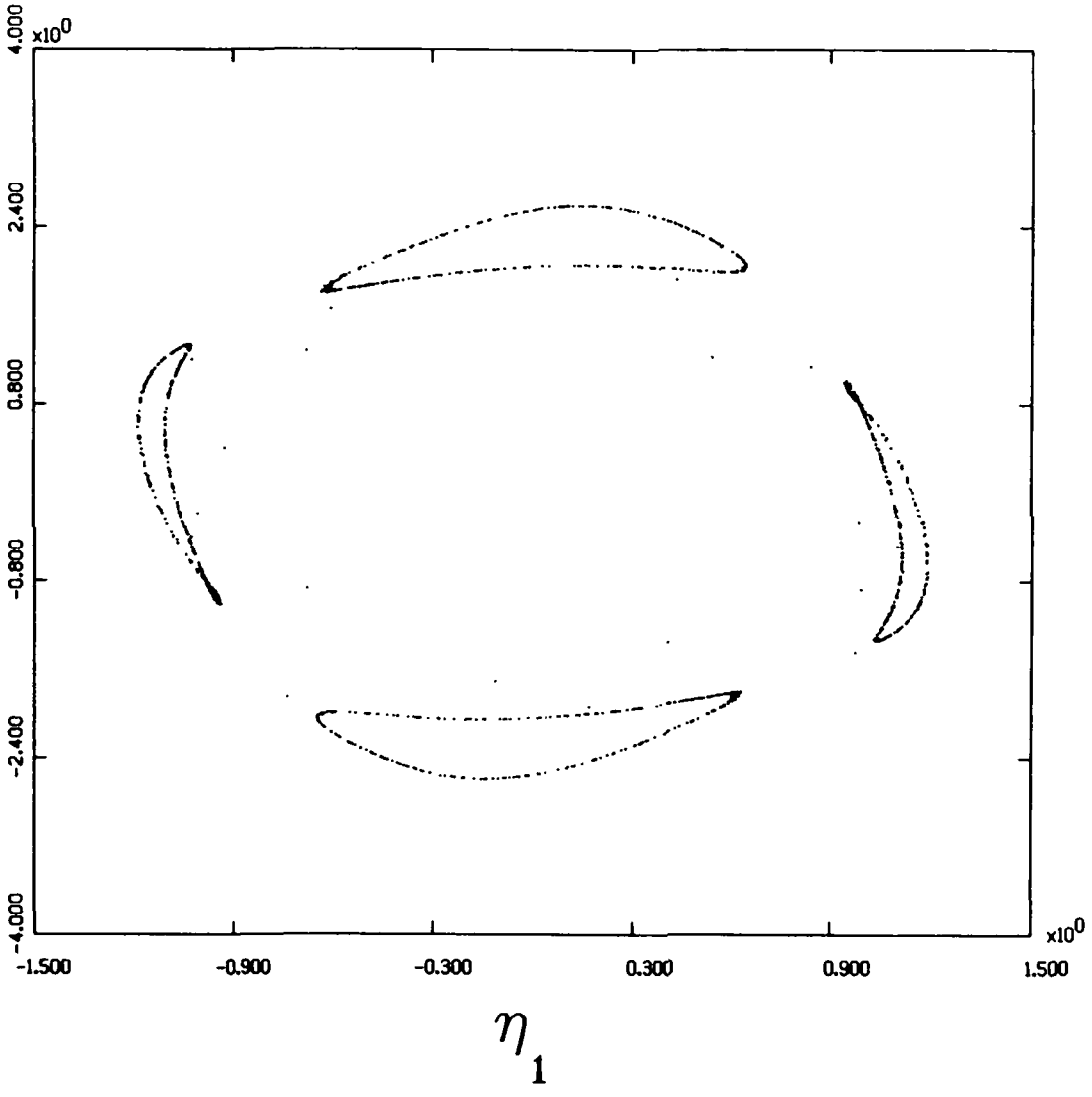

Figure 4.37 Four Pi Poincare Map of η_1 vs η_2, phase 3.6 Pi

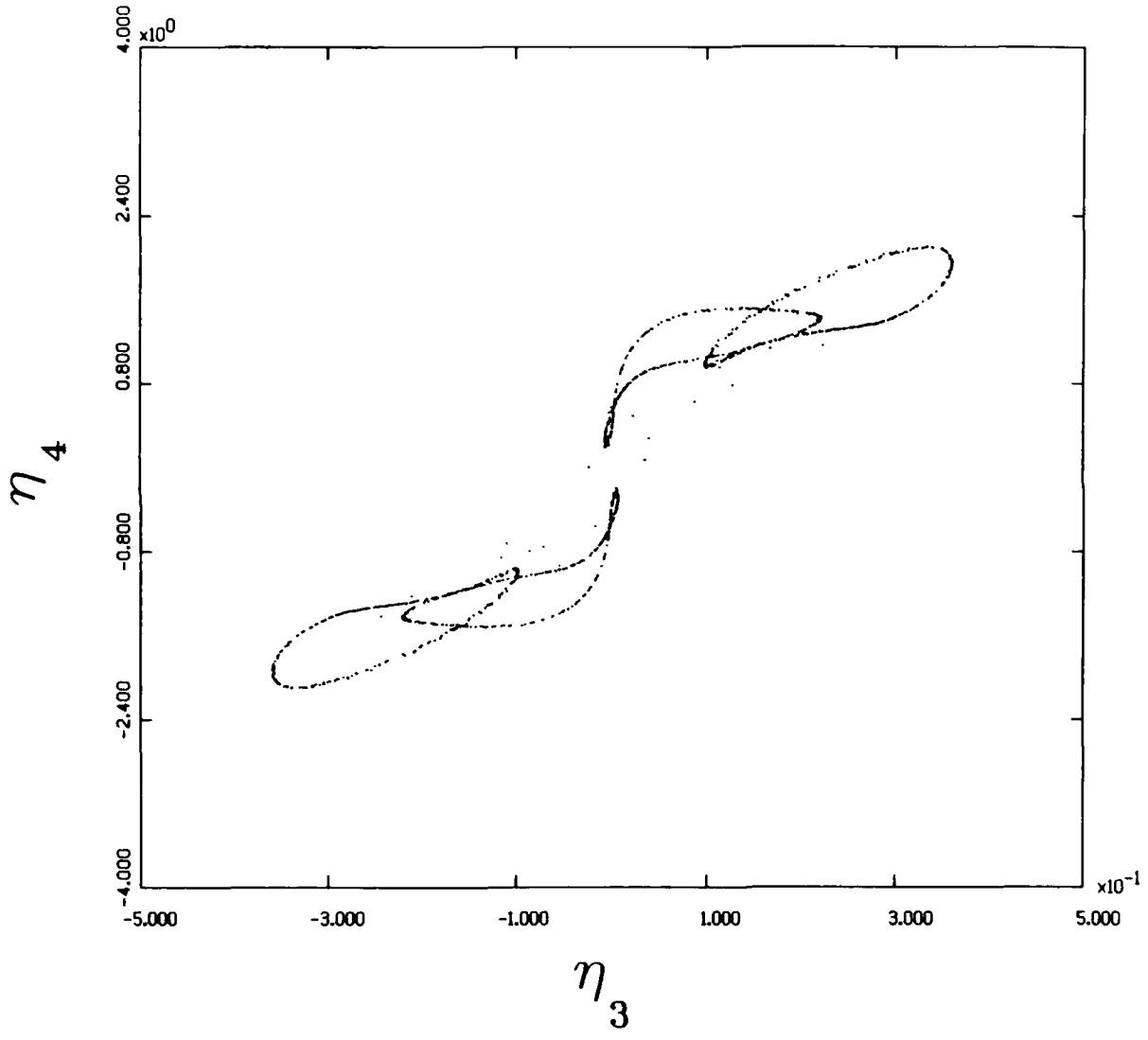

Figure 4.38 Four Pi Poincare Map of η_3 vs η_4, phase 0

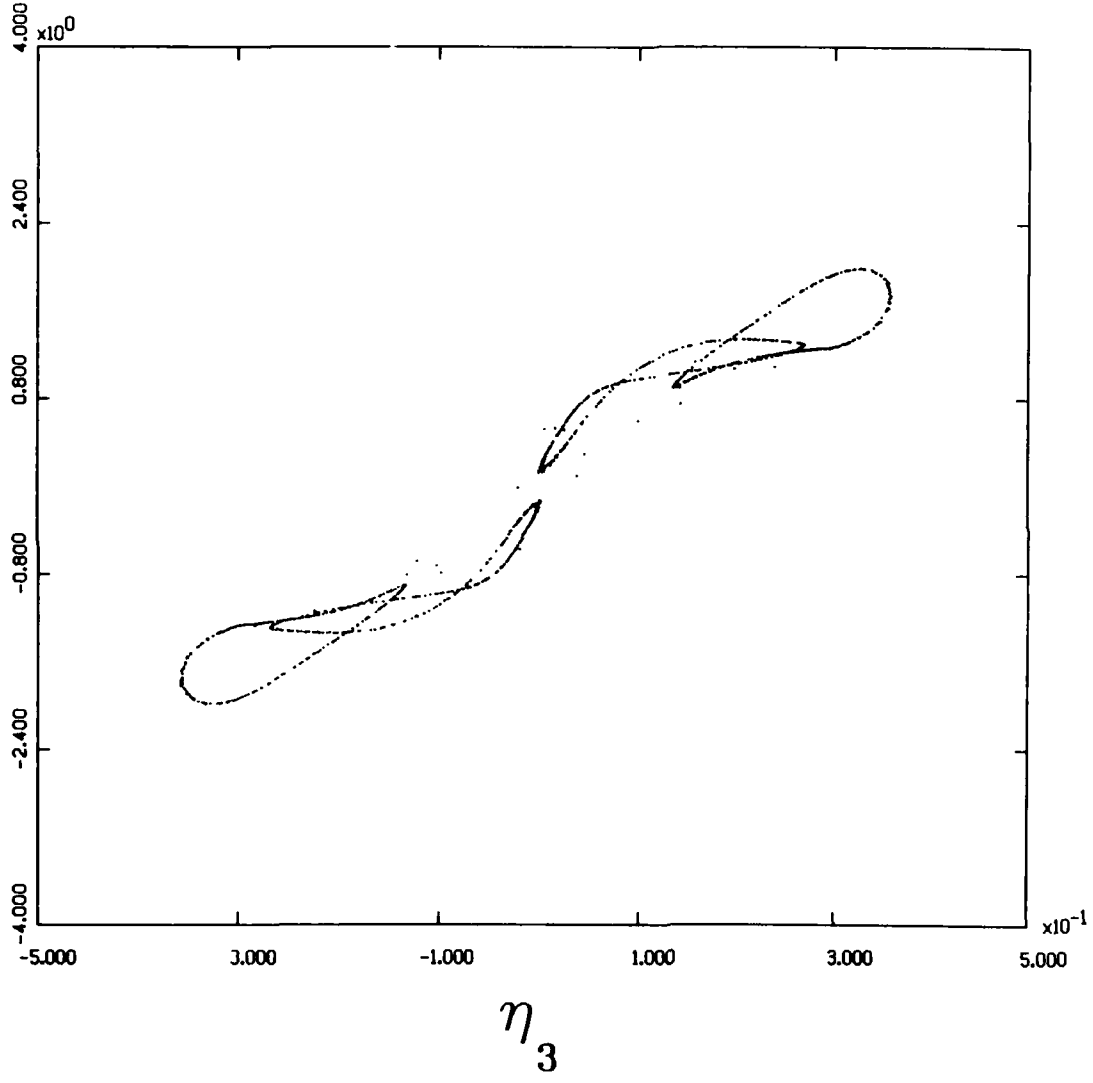

Figure 4.39 Four Pi Poincare Map of η_3 vs η_4, phase 0.4 Pi

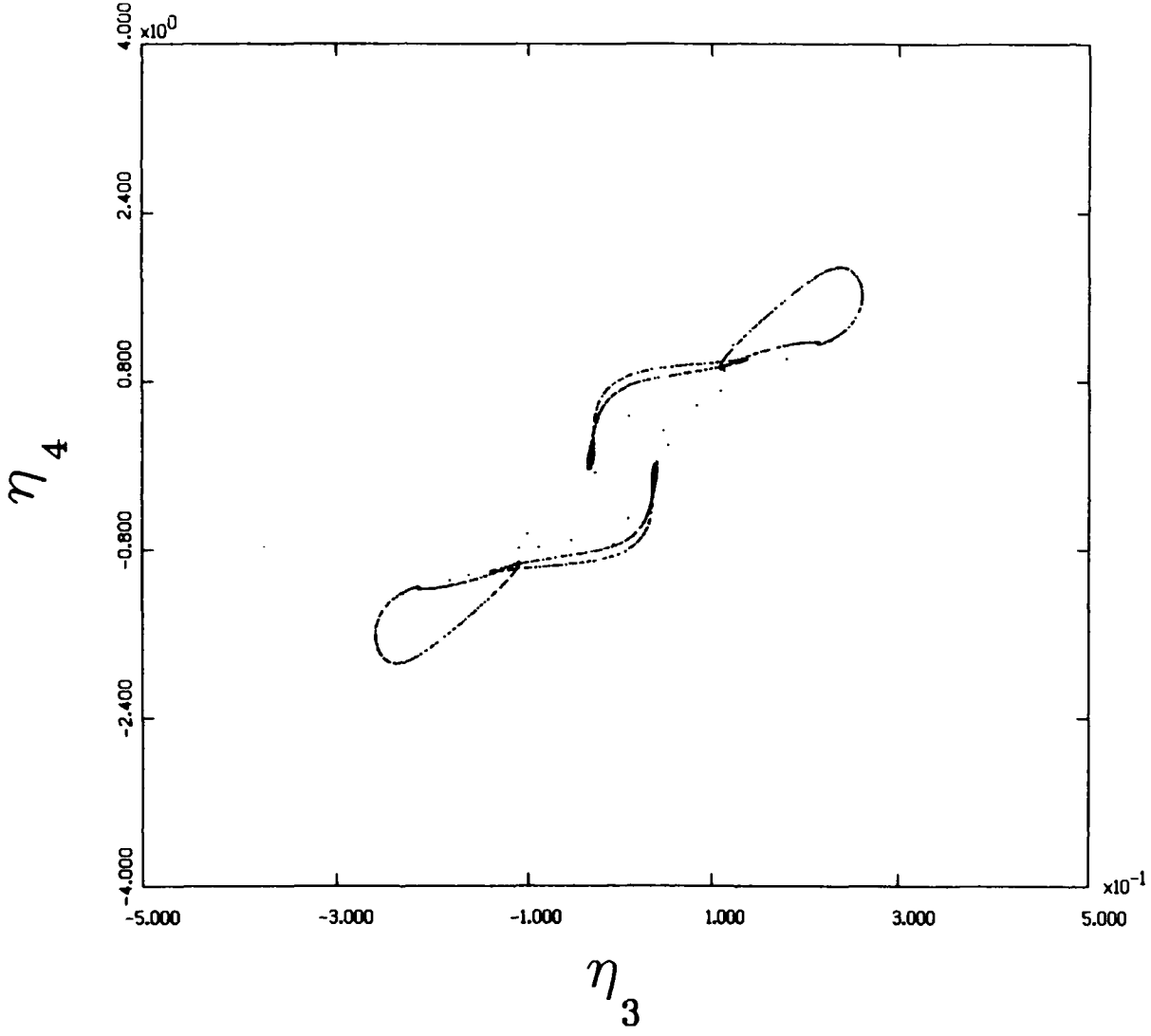

Figure 4.40 Four Pi Poincare Map of η_3 vs η_4, phase 0.8 Pi

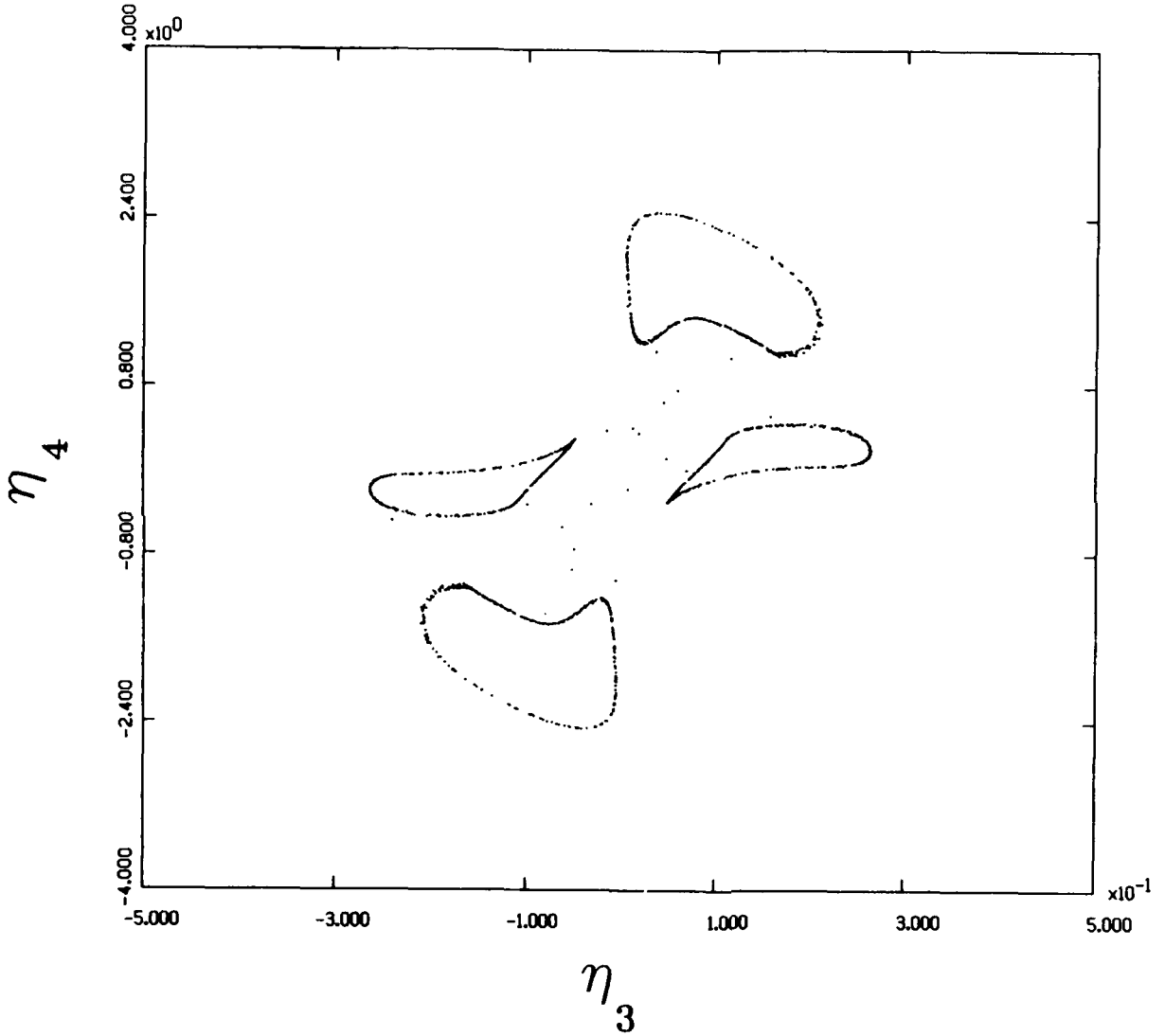

Figure 4.41 Four Pi Poincare Map of η_3 vs η_4, phase 1.2 Pi

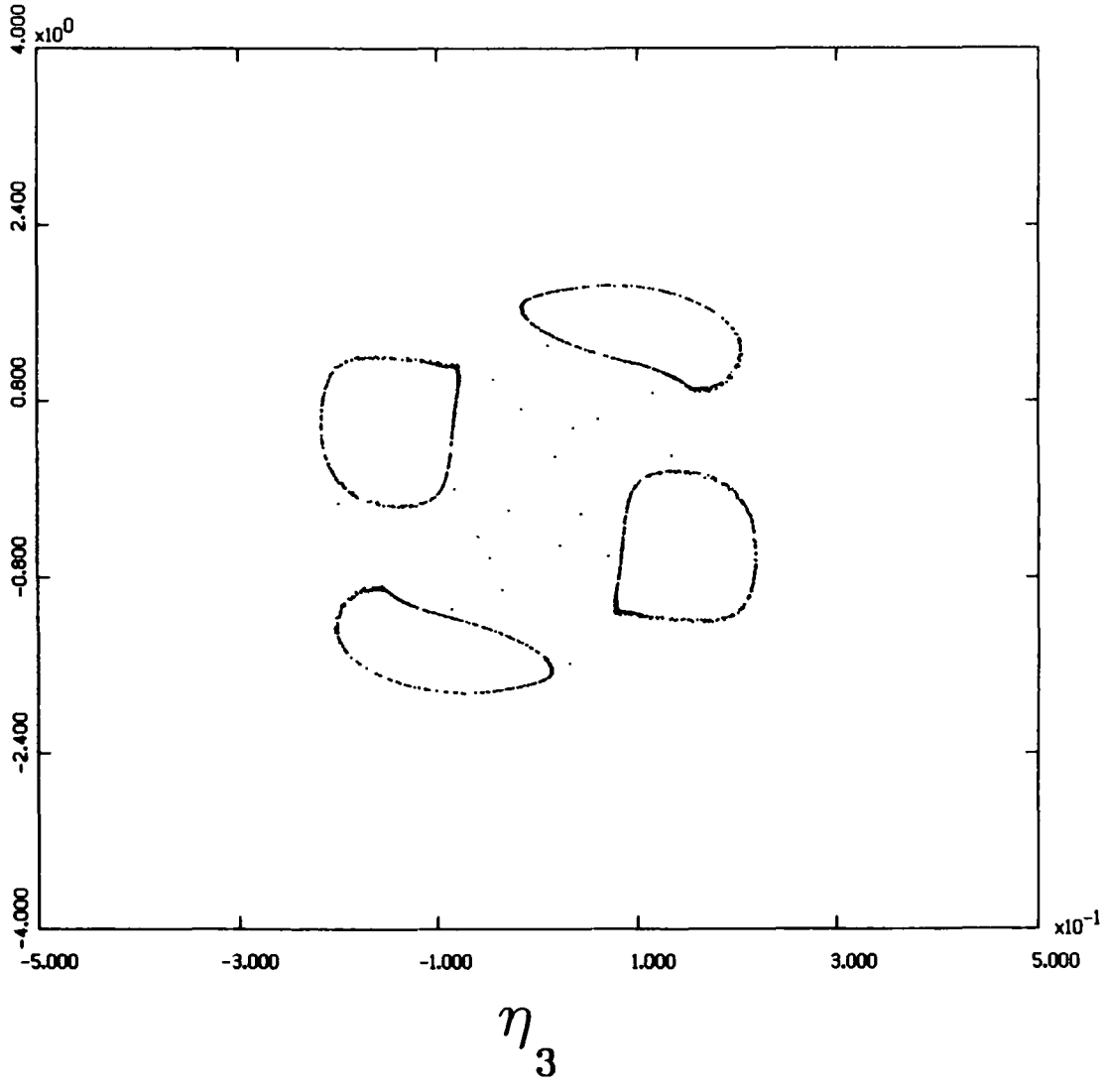

Figure 4.42 Four Pi Poincare Map of η_3 vs η_4, phase 1.6 Pi

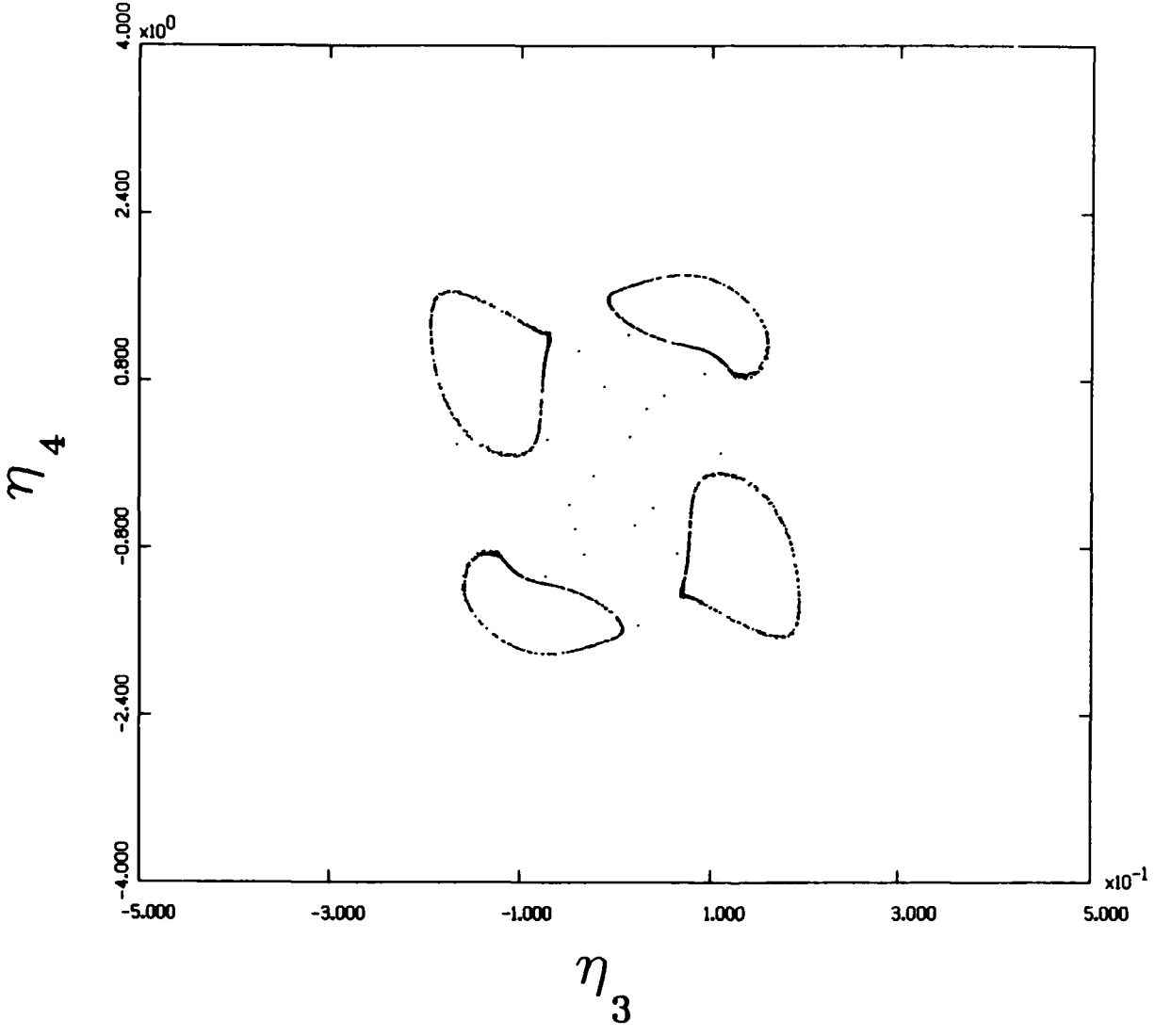

Figure 4.43 Four Pi Poincare Map of η_3 vs η_4, phase 2.0 Pi

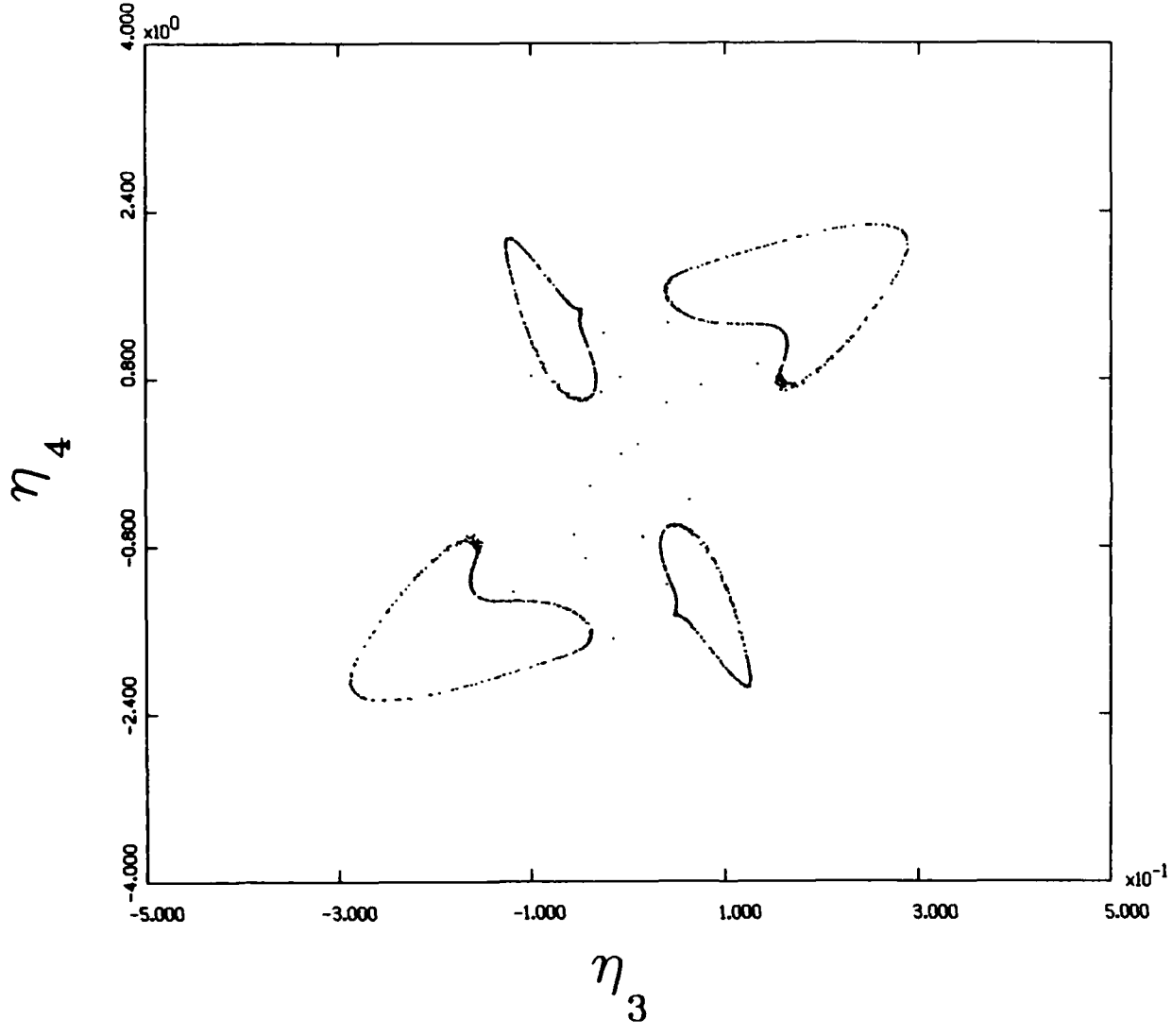

Figure 4.44 Four Pi Poincare Map of η_3 vs η_4, phase 2.4 Pi

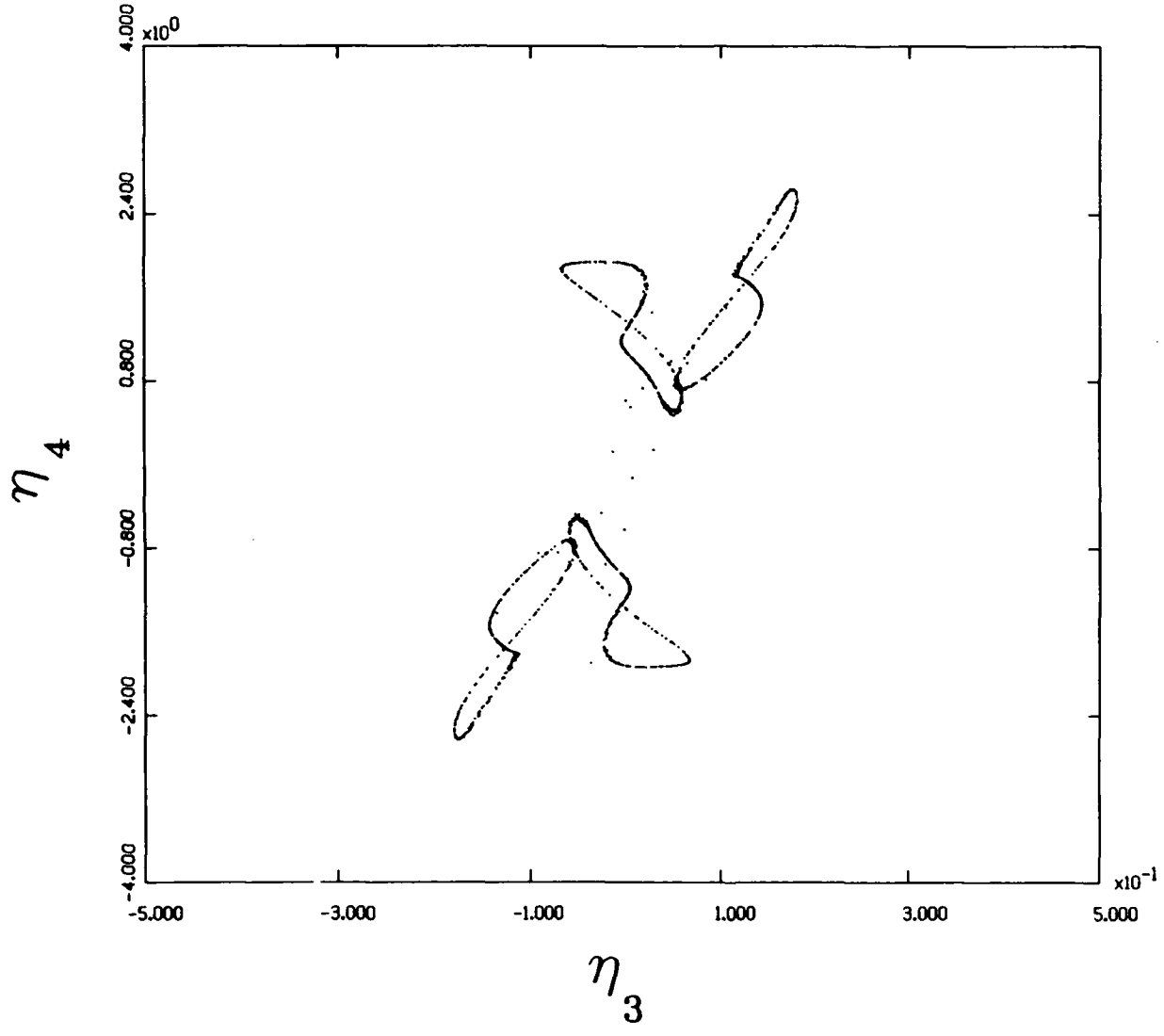

Figure 4.45 Four Pi Poincare Map of η_3 vs η_4, phase 2.8 Pi

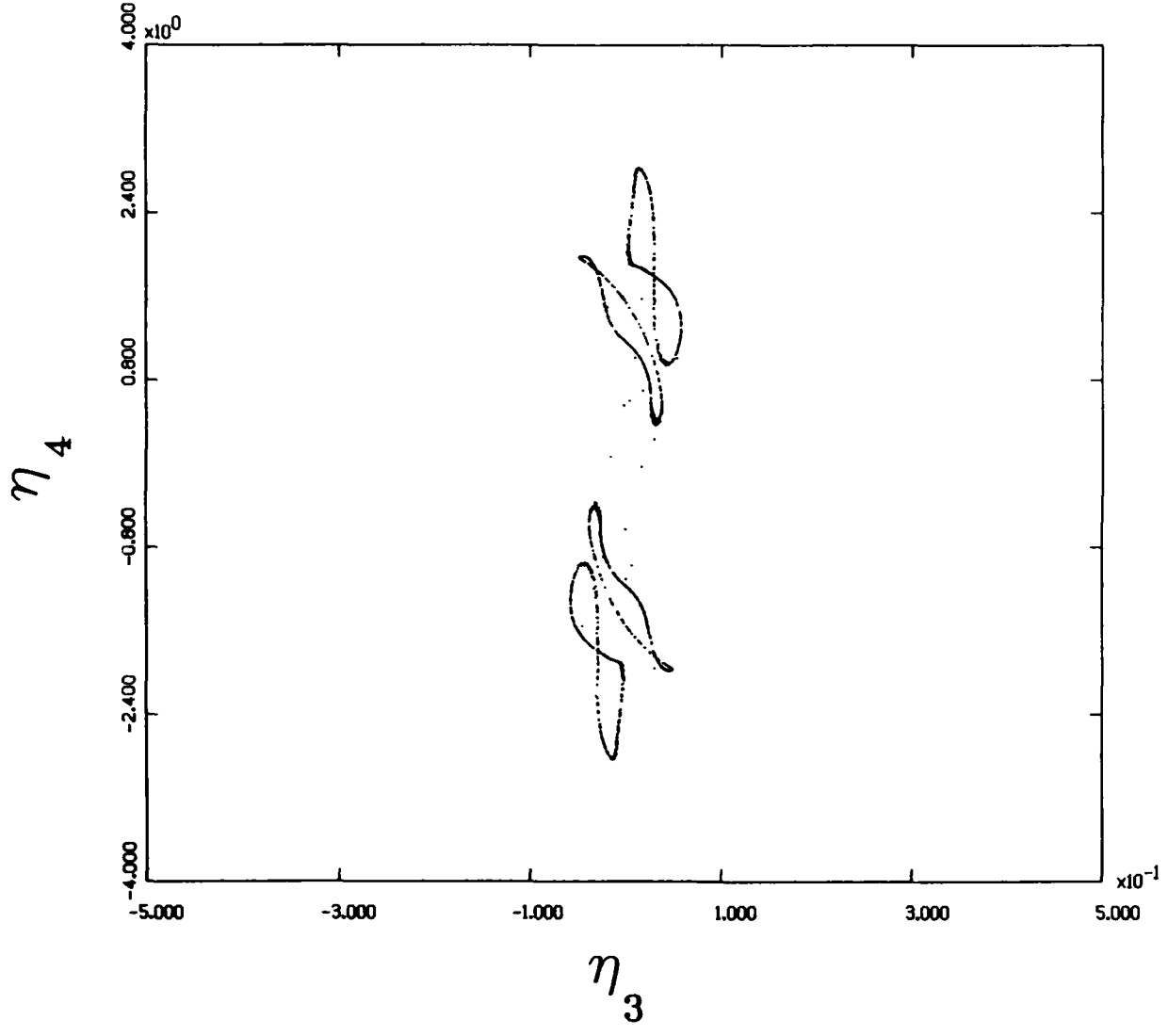

Figure 4.46 Four Pi Poincare Map of η_3 vs η_4, phase 3.2 Pi

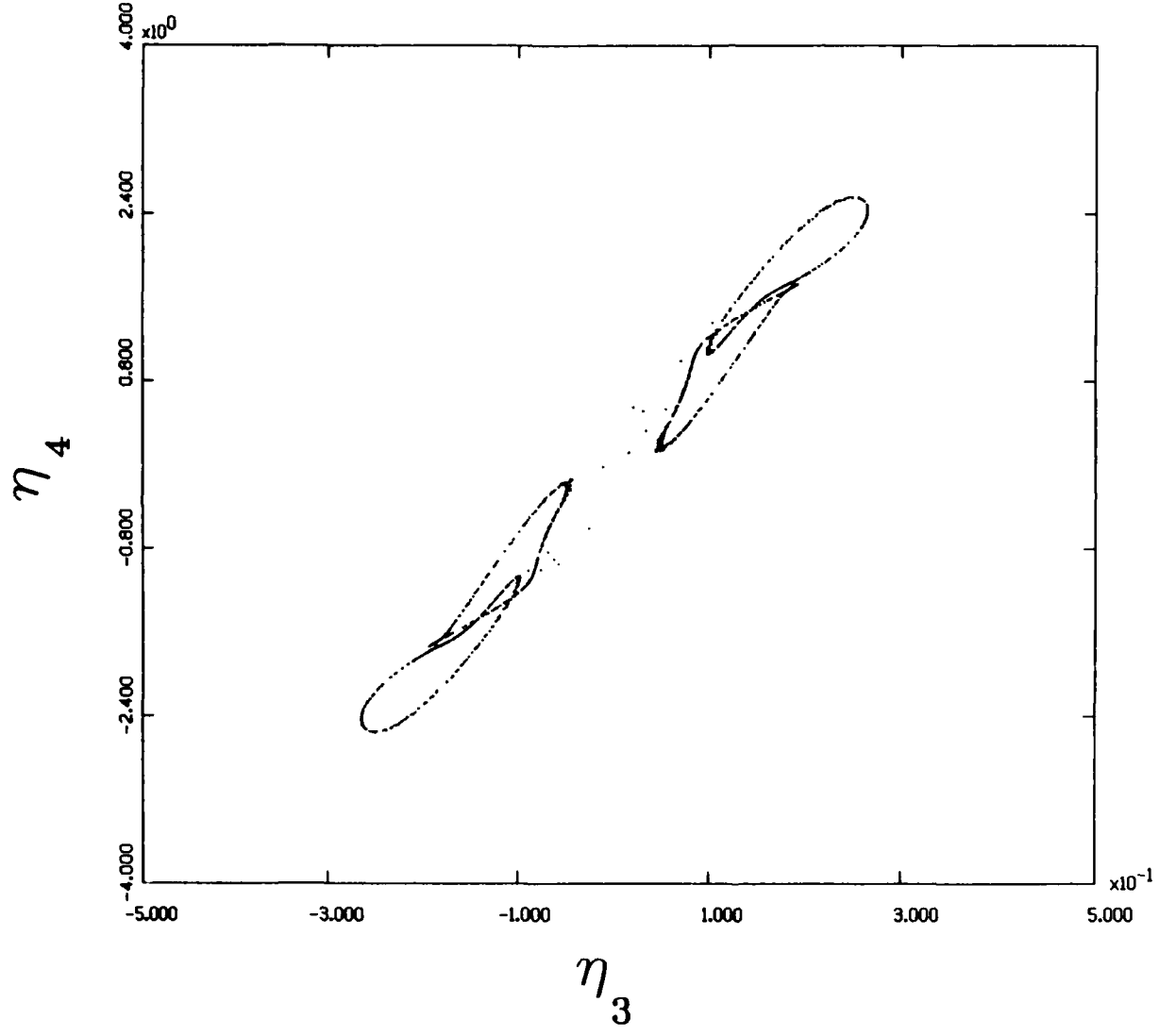

Figure 4.47 Four Pi Poincare Map of η_3 vs η_4, phase 3.6 Pi

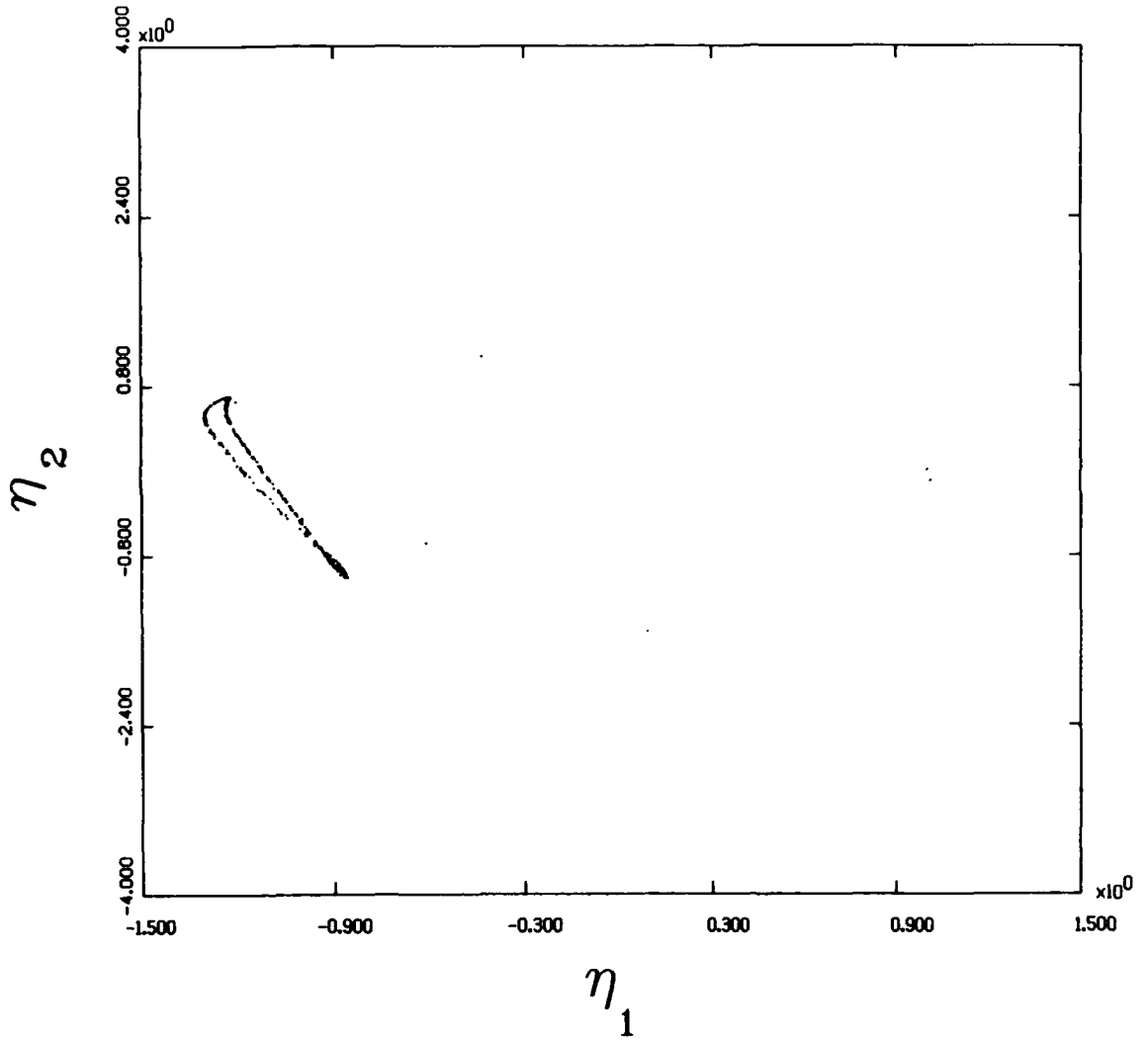

Figure 4.48 Non-linear η_1 vs η_2 16 Pi Poincare Map for 2500 orbits

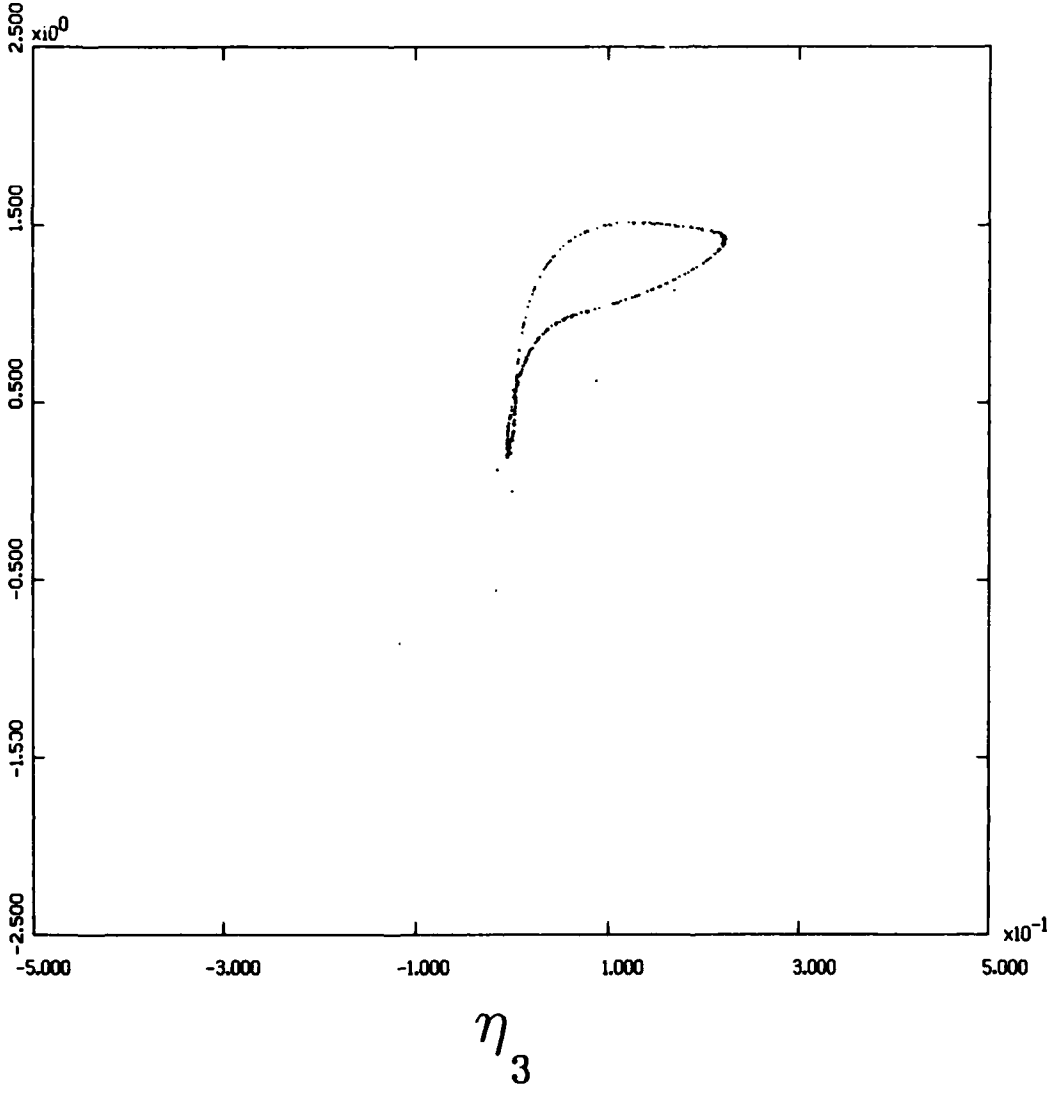

Figure 4.49 Non-linear η_3 vs η_4 16 Pi Poincare Map for 2500 orbits

Table 4.5. Starting values for η_1 axis using low gain controller

	η_1	η_2	η_3	η_4
A	0.5	0.0	0.0	0.0
B	1.0	0.0	0.0	0.0
C	1.5	0.0	0.0	0.0
D	2.0	0.0	0.0	0.0
E	3.0	0.0	0.0	0.0
F	4.0	0.0	0.0	0.0
G	5.0	0.0	0.0	0.0
H	6.0	0.0	0.0	0.0

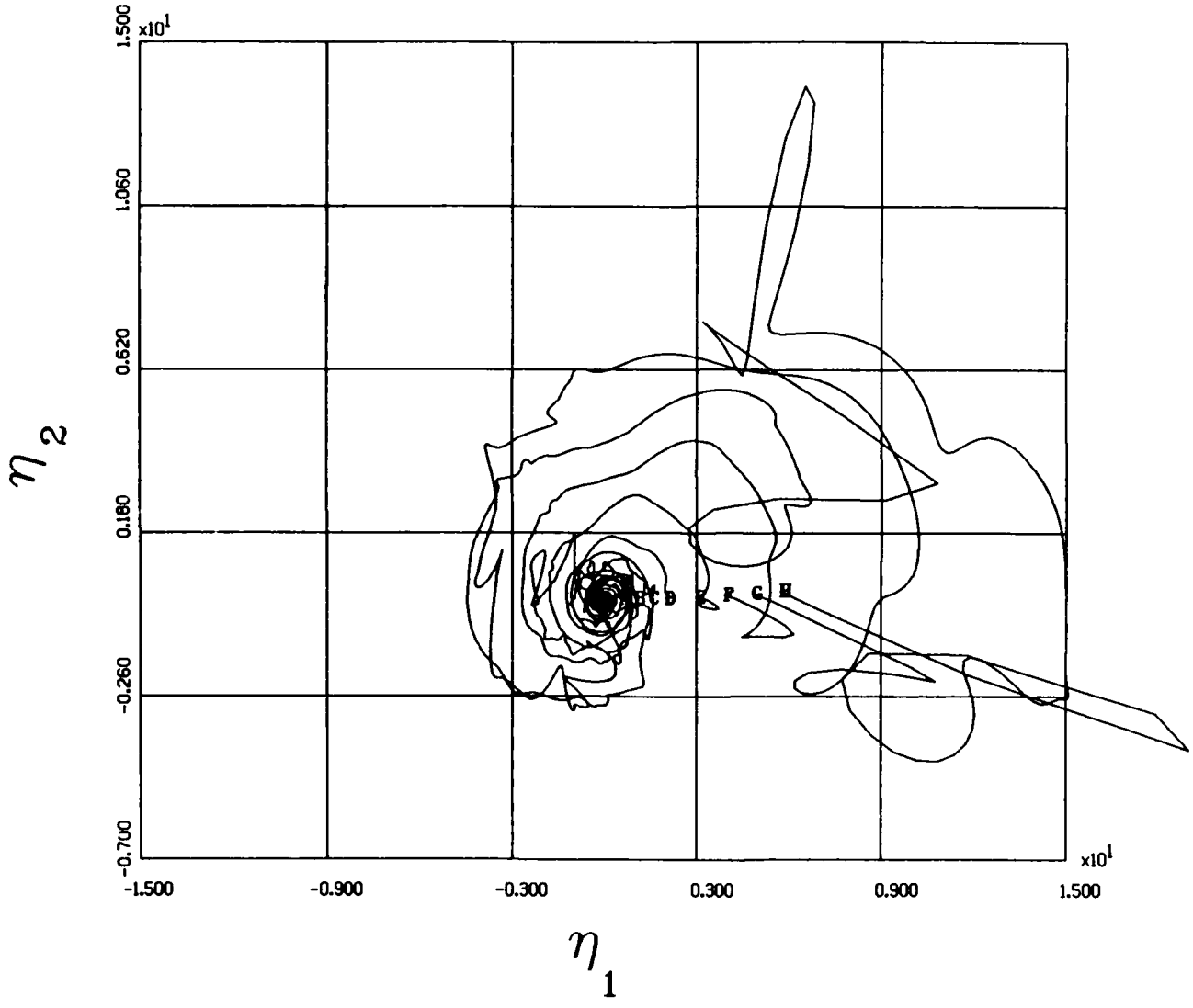

Figure 4.50 η_1 vs η_2 with low gain controller

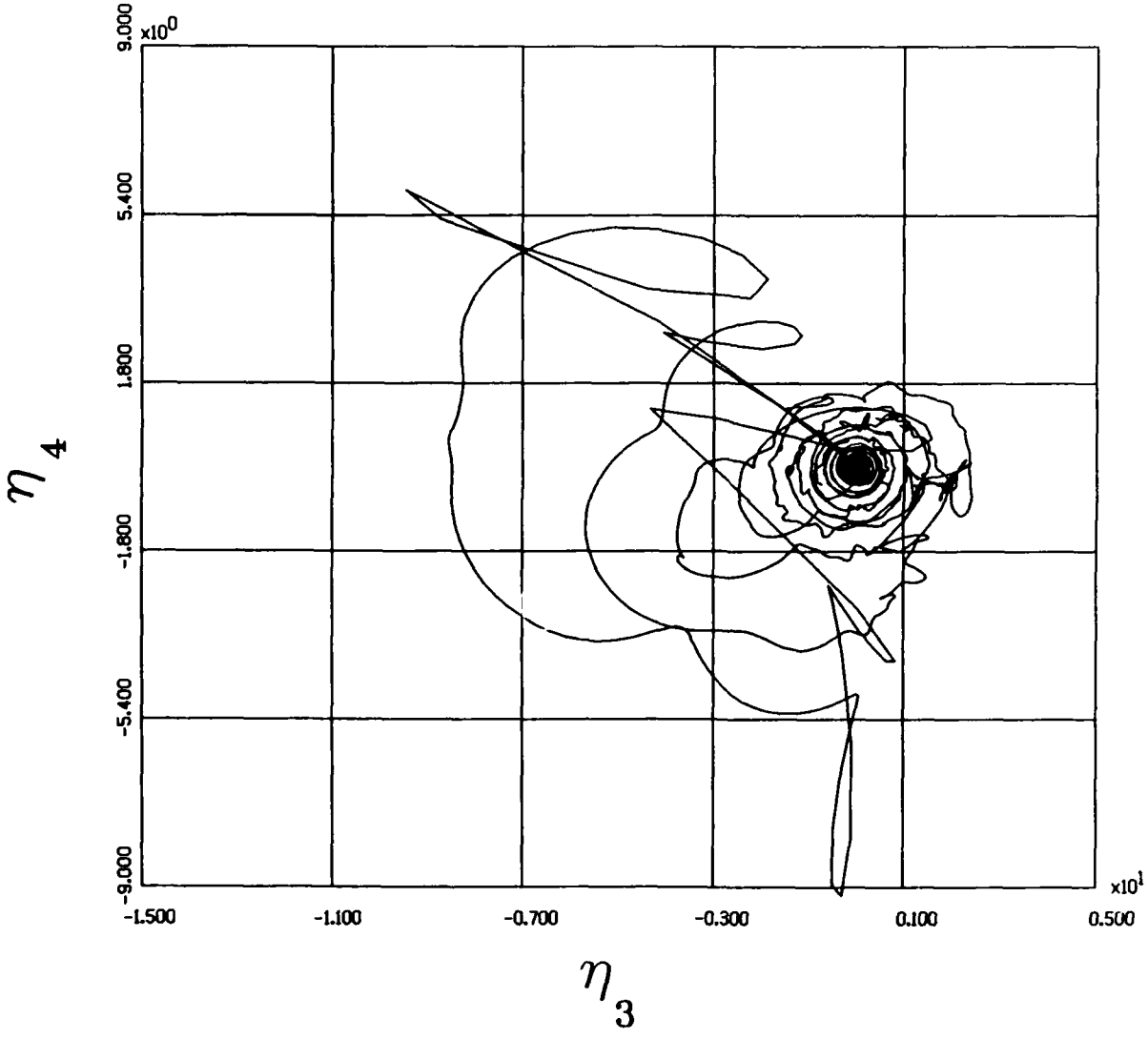

Figure 4.51 η_3 vs η_4 with low gain controller

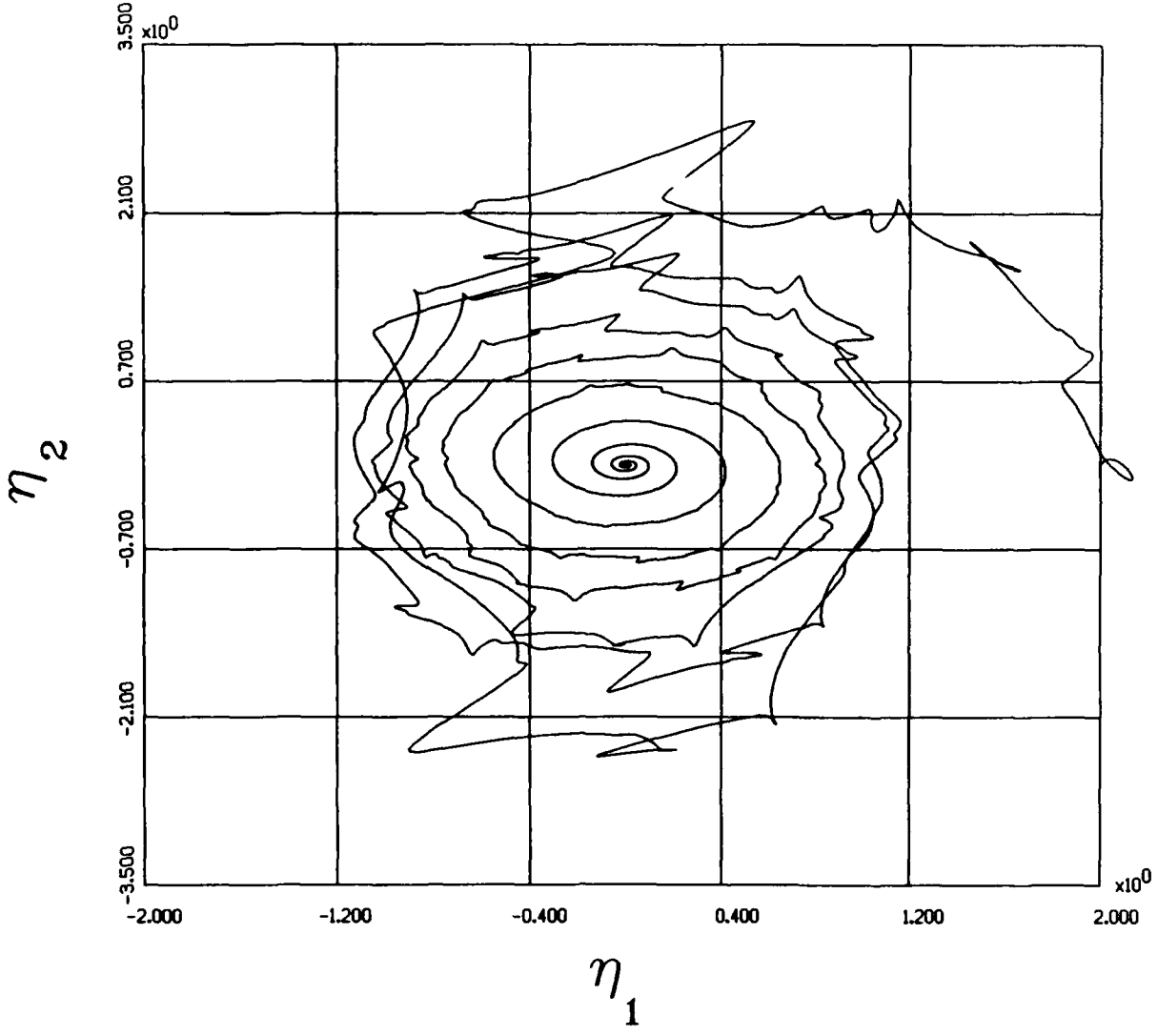

Figure 4.52 η_1 vs η_2 for 40 orbits, gain = 0.3

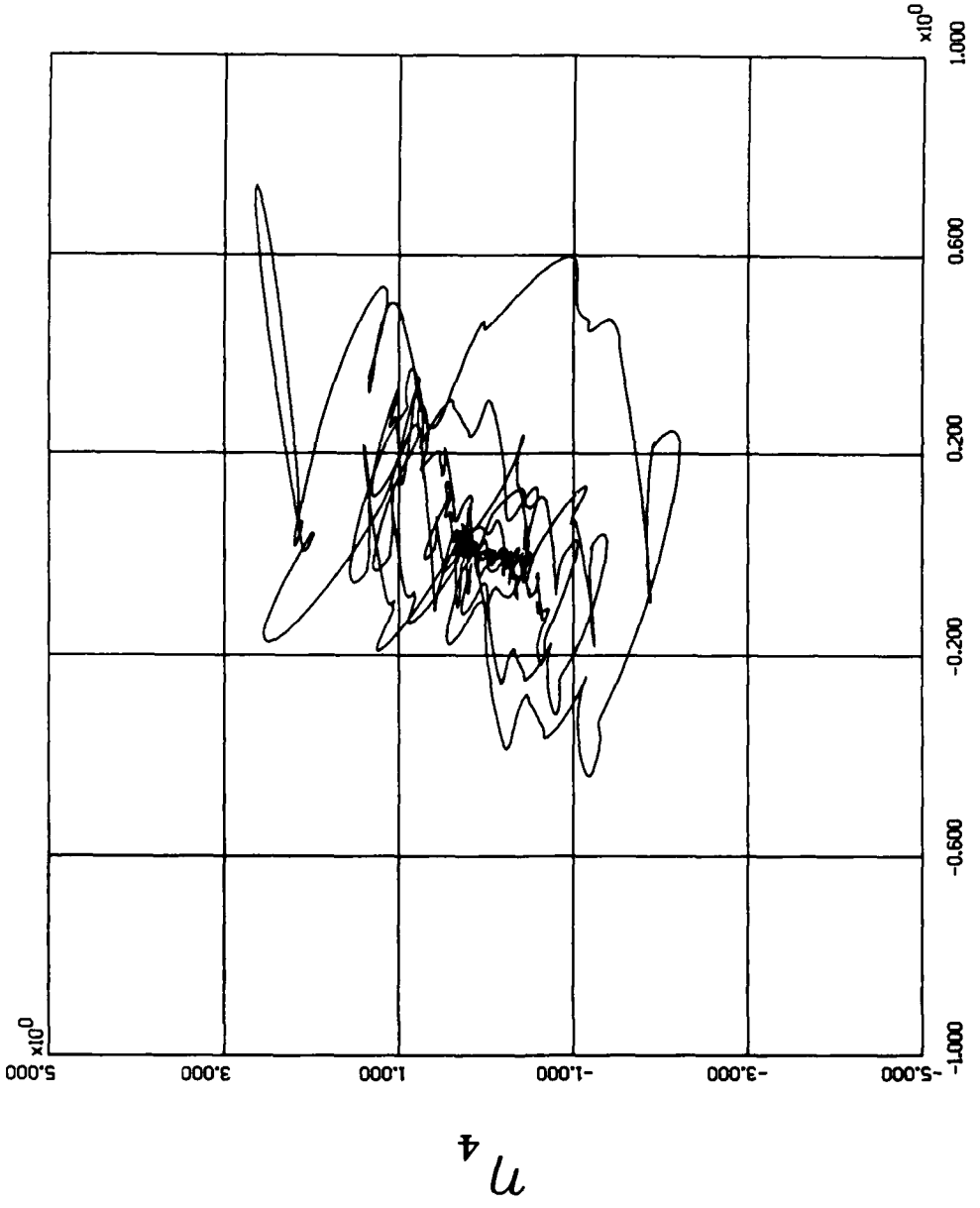

Figure 4.53 η_3 vs η_4 for 40 orbits, gain = 0.3

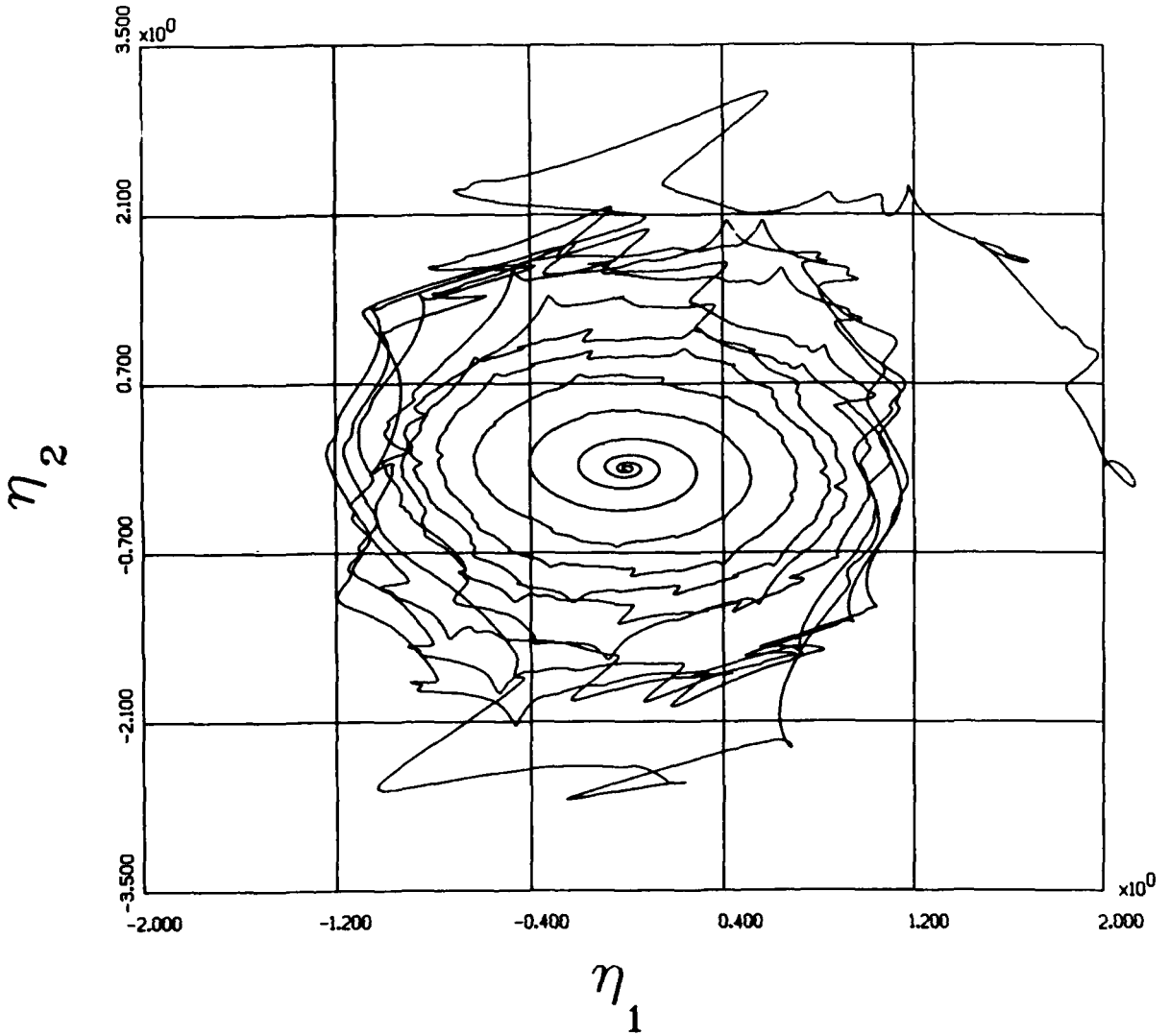

Figure 4.54 η_1 vs η_2 for 40 orbits, gain = 0.325

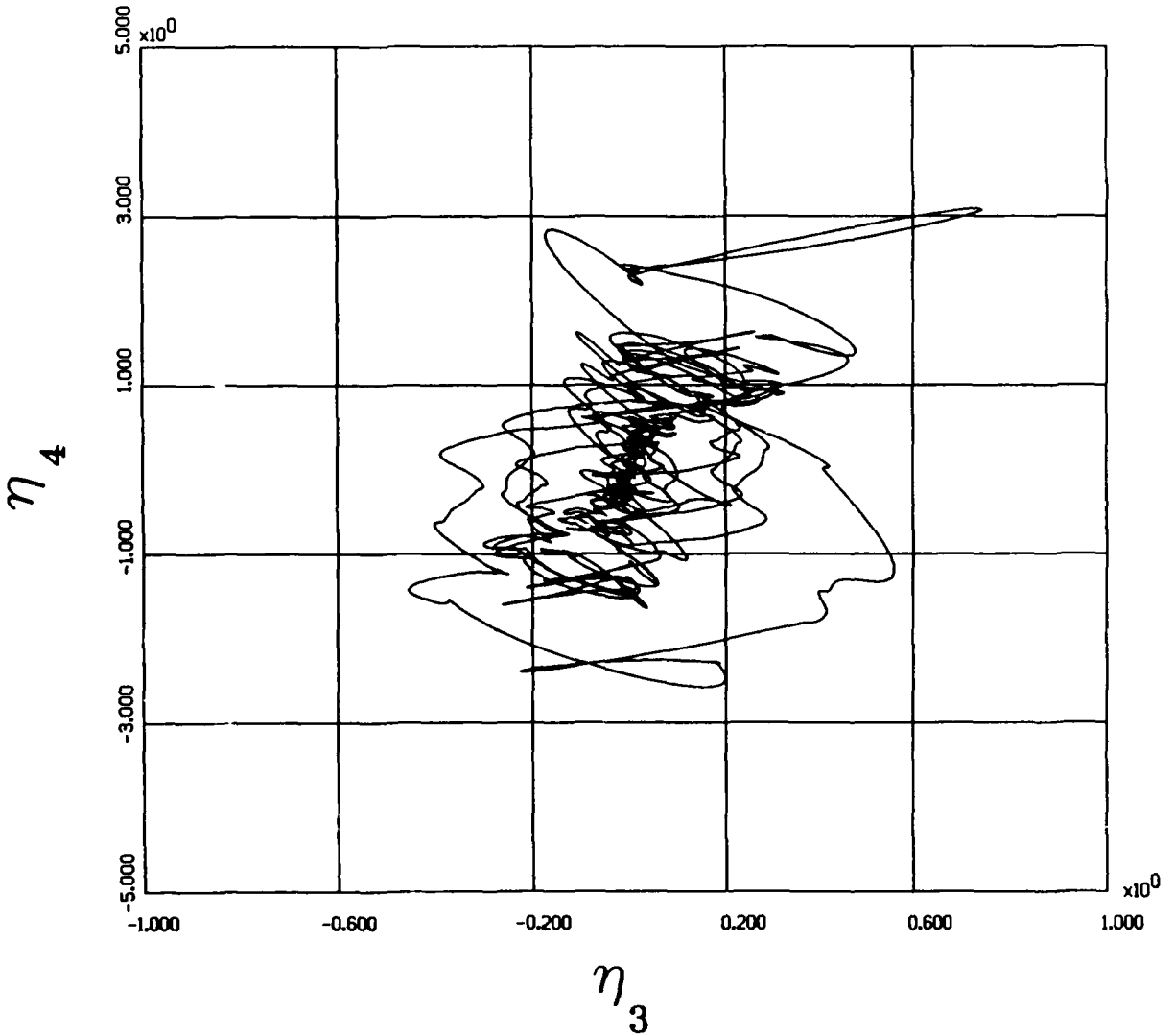

Figure 4.55 η_3 vs η_4 for 40 orbits, gain = 0.325

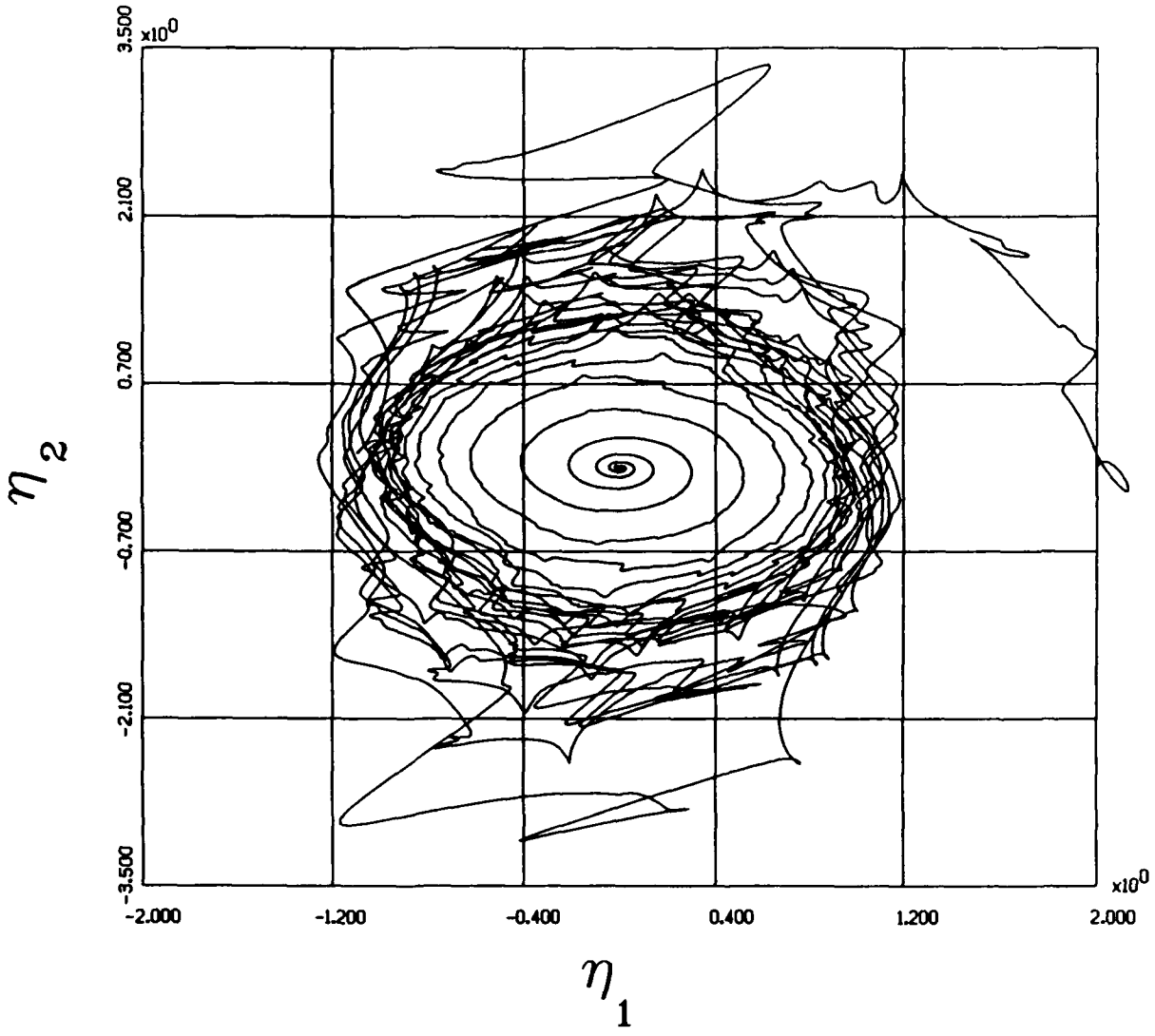

Figure 4.56 η_1 vs η_2 for 100 orbits, gain = 0.35

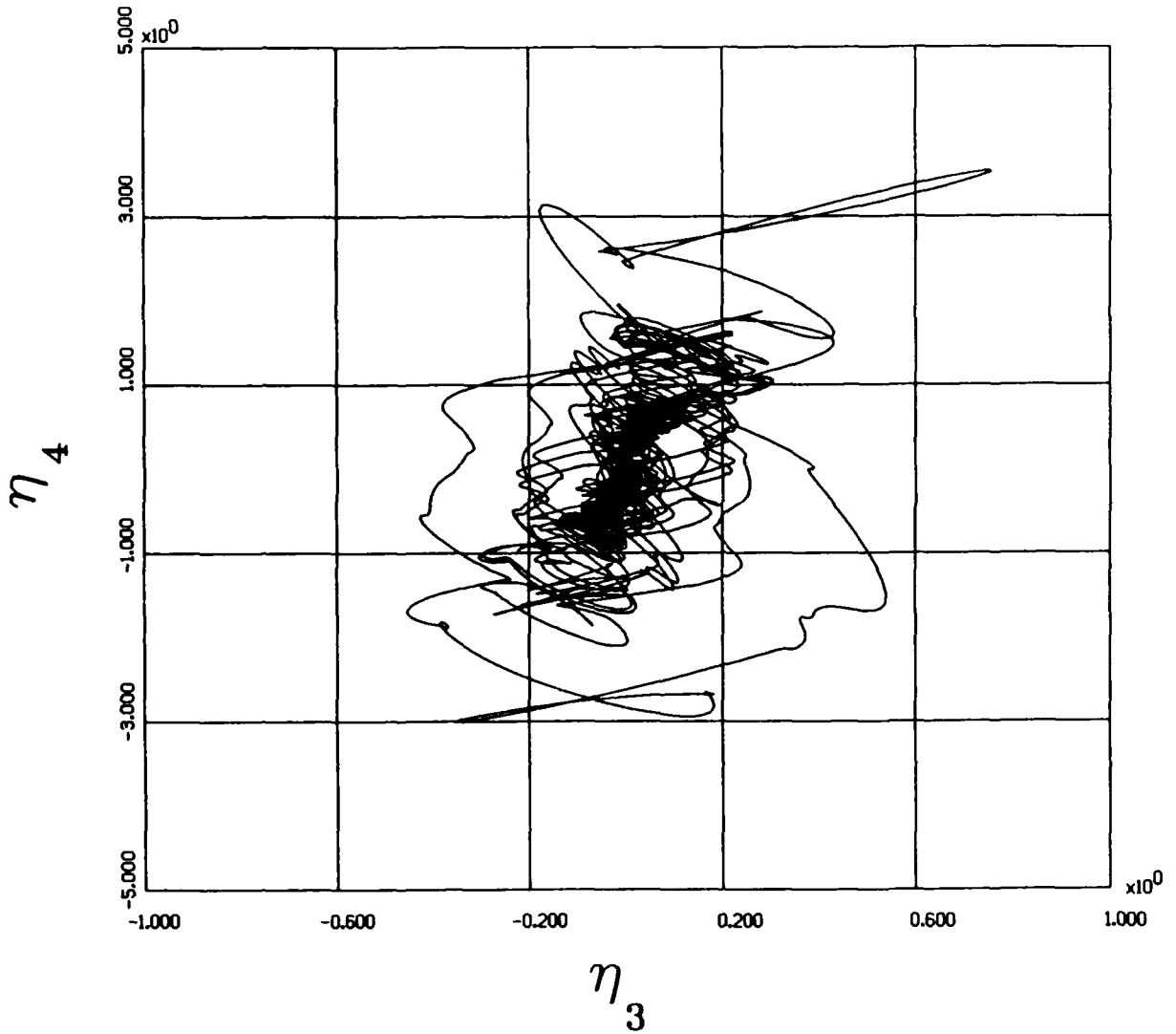

Figure 5.57 η_3 vs η_4 for 100 orbits, gain = 0.35

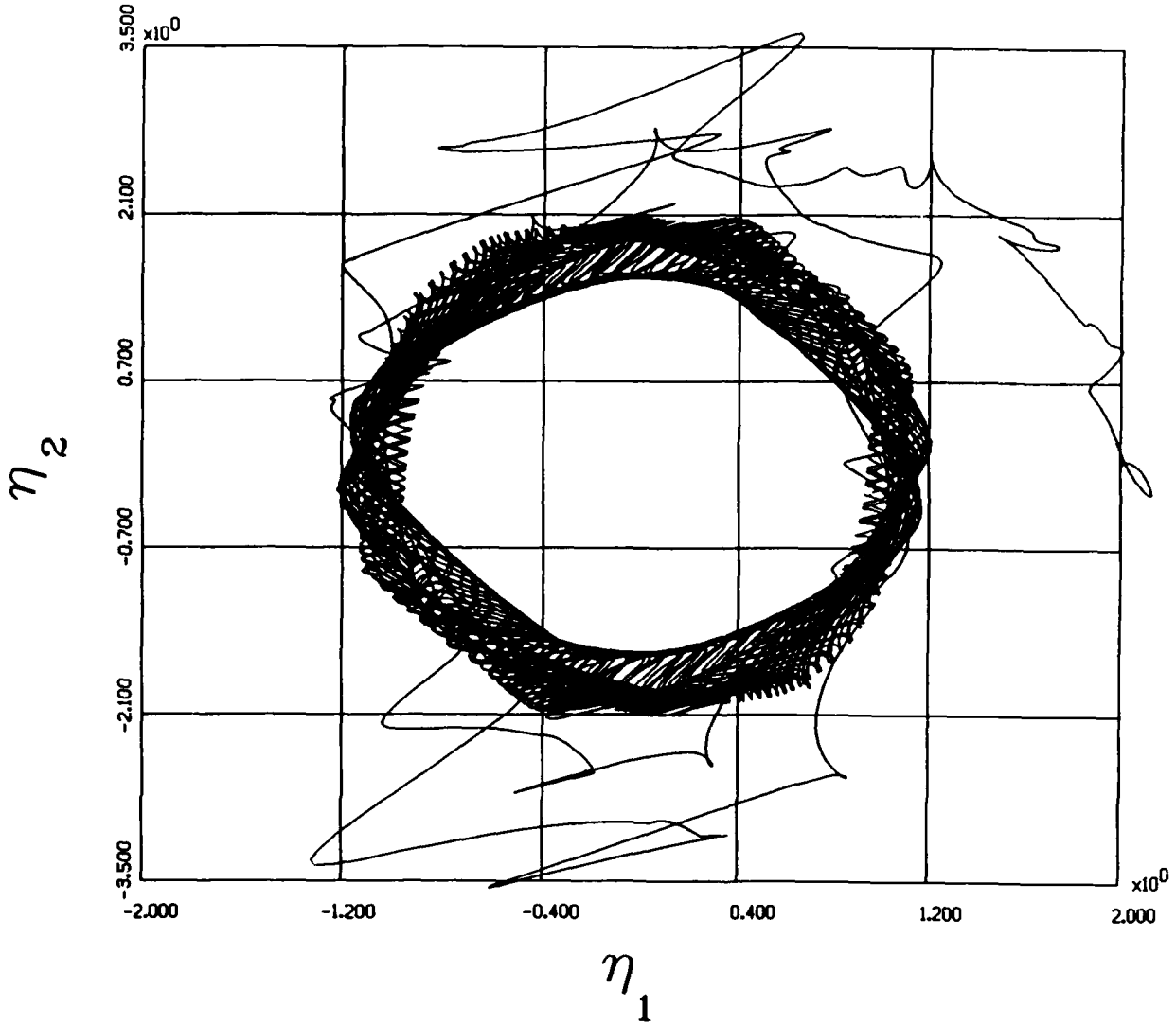

Figure 4.58 η_1 vs η_2 for 100 orbits, gain = 0.375

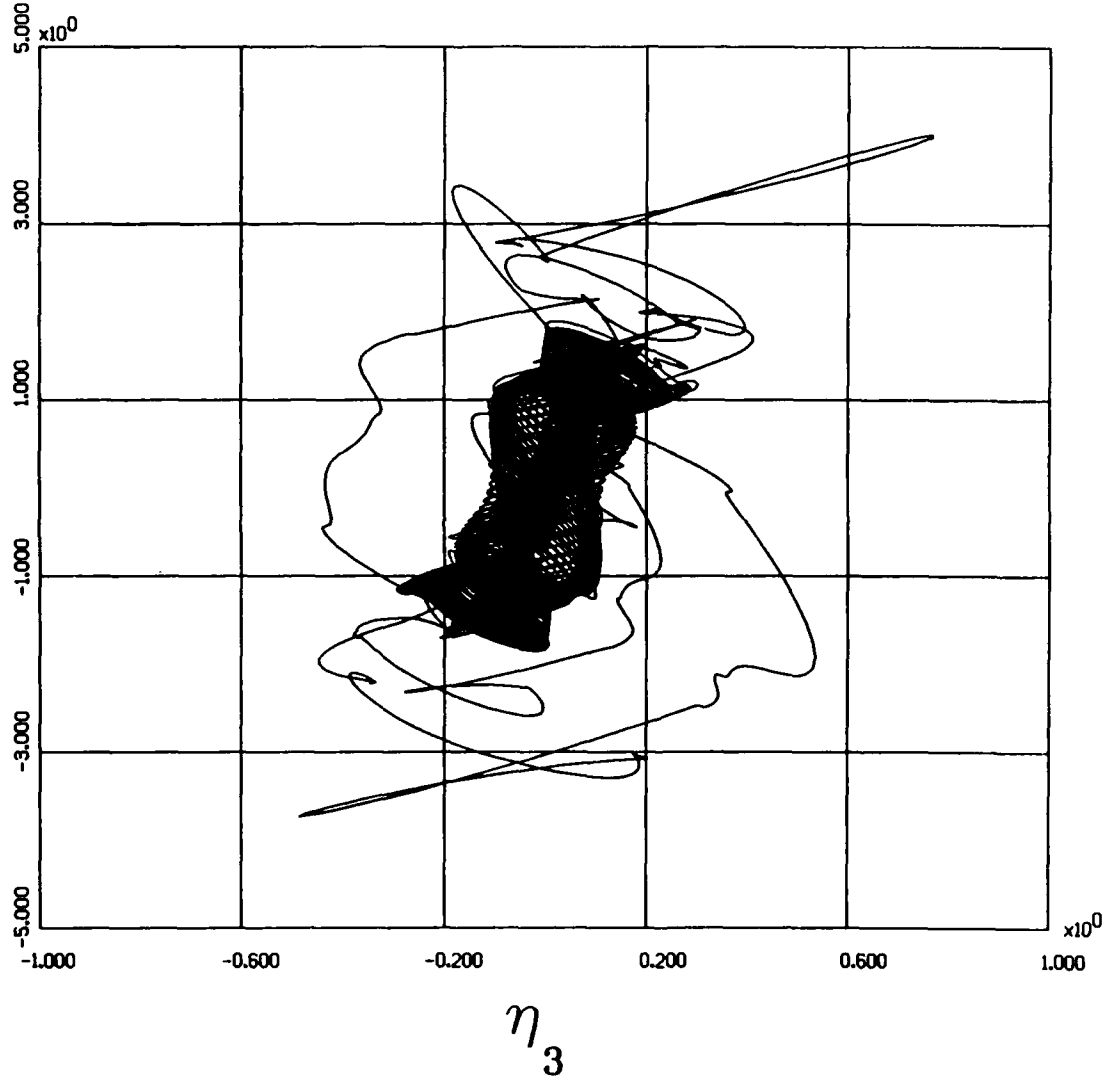

Figure 5.59 η_3 vs η_4 for 100 orbits, gain = 0.375

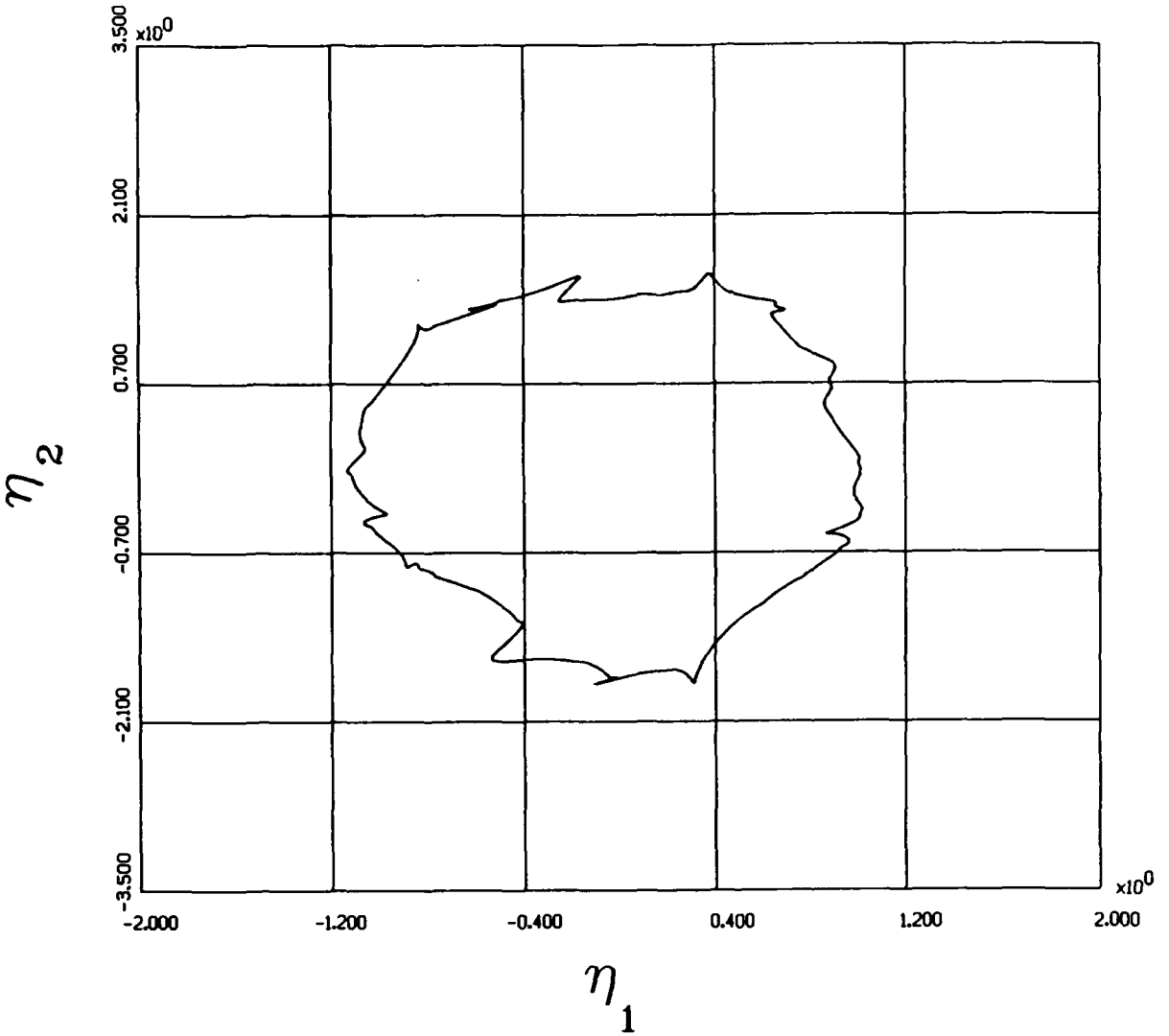

Figure 4.60 η_1 vs η_2 limit cycle behavior, gain = 0.36

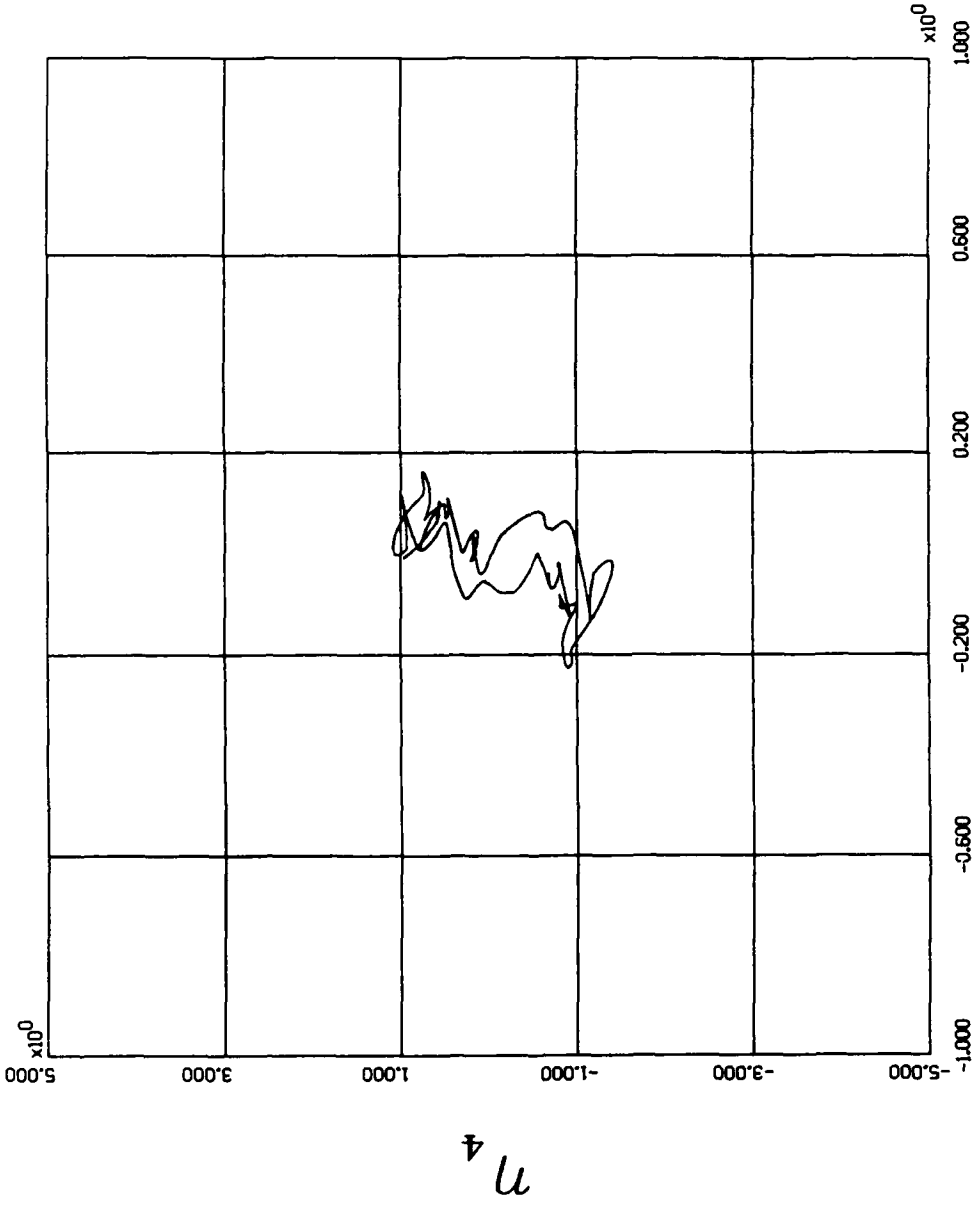

Figure 4.61 η_3 vs η_4 limit cycle behavior, gain = 0.36

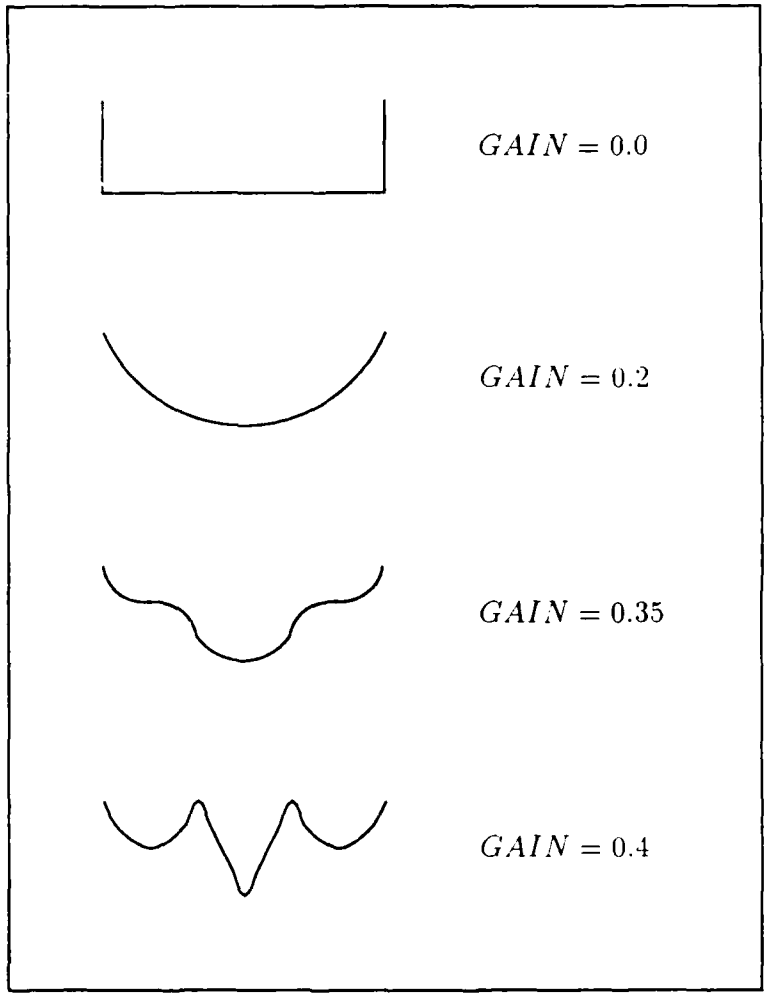

Figure 4.62. Two dimension analogy of system

V. Conclusions and Recommendations

The linearized system does give significant insight into the non-linear problem. Myers was correct in picking the intersection of the real axis as being the most stable setting for the linearized system gain. Since this is where the bifurcation occurs, this implies it is the point of highest gain that provides global stability. However, from the non-linear analysis, we can recommend gain levels up to 0.36 and still have global stability. If the risk of large perturbations is small, even higher gains could be suggested with appropriate limits. The non-linear analysis of the system has not produced an equation that will tell the control designer what value of gain to use. It does present the tools required to determine the limits of a controller in its phase space and what factors can effect its performance. Each controller will have to be evaluated individually.

Some caution needs to be taken since quick evaluations around the linearized equilibrium can be misleading. Long computer runs over a variety of starting locations is essential in evaluating the performance of a control system design. The uncontrolled system should also be examined closely to try to understand any non-linear features. Evaluation using the full non-linear equations of motion is justified in many instances. The study of higher order systems may require additional computer resources.

Sometimes performance must be traded for increased range of stability. This would be true in the example problem where one would have to set the gains for longer settling times to be prepared for the case the satellite should be bumped very far from the equilibrium. One could not risk burning up the controller resources and losing a satellite just to provide a faster correction.

The same techniques that have been used to examine this scalar controller could be applied to evaluate other controllers. The vector controller in the same satellite is an obvious next step.

Appendix A. *Equations of Motion*

This appendix develops the equations of motion of a spinning inertially symmetric satellite in an elliptical orbit around a symmetrical attracting body. The spin axis of the satellite is along the inertial axis of symmetry and perpendicular to the orbit plane. The equations that describe the attitude of the satellite are presented and they are linearized about an equilibrium point. Both the linearized and non-linear attitude equations of motion are developed.

The motion and stability of a symmetrical satellite in an elliptical orbit has been examined previously. Kane and Barba developed the linearized equations that describe the attitude motion of the satellite. This section is taken from their work [8] and the expressions for the non-linear equations of motion were taken from the thesis by Captain Dale Shell [14:2.23-2.25].

A.1 Orbit Equations

Two basic equations describe the trajectory of a satellite in orbit around a spherically symmetric attracting body. These equations are developed in any introductory astrodynamics text, for example see [16]. The equations are:

$$\ddot{r} - r\dot{\nu}^2 + \frac{n^2 a^3}{r^2} = 0 \tag{A.1}$$

and,

$$r^2\dot{\nu} = a^2 n(1-\epsilon^2)^{1/2} \tag{A.2}$$

where the "mean motion", n, is

$$n = 2\pi/T \tag{A.3}$$

and T is the period of the orbit. The orbital elements r, ν, a and ϵ are defined in Figure A.1. r and ν are the polar coordinates of the center of mass of the satellite.

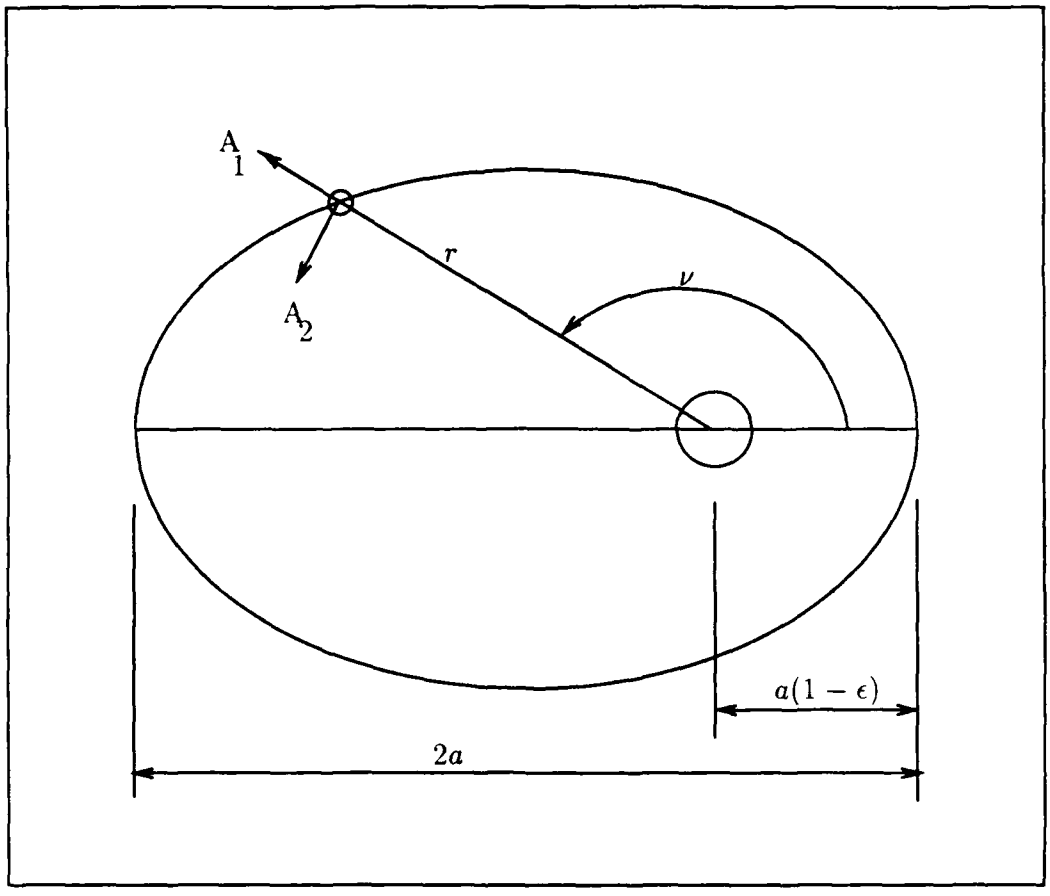

Figure A.1. Elliptical Orbit Elements

ϵ represents the eccentricity of the orbit and a is the major semidiameter.

This system can be nondimensionalized by introducing two new variables.

$$\tau = nt \tag{A.4}$$

and

$$\zeta = r/a \tag{A.5}$$

Equation A.2 can be used to eliminate $\dot{\nu}$ from equation A.1. Rearrange equation

A.2 to solve for $\dot{\nu}$

$$\dot{\nu} = \frac{a^2 n(1-\epsilon^2)^{1/2}}{r^2} \tag{A.6}$$

Substituting this into equation A.1 yields

$$\ddot{r} - \frac{a^4 n^2(1-\epsilon^2)}{r^3} + \frac{n^2 a^3}{r^2} = 0 \tag{A.7}$$

To nondimensionalize this equation, we must define differentiation with respect to the nondimensional time, τ. All derivatives that are taken with respect to τ will be shown as primes.

$$\dot{r} = \frac{dr}{dt} = \frac{d}{d\tau}\left(\frac{d\tau}{dt} r\right) = \frac{d}{d\tau}(n\zeta a) = \zeta' n a \tag{A.8}$$

and

$$\ddot{r} = \frac{d}{dt}\left(\frac{dr}{dt}\right) = \frac{d}{d\tau}\left(\frac{d\tau}{dt}\left(\frac{dr}{dt}\right)\right) = \zeta'' n^2 a \tag{A.9}$$

Now divide equation A.7 by $n^2 a$ to get

$$\frac{\ddot{r}}{n^2 a} + \frac{(\epsilon^2 - 1)a^3}{r^3} + \frac{a^2}{r^2} = 0 \tag{A.10}$$

Then substitute in equations A.8 and A.9 this reduces to the nondimensional form

$$\zeta'' + \frac{1}{\zeta^2} + \frac{\epsilon^2 - 1}{\zeta^3} = 0 \tag{A.11}$$

To nondimensionalize equation A.6 using equations A.4 and A.5 note

$$\frac{d\nu}{d\tau} = \frac{d\nu}{dt}\frac{dt}{d\tau} = \left(\frac{a^2 n(1-\epsilon^2)^{1/2}}{r^2}\right)\left(\frac{1}{n}\right) \tag{A.12}$$

this reduces to

$$\nu' = \frac{(1-\epsilon^2)^{1/2}}{\zeta^2} \tag{A.13}$$

and differentiate again with respect to τ

$$\frac{d}{d\tau}(\nu') = \frac{d}{d\tau}\left(\frac{(1-\epsilon^2)^{1/2}}{\zeta^2}\right) \tag{A.14}$$

or

$$\nu'' = \frac{2(1-\epsilon^2)^{1/2}}{\zeta^3}\zeta' \tag{A.15}$$

This is the nondimensional form of both orbit differential equations. The initial conditions are arbitrarily selected such that the satellite is at the perigee when $t = \tau = 0$. It then follows that

$$r(0) = a(1-\epsilon) \tag{A.16}$$

and

$$\dot{r}(0) = 0 \tag{A.17}$$

and converting it to the nondimensional form

$$\zeta(0) = 1 - \epsilon \tag{A.18}$$

and

$$\zeta'(0) = 0 \tag{A.19}$$

It is now possible to numerically integrate this set of equations to find the path of the center of mass of the satellite. It will be necessary to have solutions to these two equations to provide inputs to the satellite attitude equations.

A.2 Attitude Equations

The orbit equations of motion assume the motion of the center of mass of the satellite is unaffected by the orientation of the satellite. The attitude equations are not, however, independent of the orbit motion.

Figure A.2 defines an orbital reference frame A. A_1 points outward along

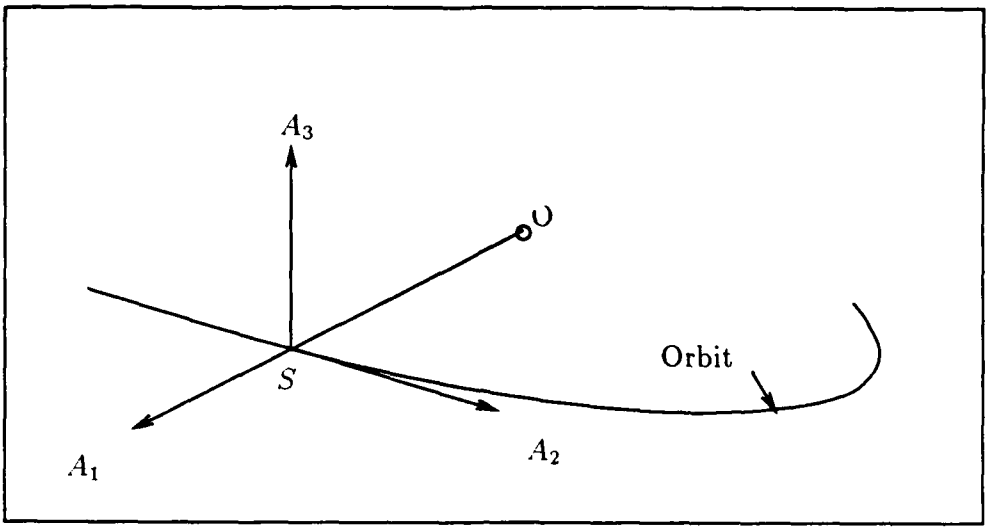

Figure A.2. Orbit Reference Frame

the orbit radius, A_2 is perpendicular to A_1 and in the orbit plane. At perigee the satellite is moving only in the positive A_2 direction. A_3 is perpendicular to A_1 and A_2, pointing out of the orbit plane to form a right-hand system.

The body axis frame D is obtained by a 1-2-3 rotation from the A frame as shown in Figure A.3. The three angles, θ_1, θ_2 and θ_3 describe the magnitude and direction of the three rotations. ϕ is the angle measured from the A_3 axis to the spin axis of the satellite, D_3. Taking advantage of the symmetry of the satellite, the nodal axis C can be used to simplify the analysis. The C axis is obtained through only a 1-2 rotation. This leaves us one rotation away from the body axis, but the body is symmetric along this axis. To develop an expression for the angular velocity of the satellite in the nodal coordinates C, we start by writing the angular velocity

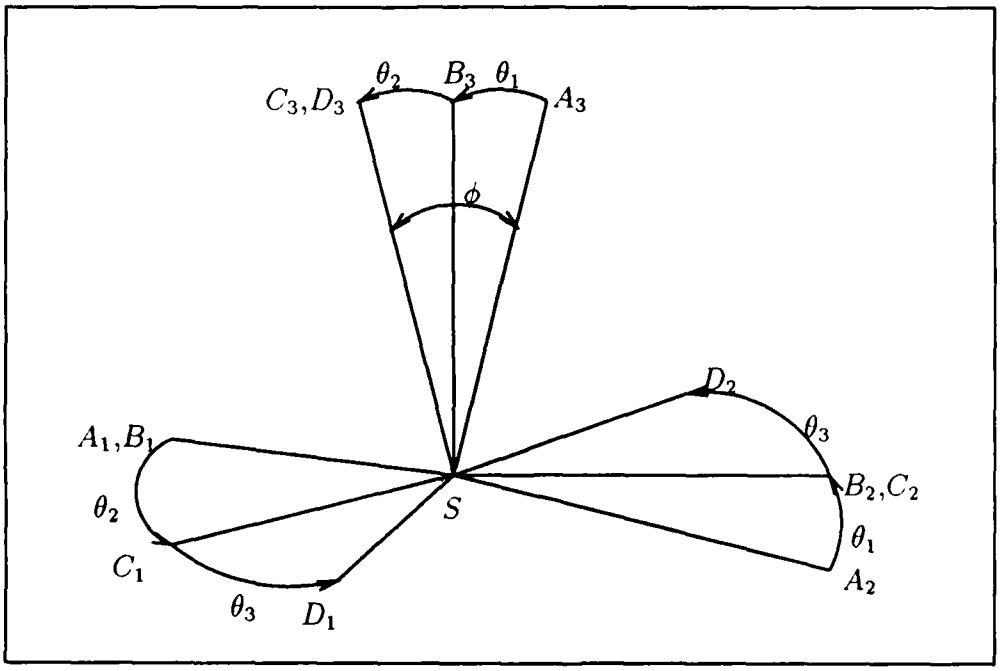

Figure A.3. Body Reference Frame

of the reference frame A with respect to an inertial frame.

$$\bar{\omega}^{A/I} = \dot{\nu}\hat{e}_{A_3} = \left\{ \begin{array}{c} 0 \\ 0 \\ \dot{\nu} \end{array} \right\} \tag{A.20}$$

The relative rotation rates of the other reference frames are

$$\bar{\omega}^{B/A} = \dot{\theta}_1\hat{e}_{B_1} = \dot{\theta}_1\hat{e}_{A_1} = \left\{ \begin{array}{c} \dot{\theta}_1 \\ 0 \\ 0 \end{array} \right\} \tag{A.21}$$

$$\bar{\omega}^{C/B} = \dot{\theta}_2\hat{e}_{B_2} = \dot{\theta}_2\hat{e}_{C_2} = \left\{ \begin{array}{c} 0 \\ \dot{\theta}_2 \\ 0 \end{array} \right\} \tag{A.22}$$

$$\bar{\omega}^{D/C} = \dot{\theta}_3\hat{e}_{C_3} = \dot{\theta}_3\hat{e}_{D_3} = \left\{ \begin{array}{c} 0 \\ 0 \\ \dot{\theta}_3 \end{array} \right\} \tag{A.23}$$

and the angular velocity of the satellite, expressed in the nodal axes is the sum of these components

$$\bar{\omega}^{D/I} = \left\{ \begin{array}{c} \omega_1 \\ \omega_2 \\ \omega_3 \end{array} \right\}_C \tag{A.24}$$

To add these components of the angular velocity, they must be expressed in the same reference frame and hence we transform all components to the nodal axis C. For more information on nodal axis usage can be found in [10].

$$\left\{\omega^{D/I}\right\}_C = \left\{\omega^{C/B}\right\}_C + L_{CB}\left\{\omega^{B/A}\right\}_B + L_{CA}\left\{\omega^{A/I}\right\}_A + L_{CD}\left\{\omega^{D/C}\right\}_D \tag{A.25}$$

Where the transformation matrices are defined as

$$L_{CB} = \begin{bmatrix} \cos\theta_2 & 0 & -\sin\theta_2 \\ 0 & 1 & 0 \\ \sin\theta_2 & 0 & \cos\theta_2 \end{bmatrix} \tag{A.26}$$

$$L_{BA} = \begin{bmatrix} 1 & 0 & 0 \\ 0 & \cos\theta_1 & \sin\theta_1 \\ 0 & -\sin\theta_1 & \cos\theta_1 \end{bmatrix} \tag{A.27}$$

$$L_{CA} = L_{CB}L_{BA} = \begin{bmatrix} \cos\theta_2 & \sin\theta_1\sin\theta_2 & -\cos\theta_1\sin\theta_2 \\ 0 & \cos\theta_1 & \sin\theta_1 \\ \sin\theta_2 & -\sin\theta_1\cos\theta_2 & \cos\theta_1\cos\theta_2 \end{bmatrix} \tag{A.28}$$

$$L_{CD} = \begin{bmatrix} \cos\theta_3 & \sin\theta_3 & 0 \\ -\sin\theta_3 & \cos\theta_3 & 0 \\ 0 & 0 & 1 \end{bmatrix} \tag{A.29}$$

Then, making the appropriate substitutions into equation A.25, all components of the angular velocity are transformed into the nodal reference frame.

$$\begin{aligned} \left\{\omega^{D/I}\right\}_C = & \begin{Bmatrix} 0 \\ \dot\theta_2 \\ 0 \end{Bmatrix} + \begin{bmatrix} \cos\theta_2 & 0 & -\sin\theta_2 \\ 0 & 1 & 0 \\ \sin\theta_2 & 0 & \cos\theta_2 \end{bmatrix} \begin{Bmatrix} \dot\theta_1 \\ 0 \\ 0 \end{Bmatrix} + \\ & \begin{bmatrix} \cos\theta_2 & \sin\theta_1\sin\theta_2 & -\cos\theta_1\sin\theta_2 \\ 0 & \cos\theta_1 & \sin\theta_1 \\ \sin\theta_2 & -\sin\theta_1\cos\theta_2 & \cos\theta_1\cos\theta_2 \end{bmatrix} \begin{Bmatrix} 0 \\ 0 \\ \dot\nu \end{Bmatrix} + \\ & \begin{bmatrix} \cos\theta_3 & \sin\theta_3 & 0 \\ -\sin\theta_3 & \cos\theta_3 & 0 \\ 0 & 0 & 1 \end{bmatrix} \begin{Bmatrix} 0 \\ 0 \\ \dot\theta_3 \end{Bmatrix} \end{aligned} \tag{A.30}$$

After performing the matrix algebra, this reduces to the final expression for the angular velocity of the satellite in nodal coordinates.

$$\left\{\omega^{D/I}\right\}_C = \left\{ \begin{array}{c} \dot{\theta}_1 \cos\theta_2 - \dot{\nu}\cos\theta_1 \sin\theta_2 \\ \dot{\theta}_2 + \dot{\nu}\sin\theta_1 \\ \dot{\theta}_1 \sin\theta_2 + \dot{\nu}\cos\theta_1 \cos\theta_2 + \dot{\theta}_3 \end{array} \right\}_C \tag{A.31}$$

By defining $\acute{\omega}_3 \equiv \omega_3 - \dot{\theta}_3$ then the angular velocity can be expressed as

$$\left\{\omega^{D/I}\right\}_C = \left\{\omega^{C/I}\right\}_C + \left\{\omega^{D/C}\right\}_C = \left\{ \begin{array}{c} \omega_1 \\ \omega_2 \\ \omega_3 \end{array} \right\}_C = \left\{ \begin{array}{c} \omega_1 \\ \omega_2 \\ \acute{\omega}_3 + \dot{\theta}_3 \end{array} \right\}_C \tag{A.32}$$

Also,

$$\acute{\omega}_3 = \dot{\theta}_1 \sin\theta_2 + \dot{\nu}\cos\theta_1 \cos\theta_2 \tag{A.33}$$

This expression will be useful in the development of Euler's moment equations.

The angular acceleration can be found by differentiating the angular velocity vector with respect to time [9].

$$\left\{\alpha^{D/I}\right\}_C = \frac{d^I}{dt}\left\{\omega^{D/I}\right\}_C = \frac{d^C}{dt}\left\{\omega^{D/I}\right\}_C + \left\{\omega^{C/I}\right\}_C X \left\{\omega^{D/I}\right\}_C \tag{A.34}$$

where

$$\frac{d^C}{dt}\left\{\omega^{D/I}\right\}_C = \left\{ \begin{array}{c} \dot{\omega}_1 \\ \dot{\omega}_2 \\ \dot{\omega}_3 \end{array} \right\}_C = \left\{ \begin{array}{c} \alpha_1 \\ \alpha_2 \\ \alpha_3 \end{array} \right\}_C \tag{A.35}$$

and

$$\left\{\omega^{C/I}\right\}_C X \left\{\omega^{D/I}\right\}_C = \left\{\begin{array}{c}\omega_1\\ \omega_2\\ \acute{\omega}_3\end{array}\right\}_C X \left\{\begin{array}{c}\omega_1\\ \omega_2\\ \omega_3\end{array}\right\}_C = \left\{\begin{array}{c}\omega_2\omega_3 - \omega_2\acute{\omega}_3\\ -\omega_1\omega_3 - \omega_1\acute{\omega}_3\\ \omega_1\omega_2 - \omega_1\omega_2\end{array}\right\}_C = \left\{\begin{array}{c}\theta_3\omega_2\\ -\theta_3\omega_1\\ 0\end{array}\right\}_C \tag{A.36}$$

This yields

$$\left\{\alpha^{D/I}\right\}_C = \left\{\begin{array}{c}-\ddot{\nu}\cos\theta_1\sin\theta_2 + \dot{\nu}\left(\dot{\theta}_1\sin\theta_1\sin\theta_2 - \dot{\theta}_2\cos\theta_1\cos\theta_2\right) +\\ \ddot{\nu}\sin\theta_1 + \dot{\nu}\dot{\theta}_1\cos\theta_1 +\\ \ddot{\nu}\cos\theta_1\cos\theta_2 - \dot{\nu}\left(\dot{\theta}_1\sin\theta_1\cos\theta_2 + \dot{\theta}_2\cos\theta_1\sin\theta_2\right) +\\ \ddot{\theta}_1\cos\theta_2 - \dot{\theta}_1\dot{\theta}_2\sin\theta_2\\ \ddot{\theta}_2\\ \ddot{\theta}_1\sin\theta_2 + \dot{\theta}_1\dot{\theta}_2\sin\theta_2 + \ddot{\theta}_3\end{array}\right\}_C \tag{A.37}$$

Having solved for the angular acceleration, use the angular velocity and write the angular momentum about the satellite center of mass, S.

$$\{H_S\}_C = [I_S]_C \left\{\omega^{D/I}\right\}_C \tag{A.38}$$

Since this satellite is symmetric about the spin axis, the inertia matrix can be written as a matrix of constants

$$[I_S]_C = \begin{bmatrix} A & 0 & 0\\ 0 & A & 0\\ 0 & 0 & C\end{bmatrix} \tag{A.39}$$

From Euler's equation of motion, the change in angular momentum is equal to the applied moments.

$$\frac{d^I}{dt}\{H_S\}_C = \{M_S\}_C \tag{A.40}$$

$$\frac{d^C}{dt}\{H_S\}_C + \left[\tilde{\omega}^{C/I}\right]\{H_S\}_C = \{M_S\}_C \tag{A.41}$$

where

$$\left[\tilde{\omega}^{C/I}\right] = \begin{bmatrix} 0 & -\dot{\omega}_3 & \omega_2 \\ \dot{\omega}_3 & 0 & -\omega_1 \\ -\omega_2 & \omega_2 & 0 \end{bmatrix} \tag{A.42}$$

Since the inertia matrix is constant, equation A.41 can be written as

$$\begin{bmatrix} A & 0 & 0 \\ 0 & A & 0 \\ 0 & 0 & C \end{bmatrix} \begin{Bmatrix} \dot{\omega}_1 \\ \dot{\omega}_2 \\ \dot{\omega}_3 \end{Bmatrix} + \begin{bmatrix} 0 & -\dot{\omega}_3 & \omega_2 \\ \dot{\omega}_3 & 0 & -\omega_1 \\ -\omega_2 & \omega_2 & 0 \end{bmatrix} \begin{bmatrix} A & 0 & 0 \\ 0 & A & 0 \\ 0 & 0 & C \end{bmatrix} \begin{Bmatrix} \omega_1 \\ \omega_2 \\ \omega_3 \end{Bmatrix} = \begin{Bmatrix} M_1 \\ M_2 \\ M_3 \end{Bmatrix} \tag{A.43}$$

This reduces to

$$\begin{Bmatrix} A\dot{\omega}_1 \\ A\dot{\omega}_2 \\ C\dot{\omega}_3 \end{Bmatrix} + \begin{bmatrix} 0 & -\dot{\omega}_3 & \omega_2 \\ \dot{\omega}_3 & 0 & -\omega_1 \\ -\omega_2 & \omega_2 & 0 \end{bmatrix} \begin{Bmatrix} A\omega_1 \\ A\omega_2 \\ C\omega_3 \end{Bmatrix} = \begin{Bmatrix} M_1 \\ M_2 \\ M_3 \end{Bmatrix} \tag{A.44}$$

Or in scalar form

$$M_1 = A\dot{\omega}_1 - A\omega_2\dot{\omega}_3 + C\omega_2\omega_3 \tag{A.45}$$

$$M_2 = A\dot{\omega}_2 + A\omega_1\dot{\omega}_3 - C\omega_1\omega_3 \tag{A.46}$$

$$M_3 = C\dot{\omega}_3 - A\omega_1\omega_2 + A\omega_1\omega_2 \tag{A.47}$$

Replacing $\dot{\omega}_3$ with $\omega_3 - \dot{\theta}_3$ this becomes

$$M_1 = A\dot{\omega}_1 - A\omega_2\omega_3 + A\omega_2\dot{\theta}_3 + C\omega_2\omega_3 \tag{A.48}$$

$$M_2 = A\dot{\omega}_2 + A\omega_1\omega_3 - A\omega_1\dot{\theta}_3 - C\omega_1\omega_3 \tag{A.49}$$

$$M_3 = C\dot{\omega}_3 \tag{A.50}$$

Dividing the first two moment equations by A, and the last by C.

$$\frac{M_1}{A} = \dot{\omega}_1 + \frac{C-A}{A}\omega_2\omega_3 + \omega_2\dot{\theta}_3 \quad (A.51)$$

$$\frac{M_2}{A} = \dot{\omega}_2 - \frac{C-A}{A}\omega_1\omega_3 - \omega_1\dot{\theta}_3 \quad (A.52)$$

$$\frac{M_3}{C} = \dot{\omega}_3 \quad (A.53)$$

The moments from gravitational potentials are given in [8]. These values are

$$M_1 = 0 \quad (A.54)$$

$$M_2 = -3n^2\zeta^{-3}(C-A)\sin\theta_2\cos\theta_2 \quad (A.55)$$

$$M_3 = 0 \quad (A.56)$$

Introducing the inertial ratio K that is defined as

$$K \equiv \frac{C-A}{A} \quad (A.57)$$

the three moment equations can be written as

$$\dot{\omega}_1 + K\omega_2\omega_3 + \omega_2\dot{\theta}_3 = 0 \quad (A.58)$$

$$\dot{\omega}_2 - K\omega_1\omega_3 - \omega_1\dot{\theta}_3 = -3n^2\zeta^{-3}K\sin\theta_2\cos\theta_2 \quad (A.59)$$

$$\dot{\omega}_3 = 0 \quad (A.60)$$

or

$$\alpha_1 + K\omega_2\omega_3 + \omega_2\dot{\theta}_3 = 0 \quad (A.61)$$

$$\alpha_2 - K\omega_1\omega_3 - \omega_1\dot{\theta}_3 = -3n^2\zeta^{-3}K\sin\theta_2\cos\theta_2 \quad (A.62)$$

$$\alpha_3 = 0 \quad (A.63)$$

where $\{\alpha\}$ is given in equation A.37 and $\{\omega\}$ is from equation A.31.

Now we consider motion of the satellite about the equilibrium point $\theta_1 = \theta_2 = 0$. The value of θ_3 can be solved for in terms of ω_3. Using small angle conditions around the equilibrium point

$$\left\{\omega^{D/I}\right\}_C = \left\{\begin{array}{c} \omega_1 \\ \omega_2 \\ \omega_3 \end{array}\right\}_C = \left\{\begin{array}{c} \dot{\theta}_1 - \dot{\nu}\theta_2 \\ \dot{\theta}_2 + \dot{\nu}\theta_1 \\ \dot{\nu} + \dot{\theta}_3 \end{array}\right\}_C \tag{A.64}$$

Integrating the equation for ω_3

$$\int_0^t \omega_3 dt = \omega_3 t = \theta_3 + \theta_3(0) + \nu + \nu(0) \tag{A.65}$$

With the initial conditions defined as $\theta_3(0) = \nu(0) = 0$ solve for θ_3.

$$\theta_3 = \omega_3 t - \nu \tag{A.66}$$

where $\omega_3 = n(1+\alpha)$, α is the spin rate of the satellite, $\left\{\omega^{D/C}\right\}$, and is a constant value, n is defined in equation A.3. For these conditions, the accelerations and moments are zero. Therefore this represents a valid equilibrium point, with the spin axis perpendicular to the orbit plane. . The next step is to transform our linearized differential equations of motion into a form where the stability of this equilibrium point can be evaluated using Floquet Theory. The desired form is

$$\bar{x}' = A\bar{x} \tag{A.67}$$

where $\bar{x}$ represents the vector of state variables.

$$\{x\} = \begin{Bmatrix} \theta_1 \\ \theta_2 \\ \dot{\theta}_1 \\ \dot{\theta}_2 \end{Bmatrix} \tag{A.68}$$

The first two rows of the A matrix are fairly simple with a one in the appropriate column and the rest of the elements zero. The last two rows can be found by differentiating equation A.64.

$$\frac{d}{dt}\left\{\omega^{D/I}\right\}_C = \begin{Bmatrix} \dot{\omega}_1 \\ \dot{\omega}_2 \\ \dot{\omega}_3 \end{Bmatrix}_C = \begin{Bmatrix} \alpha_1 \\ \alpha_2 \\ \alpha_3 \end{Bmatrix}_C = \begin{Bmatrix} \ddot{\theta}_1 - \ddot{\nu}\theta_2 - \dot{\nu}\dot{\theta}_2 \\ \ddot{\theta}_2 + \ddot{\nu}\theta_1 + \dot{\nu}\dot{\theta}_1 \\ \ddot{\nu} + \ddot{\theta}_3 \end{Bmatrix}_C \tag{A.69}$$

Substituting these values for α and the values for ω from equation A.64 into equations A.62 and A.63 the result is two linearized equations for the motion in the region near the equilibrium point.

$$\ddot{\theta}_1 - \ddot{\nu}\theta_2 - \dot{\nu}\dot{\theta}_2 + K\left(\dot{\theta}_2 + \dot{\nu}\theta_1\right)\left(\dot{\theta}_3 + \dot{\nu}\right) + \left(\dot{\theta}_2 + \dot{\nu}\theta_1\right)\dot{\theta}_3 = 0 \tag{A.70}$$

also applying the small angle assumptions to the second equation

$$\ddot{\theta}_2 + \dot{\nu}\dot{\theta}_1 + \ddot{\nu}\theta_1 - K\left(\dot{\theta}_1 - \dot{\nu}\theta_2\right)\left(\dot{\theta}_3 + \dot{\nu}\right) - \left(\dot{\theta}_1 - \dot{\nu}\theta_2\right)\dot{\theta}_3 = -3n^2 K\theta_2\zeta^{-1} \tag{A.71}$$

To put these in the proper format we must apply the chain rule and convert them to a form with the differentiation is with respect to τ. Then solve for θ_1'' and θ_2''. This results in

$$\theta_1'' = -\nu'\left(\theta_3' + K\nu' + K\theta_3'\right)\theta_1 + \nu''\theta_2 + \left(\nu' - \theta_3' - K\left(\nu' + \theta_3'\right)\right)\theta_2' \tag{A.72}$$

$$\theta_2'' = -\nu''\theta_1 + \left[-\nu'\left(\theta_3' + K\nu' + K\theta_3'\right) - 3K\zeta^{-3}\right]\theta_2 - \left(\nu' - \theta_3' - K\left(\nu' + \theta_3'\right)\right)\theta_1' \quad \text{(A.73)}$$

ν' and ν'' can be replaced by the values from equations A.13 and A.14. θ_3' can be replaced by noting that $\alpha_3 = 0$, then from equation A.64

$$\nu' + \theta_3' = constant \quad \text{(A.74)}$$

and letting the *constant* be $\alpha + 1$, then θ_3' can be expressed as

$$\theta_3' = (\alpha + 1) - \zeta^{-2}\left(1 - \epsilon^2\right)^{1/2} \quad \text{(A.75)}$$

Now the equations can be expressed in matrix form in terms satellite inertia ratio (K) , satellite spin rate (α) and orbital eccentricity (ζ and ζ'). If the spin rate and inertia ratio of the satellite are held fixed, increased eccentricity will tend to destabilize the satellite attitude.

$$A(\tau) = \begin{bmatrix} 0 & 0 & 1 & 0 \\ 0 & 0 & 0 & 1 \\ a_{31} & a_{32} & 0 & a_{34} \\ a_{41} & a_{42} & a_{43} & 0 \end{bmatrix} \quad \text{(A.76)}$$

where:

$a_{31} = (1 - \epsilon^2)\zeta^{-4} - (1 + \alpha)(1 + K)(1 - \epsilon^2)^{1/2}\zeta^{-2}$

$a_{32} = -a_{41} = -2(1 - \epsilon^2)^{1/2}\zeta'\zeta^{-3}$

$a_{34} = -a_{43} = 2(1 - \epsilon^2)^{1/2}\zeta^{-2} - (1 + \alpha)(1 + K)$

$a_{42} = a_{31} - 3K\zeta^{-3}$

It should be noted all the elements of A are periodic with a period of one orbit, T. This is the proper form needed to apply Floquet Theory. Now the stability can be determined in the region of an equilibrium point.

A.3 Non-linear Equations of Motion

All of the previous development has been based on the linearized equations of motion around an equilibrium point. To fully evaluate the system requires its non-linear behavior to be examined in the phase space. To do this requires the non-linear equations of motion. The expressions for these can be found by replacing ω_1, ω_2, α_1 and α_2 in equations A.62 and A.63 with the expressions from equations A.31 and A.37. ω_3 is still a constant, $\alpha + 1$, that is the spin rate about the axis of symmetry. Using this value and solving equation A.31, to remove $\dot{\theta}_3$ from the equations yields.

$$\dot{\theta}_3 = \alpha + 1 - \dot{\theta}_1 \sin\theta_2 - \dot{\nu}\cos\theta_1\cos\theta_2 \tag{A.77}$$

Making the appropriate substitutions into equation A.62 yields.

$$\begin{aligned} 0 \;=\; & \ddot{\theta}_1\cos\theta_2 - \dot{\theta}_1\dot{\theta}_2\sin\theta_2 - \ddot{\nu}\cos\theta_1\sin\theta_2 + \dot{\nu}\dot{\theta}_1\sin\theta_1\sin\theta_2 - \dot{\nu}\dot{\theta}_2\cos\theta_1\cos\theta_2 + \\ & K(\dot{\theta}_2 + \dot{\nu}\sin\theta_1)(\alpha+1) + (\dot{\theta}_2 + \dot{\nu}\sin\theta_1)\dot{\theta}_3 \end{aligned} \tag{A.78}$$

Converting the derivative from dt to $d\tau$, replacing $\dot{\theta}_3$ then solving for θ_1''

$$\begin{aligned} \theta_1'' \;=\; & 2\theta_1'\theta_2'\tan\theta_2 + 2\nu'\theta_2'\cos\theta_1 - (K+1)(\alpha+1)(\theta_2' + \nu'\sin\theta_1)\sec\theta_2 \\ & + \nu''\cos\theta_1\tan\theta_2 + \nu'\nu'\sin\theta_1\cos\theta_1 \end{aligned} \tag{A.79}$$

And in a similar manner solve for θ_2''

$$\begin{aligned} \theta_2'' \;=\; & (K+1)(\alpha+1)(\theta_1'\cos\theta_2 - \nu'\cos\theta_1\ sin\theta_2) - \nu''\sin\theta_1 - 2\nu'\theta_1'\cos\theta_1\cos^2\theta_2 - \\ & (\theta_1'^2 - \nu'^2\cos^2\theta_1 + 3K\zeta^{-3})\sin\theta_2\cos\theta_2 \end{aligned} \tag{A.80}$$

Expressions for ν' and ν'' are in equations A.6 and A.7. Numerical integration of this equation set will allow us to determine the motion of the satellite described by the non-linear equations of motion.

Bibliography

1. Bai-Lin, Hao. *Chaos*. Singapore,China: World Scientific Publishing Co Pte Ltd., 1984.
2. Calico, R.A. and W.E. Wiesel. "Control of Time-Periodic Systems," *Journal of Guidance, Control, and Dynamics*, 7(6):671–676 (November-December 1984).
3. Calico, R.A. and G.S. Yeakel. "Active Attitude Control of a Spinning Symmetrical Satellite in an Elliptic Orbit," *Journal of Guidance, Control, and Dynamics*, *6*(4):315–318 (July-August 1983).
4. Glass, Leon and Michael C. Mackey. *From Clocks to Chaos*. Princeton, New Jersey: Princeton University Press, 1988.
5. Gleick, James. *Chaos, Making a New Science*. New York, NY: Viking Penguin Inc, 1988.
6. Grouwer, D. and G.M. Clemence. *Methods of Celestial Mechanics*. New York, NY: Academic Press, 1961.
7. Jordan, D.W. and P. Smith. *Nonlinear Ordinary Differential Equations* (second Edition). New York, NY: Oxford University Press, 1988.
8. Kane, T.R. and P.M. Barba. "Attitude Stability of a Spinning Satellite in an Elliptic Orbit," *Journal of Applied Mechanics*, *33*:402–405 (June 1966).
9. Likins, Peter W. *Elements of Engineering Mechanics*. New York, NY: McGraw-Hill Book Company, 1973.
10. Meirovitch, Leonard. *Methods of Analytical Dynamics*. New York, NY: McGraw-Hill Book Company, 1970.
11. Moon, Francis C. *Chaotic Vibrations*. New York, NY: John Wiley and Sons Ltd., 1987.
12. Myers, Gregory E. *Active Control of Linear Periodic System with Two Unstable Modes*. MS thesis, AFIT/GAE/AA/82D-21, 1982.
13. Pagels, Heinz R. *The Dreams of Reason*. New York, NY: Bantum Books, 1988.
14. Shell, Dale E. *Stability Solution to Linearized Equations of Motion for a Symmetric Spinning Satellite in an Elliptical Orbit Applied to the Non-linear Equations*. MS thesis, AFIT/GA/AA/88D-09, 1988.
15. Thompson, J.M.T. and H.B. Stewart. *Nonlinear Dynamics and Chaos*. New York, NY: John Wiley and Sons Ltd., 1987.
16. Wiesel, William E. *Spaceflight Dynamics*. New York, NY: McGraw-Hill Book Company, 1989.

Vita

James W. Cole

attended the University of Central Arkansas for two and one half years, enlisted in the Air Force on 17 August 1973. In August of 1978 he returned to school at the University of Texas at Austin under the Airman Education and Commissioning Program. In December of 1980 he graduated with a Bachelor of Science in Mechanical Engineering and was awarded Highest Honors. He completed Officers Training School on 6 May 1981 and was assigned to the 6595 Shuttle Test Group at Vandenberg AFB. From there he received an assignment to Kennedy Space Center to train as a Shuttle Avionics Engineer. After the Challenger accident and the cancellation of the AF Shuttle program, he transferred to the 6555 Aerospace Test Group at Cape Canaveral Air Force Station, Florida, where he worked as the Chief of Inertial Upper Stage Engineering for two years. He then accepted an assignment to AFIT. Upon completion of the Reliability and Maintainability PSC course, he will be assigned to AFLC/MM at Hill AFB, Utah.

SECURITY CLASSIFICATION OF THIS PAGE

REPORT DOCUMENTATION PAGE

Form Approved OMB No. 0704-0188

1a. REPORT SECURITY CLASSIFICATION: UNCLASSIFIED	1b. RESTRICTIVE MARKINGS
2a. SECURITY CLASSIFICATION AUTHORITY	3. DISTRIBUTION/AVAILABILITY OF REPORT: Approved for public release; Distribution Unlimited
2b. DECLASSIFICATION/DOWNGRADING SCHEDULE	
4. PERFORMING ORGANIZATION REPORT NUMBER(S): AFIT/GAE/ENY/89D-05	5. MONITORING ORGANIZATION REPORT NUMBER(S)
6a. NAME OF PERFORMING ORGANIZATION: School of Engineering; 6b. OFFICE SYMBOL (If applicable): AFIT/ENY	7a. NAME OF MONITORING ORGANIZATION
6c. ADDRESS (City, State, and ZIP Code): Air Force Institute of Technology, Wright-Patterson AFB OH 45433	7b. ADDRESS (City, State, and ZIP Code)
8a. NAME OF FUNDING/SPONSORING ORGANIZATION; 8b. OFFICE SYMBOL (If applicable)	9. PROCUREMENT INSTRUMENT IDENTIFICATION NUMBER
8c. ADDRESS (City, State, and ZIP Code)	10. SOURCE OF FUNDING NUMBERS: PROGRAM ELEMENT NO. / PROJECT NO. / TASK NO. / WORK UNIT ACCESSION NO.

11. TITLE (Include Security Classification): Stability and Control of a Spinning Symmetric Satellite in an Elliptical Orbit (unclassified)

12. PERSONAL AUTHOR(S): James W. Cole, Captain USAF

13a. TYPE OF REPORT	13b. TIME COVERED	14. DATE OF REPORT (Year, Month, Day)	15. PAGE COUNT
M.S. Thesis	FROM _____ TO _____	1989 December	127

16. SUPPLEMENTARY NOTATION

17. COSATI CODES			18. SUBJECT TERMS (Continue on reverse if necessary and identify by block number)
FIELD	GROUP	SUB-GROUP	Satellite Attitude, Floquet Theory, Modal Control, Non-linear Analysis, Poincaré Maps, Chaos
22	01		
22	02		

19. ABSTRACT (Continue on reverse if necessary and identify by block number)

The stability of a spinning symmetric satellite in an elliptical orbit is analyzed using phase planes and surface of section techniques. The equations of motion for the satellite attitude are presented in a linearized and a non-linear form. Floquet Theory is applied to the development of a control system for two unstable modes of the satellite. A scalar control is applied using angle rates as feedback. The stability of the controlled system is examined in controlled modal coordinates. Comparisons of the linear and non-linear system motions are made relative to changes in the control gains. Potential chaotic motion limits the controller gains of the non-linear system.

20. DISTRIBUTION/AVAILABILITY OF ABSTRACT: ☒ UNCLASSIFIED/UNLIMITED ☐ SAME AS RPT. ☐ DTIC USERS	21. ABSTRACT SECURITY CLASSIFICATION: UNCLASSIFIED
22a. NAME OF RESPONSIBLE INDIVIDUAL: Dr. Robert A. Calico	22b. TELEPHONE (Include Area Code): 513-255-3517; 22c. OFFICE SYMBOL: AFIT/EN

DD Form 1473, JUN 86 — Previous editions are obsolete. — SECURITY CLASSIFICATION OF THIS PAGE